ABRUPT CLIMATE VARIABILITY DURING THE LAST GLACIAL AND THE LATE HOLOCENE FROM THE WESTERN TROPICAL PACIFIC PERSPECTIVE

by

Reetta Maaria Saikku

A Dissertation Presented to the
FACULTY OF THE GRADUATE SCHOOL
UNIVERSITY OF SOUTHERN CALIFORNIA
In Partial Fulfillment of the
Requirements for the Degree
DOCTOR OF PHILOSOPHY
(EARTH SCIENCES)

May 2009

Acknowledgments

I would like to thank my advisor Lowell Stott as well as my other committee members Robert Douglas, Douglas Hammond and Donal Manahan for their help and guidance.

Thank you also to Miguel Rincon for teaching me the laboratory techniques and for assistance with running samples. I would also like to thank Steve Lund for providing his paleomagnetic data for Project I and for helpful discussions.

Thank you also to my lab mates in the paleoclimatology lab through my years at USC: Andres Martinez, Paola Gomez, Max Berkelhammer, Pat Horan, Deborah Khider, Mengfan Zhu and Justin Reuter.

I would like to thank the Department of Earth Sciences at the University of Southern California for funding. Thank you to Cynthia Waite, John McRaney and Vardui Ter-Simonian for their help through the years. I would also like to thank the American-Scandinavian Foundation for funding my research.

Table of contents

List of Tables

List of Figures

Abstract

In Project I, Western tropical Pacific sea surface temperatures and Pacific Deep Water temperatures during Marine Isotope Stage 3 have been reconstructed from the $\delta^{18}O$ and Mg/Ca of planktonic and benthic foraminifera from *Marion Dufresne* core MD98-2181. This 36m marine core was collected at 6.3°N from a water depth of 2114m. With sediment accumulation rates of up to 80cm/ky, it provides a decadally-resolved history of ocean variability during the last glacial period. Surface temperatures and salinities at this site varied in close association with millennial-scale atmospheric temperature swings at high northern latitudes as reflected in the GISP2 ice core. At times of colder atmospheric temperatures over Greenland, the western Pacific was more saline and summer season SSTs were ~2^{o}C colder. These millennial scale changes within the tropics are attributed to a southward displacement of the summer season ITCZ in response to steeper meridional temperature gradients within the Pacific. The benthic $\delta^{18}O$ record from MD98-2181 documents upper Pacific Deep Water temperature and salinity variability. Benthic $\delta^{18}O$ variations of 0.3-0.5‰ during MIS 3 indicate deep waters within the Pacific were varying by ~1-1.5°C, with the possibility that some of the variability was due to changing salinity and minor glacial-eustatic changes. The observed deep water variability correlates to changes in Antarctic surface temperatures and thus reflects changes in Southern Ocean temperatures at the site of Pacific Deep Water formation. The combined planktonic and benthic records from MD98-2181 thus provides a northern and southern hemispheric climate record of anti-

phased variability during MIS 3 as has been inferred previously from ice core records. Furthermore, the deep sea temperature excursions appear to have led millennial variations in atmospheric CO_2 as recorded in the EDML ice core by ~1kyr. It is therefore hypothesized that the CO_2 may have been outgassed from a less stratified Southern Ocean.

Project II presents a 2000-year record of Mg/Ca and $\delta^{18}O$ measurements on planktonic, and $\delta^{18}O$ measurements on benthic foraminifera from continuous marine cores taken from high sedimentation sites in the Western Pacific Warm Pool. The western Pacific warm pool exhibits decadal- to centennial-scale variability. The Little Ice Age is recorded as the coldest and Medieval Warm Period as the warmest over last 2ka (data does not include the last 150yrBP).

The MD81 benthic record suggests a large drop in temperature of ~1°C, which may also include a salinity component. This event correlates with other proxy records from the Southern Ocean confirming the event as Southern Hemisphere-wide.

Due to the ideal core location of MD81 it was also possible to address the question of phasing of the northern and southern climate records and whether the "bipolar seesaw" was still active during the Holocene. The 2000-year surface record from the western Pacific warm pool exhibits centennial scale variability, with larger, potentially millennial-scale oscillations present within the last 1000 years, as recorded by two marine sediment cores. However, based on the available data there is no evidence for a bipolar seesaw during the large benthic cooling event.

Preface

This research presents two studies of high resolution marine climate proxy data from the climatically important region of the western tropical Pacific. The purpose is to address questions of the extent and probable source of abrupt climate change events during the Last Glacial and during the late Holocene on millennial, centennial and decadal-timescales.

Chapters 1-6 deal with Project I – Marine Isotope Stage 3; Chapter 1 is the introduction, Chapter 2 describes the regional setting and oceanography, Chapter 3 the materials and methods. The results are presented in Chapter 4. Chapter 5 and 6 are the discussion and conclusions respectively.

Chapters 7-12 deal with Project II – Past two millennia. Chapter 7 is the introduction, and the regional setting and oceanography are described in Chapter 8. The materials and methods are outlined in Chapter 9. This is a briefer description as the methodology is identical between Project I and II. For the more detailed version of the methodology, please see Chapter 3. The results are presented in Chapter 10, and the discussion and conclusions in Chapters 11 and 12 respectively.

Chapter 1: Introduction

In Project I, Western tropical Pacific sea surface temperatures and Pacific Deep Water temperatures during Marine Isotope Stage 3 have been reconstructed from the $\delta^{18}O$ and Mg/Ca of planktonic and benthic foraminifera from Marion Dufresne core MD98-2181.

1-1. Ice cores

Marine Isotope Stage 3 (MIS3), which lasted from approximately 60000 to 30000 years ago, is now known to have been a time during which the climate underwent rapid changes. Ice core records drilled in Greenland were the first to show these climate events, now known as Dansgaard-Oeschger (D/O) events (Dansgaard et al., 1993), which involved rapid warming in the North Atlantic region followed by more gradual cooling. These events occurred repeatedly through the last ice age. The first ice core drilling through a polar ice sheet was accomplished at Camp Century, Greenland in 1966 showing climatic changes during the last 70,000-10,000 years reflected in the oxygen isotopic composition of ice. In a preliminary study (Dansgaard et al., 1969) the oxygen isotope composition of the ice core were plotted against ice age, which was calculated from an age-versus-depth equation. A comparison with other paleoclimate archives revealed a fairly good agreement between the main features of climatic history among the various records (such as pollen, ice sheet retreats and advances, deep-sea cores). Dansgaard et al. (1969) identified features such as two long-lasting periods with relatively high oxygen delta-values ($\delta^{18}O$) at ~29,000 to 35,000 yrs BP and 41,900 to

49,000 yrs BP, both of which coincided with well-known interstadial climatic periods known as the Plum Point and Port Talbot interstadials in the American and European pollen terminology (Dansgaard et al., 1969), now named D/O event 8 and 12.

The first ice core drilled in Antarctica was obtained at Byrd Station (West Antarctica) in 1968. By 1972 only two deep ice cores had been recovered, one from Camp Century, North-West Greenland and one from Byrd Station. Most of the major climatic changes documented for the past 100,000 years (known from other geochronological studies) were recognized in the Camp Century core and these were thought to be caused by solar variability (Dansgaard et al., 1969). Therefore, on this basis Johnsen et al. (1972) expected to find the same climate oscillations in the Antarctic ice core. However, at Byrd station the climatology of the site made it difficult to interpret time varying history of climate change because the site is characterized by very slow snow accumulation rate. Indeed, the reason that made this location so appropriate for obtaining a long ice core record (low accumulation rates) also made it a difficult climate record to interpret. To establish a reasonable timescale for the Byrd ice core, $\delta^{18}O$ variations from this core were compared to the ice core from Greenland. However, this method assumed that there would be a direct correlation between the two sites reflected in the oxygen isotopic stratigraphies. In fact, it was not possible to establish an exact time interval for the Wisconsin glacial phase or any of the intervening climatic events in the Byrd ice core as had been observed in the Camp Century record. It was therefore concluded that Camp Century must have been more sensitive to

climatic change during glacial periods compared to the Antarctic. Furthermore, because of the uncertainties in the Byrd timescale, no pole-to-pole correlations could be made apart from the more pronounced features and general trends.

Dansgaard et al. (1982) further discussed the large amplitude oscillations observed in the $\delta^{18}O$ stratigraphy from the Camp Century and Dye 3 ice cores during the interval between ~77,000-10,000 yrs BP, which appeared to have a quasi-periodicity of ~2550 years. The acquisition of an additional Antarctic (Vostok) data set was still considered of insufficient resolution to observe the same higher frequency climatic variability seen at Greenland (Lorius et al., 1985). In 1993 Dansgaard et al. presented a detailed stable-isotope record of the Greenland GRIP ice core, listing and numbering 24 discrete glacial interstadials, abrupt climate changes of at least regional extent. The timescale was obtained by counting individual annual layers back to 14,500 yrs BP and then applying a comparable age/depth model back to 250,000 yrs BP. This study showed that at least the climate within the North Atlantic region could reorganize itself rapidly, perhaps even within decades. The large δ-shifts observed in Greenland cores were found to be much less pronounced in the δ-record in the Antarctic Vostok core. This was thought to be because Greenland was connected to a rapidly altered ocean/atmosphere circulation change that involved increased and decreased advection of warm water currents into the North Atlantic (Dansgaard et al., 1993). The multiple ice cores from Greenland also allowed a closer examination of the regional differences between ice cores. Andersen et al. (2004) made a detailed comparison of the North Grip

ice core (NGRIP) $\delta^{18}O$ ice profile, combining it with the GRIP ice isotopic record over their common intervals. In doing so Andersen et al. (2004) found significant differences between the records that illustrated the importance of regional climate variations over Greenland. Whereas NGRIP and GRIP have very similar $\delta^{18}O$ records during the Holocene, glacial isotopic values in the NGRIP record are systematically depleted by 1-2 per mil (‰) in the glacial intervals suggesting that air masses that influenced the two sites during the glacial had different sources. Andersen et al. (2004) argued that sea ice and extensive North Atlantic ice shelves in the glacial meant that NGRIP had become further from the ocean, and may have seen a higher fraction of air coming over the northern side of the Laurentide ice sheet, bringing with it colder and more isotopically depleted moisture than GRIP might have seen. Andersen et al. (2004) therefore concluded that the atmospheric hydrologic cycle over Greenland was probably substantially different between the modern and glacial worlds.

Even though the climatic shifts in the Antarctic cores were of smaller magnitude, the next step was to more accurately match the timing of the Greenland and Antarctic ice cores to see the connection between the two.

1-2. Bipolar seesaw?

By 1995, a two-step character to the last deglaciation had been recognized in paleo-temperature records, including the ice core isotope stratigraphies. The last deglaciation was marked by a gradual temperature increase starting at the Bölling, around 14,500 yrs BP and continued through the Alleröd but the warming was interrupted by a return to near glacial conditions in the North Atlantic region known as

the cold Younger Dryas (YD). This cold event began at approximately 12,900 yrs BP and terminated abruptly around 11,500 yrs BP (Jouzel et al., 1995). All of the available paleoclimate records from long ice cores that had been recovered from the interior of the Antarctic ice sheet exhibited a similar two-step deglacial history with two warming intervals interrupted by a prominent plateau in the rise in the $\delta^{18}O$ and δD (deuterium) during the deglaciation interval (the Antarctic Cold Reversal, ACR) (Jouzel et al., 1995), but with a less accentuated return to cold conditions than in Greenland and the North Atlantic regions. For many years this pause in the warming of the Antarctic continent was thought to correlate with the YD. However, in their Dome B (Antarctica) and GRIP (Greenland) ice core data comparison Jouzel et al. (1995) showed that the coldest part of the ACR (~13,500 and 12,500 yrs BP) lead the YD by ~1000 years and the two warming periods started in Antarctica before they started in Greenland. Similar results had also been produced by Labracherie et al. (1989) from the deep-sea cores in the Indian Ocean sector of the Southern Ocean. By 13,000 yrs BP, sea surface temperatures in the Indian Ocean had reached values similar to the present. A cool oscillation abruptly interrupted this warming between 12,000 and 11,000 yrs BP. Initiation of this cooling appeared therefore to precede the northern hemisphere YD by ~1000yrs. Biostratigraphic studies seemed to indicate that the surface waters warmed earlier, by a few thousand years, in the southern ocean than in the northern Atlantic, both at the last and the penultimate glacial-interglacial transitions (Labracherie et al., 1989). When methane concentration and oxygen isotope ratios in O_2 measurements become available, this revision appeared to be confirmed (Blunier at al, 1998). A

consistent method for assessing the phasing of climatic events in Greenland and Antarctic ice-cores was needed and the synchronization of atmospheric methane variations in ice cores provided such a method because the atmospheric mixing time for methane is about 1 year or less. There are two limitations to the use of gases for synchronization: (i) it is applicable only at times where there is a rapid change in the atmospheric value, (ii) the signal is retained at the "close-off" depth (typically about 80 m) where the bubbles in the ice are isolated from the overlying atmosphere. Also, the mixing-time argument supposes that there are no persistently different hemispheric sources of methane. Using the $\delta^{18}O$ of atmospheric O_2, Sowers and Bender (1995) calculated that the plateau in the deglacial warming correlated instead with the Bölling-Alleröd warm interval which preceded the YD and that during the YD the Antarctic continent rapidly warmed. Sowers and Bender (1995) also concluded that the Antarctic climate oscillation during glacial termination I occurred before the YD event in Greenland and that given the magnitude and timing of the cold events over Greenland and Antarctica, it is not clear how they may have been related to one another. Also the length of this anti-phase was still unclear. Blunier et al. (1997) subsequently concluded that the ACR preceded the YD by at least 1800 yrs. Blunier et al. (1998) further concluded that the long-lasting Greenland warming events D/O 8 and 12 (around 36,000 and 45,000 yrs BP) lagged their Antarctic counterparts by an average of 2000-3000 yrs. A time lag of this length was interpreted to suggest a connection via the ocean instead of the atmosphere.

By 1998 climate model studies suggested that heat is extracted from the Southern Hemisphere when the North Atlantic Deep Water (NADW) formation switches on (Stocker et al., 1992, Crowley, 1992, Stocker and Wright, 1996). This inter-hemispheric coupling via the ocean thermohaline circulation was identified for the D/O events 8 and 12 and also for the termination of the last glaciation (Blunier et al., 1998), implying that during the last deglaciation the magnitude of heat released from the Southern Ocean was out of phase with that in the northern Atlantic. During the Bölling-Alleröd, when heat release in the northern Atlantic was strong, there was a reduction in heat released in the southern hemisphere. During the YD, when the heat release from the ocean in the northern Atlantic was reduced, heat released in the Southern Ocean appears to have been increased. Broecker (1998) and Charles et al. (1996) provided evidence that suggested a bipolar seesaw mechanism existed within the ocean that shifted heat between the hemispheres. It may have operated during MIS 3 where tie lines between similar looking events are not perpendicular to the time axis and instead have an offset of ~1500 years. Blunier et al. (1998) and Blunier and Brook (2001) pointed out in the Northern and Southern Hemisphere ice core records that Antarctic warm temperature variations were characterized by a gradual increase and decrease, whereas Greenland D/O events had a rapid increase and slow decrease. While the Antarctic temperature is increasing, Greenland is cooling. The Antarctic temperature rise is interrupted once Greenland temperature jumps to an interstadial state within a few decades. The temperatures then decrease in both hemispheres to full glacial levels, but Antarctica reaches this level before Greenland.

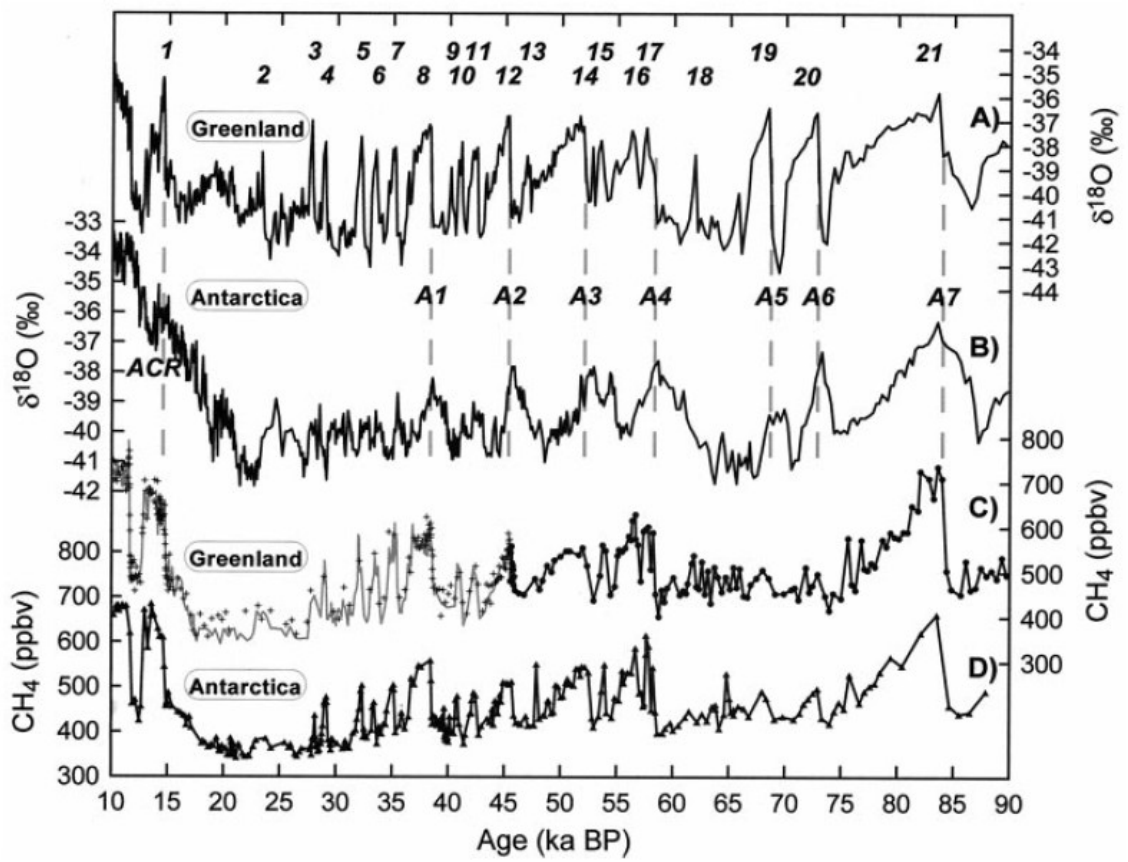

Figure 1-1: Isotopic and CH_4 data from Greenland and Antarctica on the GISP2 time scale. Dashed lines indicate the onset of major D/O-events. (A) $\delta^{18}O_{ice}$ from GISP2, Greenland. (B) $\delta^{18}O_{ice}$ from Byrd Station, West Antarctica. (C) CH_4 data from GISP2 and GRIP Greenland ice cores. Crosses and dots are from GISP2; the solid gray line is from GRIP. (D) CH_4 data from Byrd station. From Blunier and Brook, 2001.

According to Blunier and Brook (2001) the differences in timing of millennial scale climate variations in West Antarctica and in Greenland are a pervasive characteristic of the last glacial period and this temporal behavior is maintained despite large changes in the background state of climate system (ice volume, sea level and orbital geometry between 10,000-90,000 yrsBP) (Figure 1-1). The Greenland and Antarctic warm maxima are in phase, but warming began several thousand years earlier in the Antarctic Byrd and Vostok $\delta^{18}O$ records. More recent correlations include those of GISP2 (Greenland) with the Siple Dome (West Antarctica) (Brook et al., 2005) again

using methane to synchronize the oxygen isotope records. They concluded that Antarctica leads Greenland during major millennial warming events, but not necessarily for the shorter-lived D/O events and their possible Antarctic counterparts. The pattern of change at Siple Dome is similar, but not identical to the Byrd record. Therefore the Siple Dome data does support the case for a coherent regional pattern of millennial-scale climate change in Antarctica, but also highlights the small regional differences between ice cores as was also identified for Greenland. Most recent ice core work includes methane synchronization for a core from East Antarctica in Dronning Maud Land (EDML) and the cores from Greenland (GRIP and NGRIP), concluding that all the D/O events have Antarctic counterparts. This has also improved the relative Greenland-Antarctic chronologic relationships to within 400–800 years for the last glacial period (EPICA Community Members, 2006). However, there are limitations to the use of gases for synchronization and this is especially important in low accumulation rate regions such as the Antarctic plateau where the ice age/gas age offset can be as large as 5000 years or more during glacial periods. Raisbeck et al. (2007) used ^{10}Be peak correlations in an attempt to overcome the gas-ice uncertainties. They argued that the cosmogenic isotope ^{10}Be is suitable for synchronization of paleoclimatic records, because large changes in its production (caused by modulation of the galactic cosmic ray intensity by the geomagnetic field and the electric and magnetic fields associated with the out-flowing solar wind) are globally synchronous and independent of climate. A decadally resolved record of the ^{10}Be peak at 41,000 years from the EPICA Dome C ice core was matched with the same peak in the GRIP ice core

(Raisbeck et al., 2007). They conclude that between Antarctic warming events A1 and A2 three additional Antarctic temperature maxima can be identified in the EPICA Dome C ice core, and the middle of these can be precisely synchronized with D/O 10 in the Greenland ice cores via the 10Be peak, therefore lending support for the thermal bipolar seesaw theory and its operating throughout the sequence of D/O events.

1-3. Abrupt climate change outside of Greenland and Antarctica

Since the climate oscillations of MIS3 were first observed in the ice core records, there have been a multitude of studies that have observed similar or corresponding climate oscillations around the globe, which have then been tied back to the ice cores.

Benthic foraminiferal $\delta^{18}O$ is mainly thought to reflect ice volume changes on time scales of millennia. The buildup of large ice sheets during glacial periods increases the oxygen isotopic composition of the global ocean as isotopically light moisture is evaporated and deposited on land as ice. However, these changes occur progressively and over longer time scales than the more abrupt oxygen isotopic variability during the D/O events in the Greenland record. The deep sea may also record shorter-term changes and correspond to the D/O climatic changes and these would be superimposed upon the longer-term glacioeustatic changes. Shackleton et al. (1983) and Shackleton and Pisias (1985) published a detailed record of benthic foraminifera $\delta^{18}O$ and $\delta^{13}C$ for marine core V19-30 that documented oxygen and carbon isotope variability in the deep Pacific. The record included abrupt changes during MIS3. The carbon isotopic difference between the Pacific and the Atlantic is presently about 1‰, but during Stage 3 the

interocean 13C difference was close to zero (Shackleton et al., 1983). The $\delta^{13}C$ isotope record was interpreted to reflect a diminished role of the NADW during the glacial period and that NADW was replaced by a water mass with very different characteristics, a potentially increased relative contribution of AABW, at least in this part of the North Atlantic during the full glacial conditions (Shackleton et al., 1983).

A record of ocean oxygenation and circulation from the high sedimentation rate Santa Barbara basin is also thought to reflect a pattern of variability in concert with the Greenland ice-core D/O (Behl and Kennett, 1996). An apparent relationship between more oxygenated deep waters in the marine basin during stadials and reduced oxygenation during the intestadials was observed. Behl and Kennett (1996) concluded that the absence of significant lags between the GISP2 ice core record and the marine core suggested that ocean circulation was tightly linked with global climate changes through atmospheric changes (Figure 1-2). However it was not possible to distinguish whether the northeast Pacific intermediate water was changed by production of young, proximally derived intermediate water or by an influx of older, distally derived waters (Behl and Kennett, 1996). $\delta^{18}O$ data for planktonic foraminifera *Globigerina bulloides* from Mediterranean marine cores MD95-2043 and ODP-977A revealed consistency with the D/O cycles observed in Greenland as well (Martrat et al., 2004). Corresponding D/O-associated changes have also been found in North American lake records (Benson et al., 2003) although the absolute phasing between lake-size and ice-core $\delta^{18}O$ is difficult to determine.

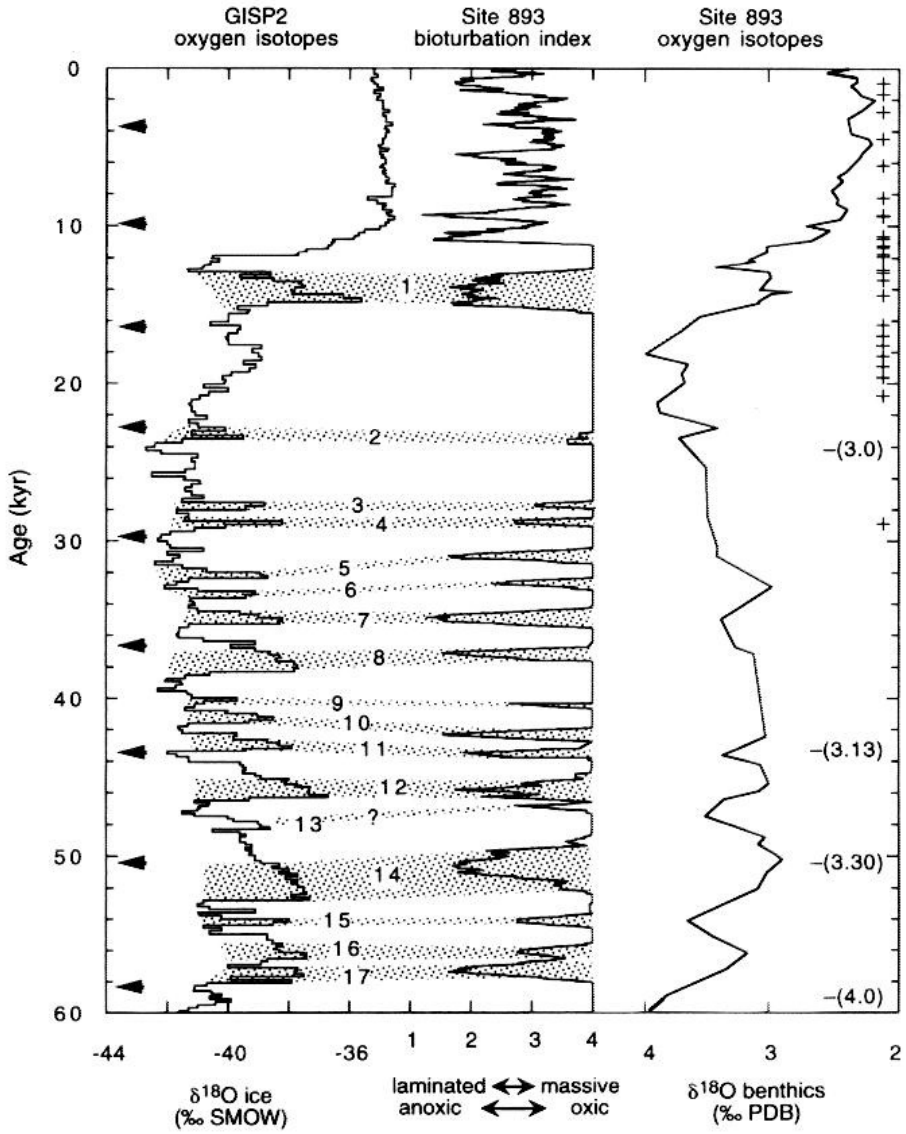

Figure 1-2: Comparison of Santa Barbara basin site 893 bioturbation index and benthic foraminiferal $\delta^{18}O$ records with $\delta^{18}O_{ice}$ time-series from GISP2. Correlation of the anoxia (lamination) events to the warm interstadials of GISP2 is shown by shading. From Behl and Kennett, 1996.

An equivalent pattern of atmospheric variability associated with the D/O events is also thought to have operated at low latitudes. Changes in monsoon-related dust flux, upwelling and ventilation records from within the Arabian Sea, northern Indian Ocean (Schulz et al., 1998, Sirocko et al., 1999) suggest a teleconnection between the monsoonal and North Atlantic/Greenland climate (Sirocko et al., 1999) and the

importance of common forcing agents such as atmospheric moisture and other greenhouse gases. Genty et al. (2003) compiled a record of carbon and oxygen isotope data from a stalagmite collected in southwest France, which has been precisely dated using U/Th, finding rapid climate oscillations that coincided with D/O events between 83,000 and 32,000 years ago BP.

Cruz et al. (2005) presented a high-resolution oxygen isotope record of a U/Th-dated stalagmite BT2 from subtropical southern Brazil. The oxygen isotope signal varies with shifts in the source region and amount of rainfall in the area, and therefore records changes in atmospheric circulation and convective intensity over South America. Cruz et al. (2005) concluded that the variations in rainfall source and amount were primarily driven by summer solar radiation, which is controlled by the Earth's precessional cycle. The D/O cycles can be detected in the record and therefore are assumed to affect the tropical hydrological cycle as well. However, the individual D/O events cannot be identified with certainty as millennial-scale climate changes are not as dominant in southern subtropical Brazil as they are in the Northern Hemisphere. The ages of the more prominent and more easily identifiable D/O events in the BT2 record match the absolute chronology of the Hulu Cave in China quite well.

The independently ^{230}Th-dated Hulu Cave speleothem record from China provides oxygen isotope data that resembles the Greenland $\delta^{18}O$ history through MIS3 (Wang et al., 2001) (Figure 1-3). When Greenland experienced stadial conditions

(cooling), the Asian summer monsoon and the Indian summer monsoon were weaker (Altabet et al., 2002). This suggests that the East Asian Monsoon intensity changed along with Greenland temperatures and changes in the North Atlantic climate appear to be coupled to changes in meridional transport of heat and moisture from the warmest parts of the ocean where the summer East Asian Monsoon originates. Burns et al. (2003) presented stalagmite data from Socotra Island in the Indian Ocean and observed D/O-like variation in the speleothem $\delta^{18}O$ (Figure 1-3). The Indian Ocean record suggests that the tropics may act as an amplifier of climate change, although the question of whether the warming and cooling in the North Atlantic was initiated at high or low latitudes remains an open question (Burns et al., 2003). As they are the benchmark chronologies for MIS3 studies, the ice core chronologies are usually taken to be the most accurate timescale by which all other records are evaluated. However, Burns et al. (2003) argued that instead of interpreting the differences in age between a stalagmite and the GRIP chronology in terms of a lead-lag relationship, the ice core chronologies are perhaps several thousand years too young and need to be revised over the interval of D/O events 9-13 and should be tied to the absolute chronology of the M1-2 stalagmite.

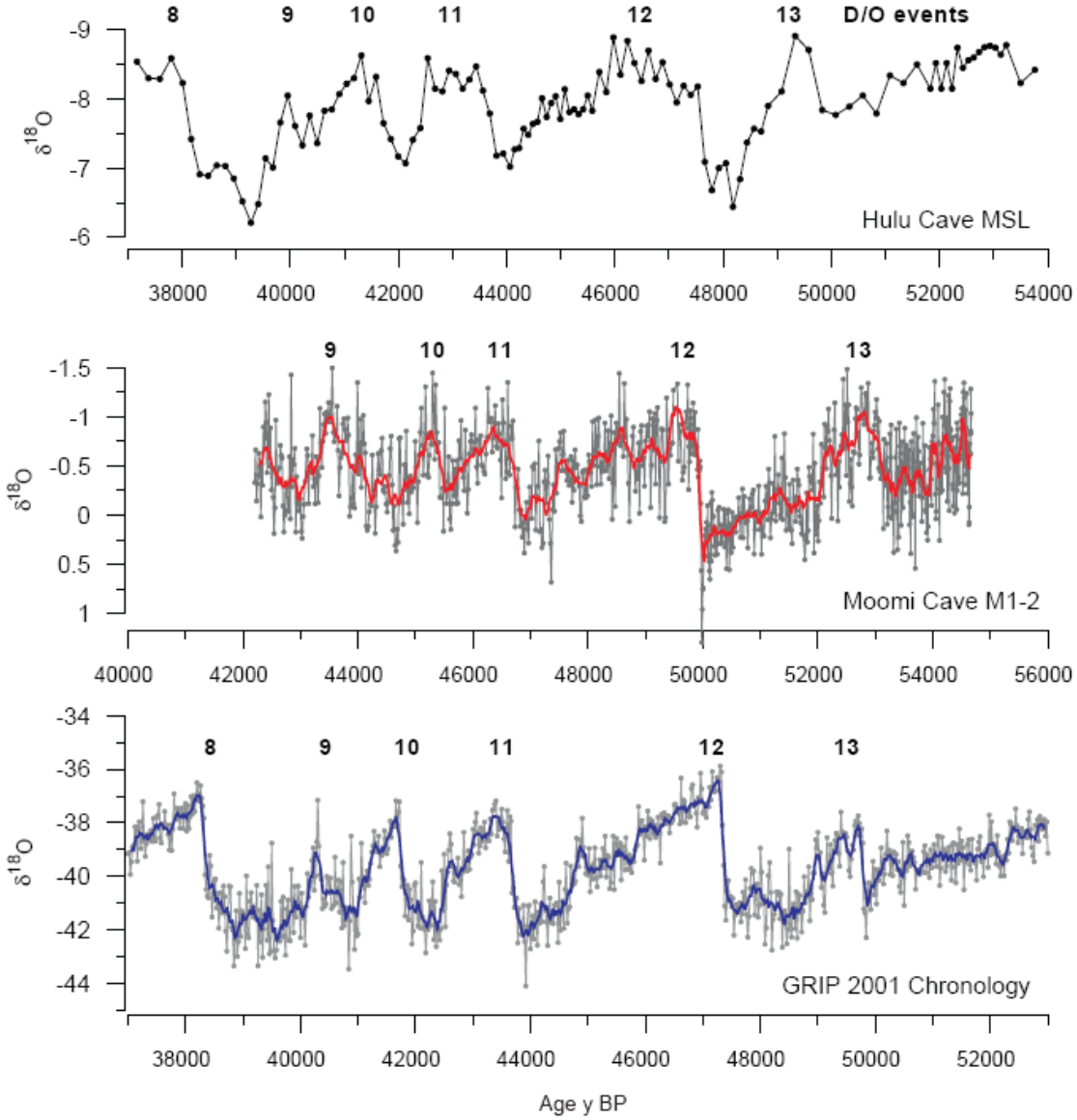

Figure 1-3: Comparison of the oxygen-isotope ratios of the Socotra Island Moomi Cave stalagmite M1-2 with oxygen isotopes from the GRIP ice core and the $\delta^{18}O$ record of a stalagmite from Hulu Cave in central China. The time scales are independent and shifted to give a best fit for D/O events. The oxygen isotopic scales for the stalagmite records are reversed. The locations of D/O events 9 through 13 as identified in each record are also shown. From Burns et al., 2003.

1-4. Mechanisms of abrupt climate change

On the basis of a simplified ocean-atmosphere model, Stocker et al. (1992) has shown that heat is drawn from the South Atlantic when North Atlantic Deep Water (NADW) switches on at the onset of a D/O event, suggesting therefore that the

corresponding events in both hemispheres are out of phase. In subsequent papers Stocker and Johnsen (2003) tried to explain the major features of interhemispheric coupling mediated by Atlantic thermohaline circulation (THC). They modified what has become known as the "bipolar seesaw" (Stocker, 1998) by coupling it to a southern heat reservoir which dampens and integrates the abrupt climate signals that are coming from the North Atlantic. In their model the Southern Ocean is assumed to act as a heat reservoir that takes time to warm or to cool, with a timescale that matches the estimated lag between the hemispheres. The mechanism makes adjustments in the warm thermocline water and sets up a southward cross-equatorial ocean current in the Atlantic transporting heat from north to south. Stocker and Johnsen (2003) suggest that this temperature signal is fully explained as an oceanic signal being made up of a thermocline as well as large-scale meridional overturning circulation (MOC) change. The thermal bipolar seesaw involves a typical heat exchange time scale, τ. The best correlation between the simulated southern signal based on the seesaw model and the reconstructed Antarctic temperature was obtained with τ=1200 years (Stocker and Johnsen, 2003). They concluded that the model demonstrates both the prominent D/O events and also the shorter events appear to have an Antarctic counterpart. Knutti et al. (2004) revised this model by using a coupled ocean-atmosphere-sea ice model which simulates processes in both the ocean and the atmosphere. The results show that in addition to a reduction of the THC, fresh water from the Northern Hemisphere ice sheets might have amplified the temperature response in the Southern Hemisphere by another, more direct mechanism. They find evidence of anomalous transport of heat

from the North to the South Atlantic Ocean in response to a large freshwater perturbation at high northern latitudes.

Various versions of the bipolar seesaw model have assumed that climate changes in the Northern Hemisphere trigger a response in the Southern Hemisphere. But since an increasing number of records suggest that Antarctic temperature changes preceded the Greenland ones by 1000-2000 years (such as Blunier et al., 1998, Brook et al., 2005 and Raisbeck et al., 2007), as per the bipolar seesaw, an alternative theory is that the trigger lies elsewhere, such as in the Southern Hemisphere (Weaver et al., 2003). Climate model work by Weaver et al. (2003) suggests melt water pulse **MWP-1a** during the last deglaciation originated from the Antarctic Ice Sheet and caused the strength of the NADW formation to increase and warm the North Atlantic region. Work by Bond et al. (1993) and Broecker (1994) pointed out that the timing of Heinrich events seems to coincide with the pattern of ice core climate oscillations and Broecker hypothesized that millennial-scale climate changes are driven by rapid freshwater input to the North Atlantic from the melting of continental ice sheets. However, there are many more D/O events than there are recorded Heinrich events or other freshwater pulses into the North Atlantic.

Ganopolski and Rahmstorf (2001) used the CLIMBER-2 coupled climate model of intermediate complexity, which is designed for long-term climate simulations. They tested the effect of a forcing, such as a fresh water pulse, in triggering a D/O event and a

threshold behavior became clear. For a fresh water forcing of 0.015Sv there is no D/O event triggered whereas for a forcing of 0.045Sv a D/O event is triggered, which then follows its own internal dynamics that produces a characteristic pattern: in Greenland an abrupt initial warming and a gradual cooling trend which is terminated by a rapid temperature drop back to stadial conditions and in Antarctica temperatures are still increasing during the stadial phase and decreasing during the warm event, but the amplitude of the response is small. The region of maximum response is centered in North Atlantic, but due to the thermal inertia of the oceans the transient response has the same sign globally and there is stronger D/O warming in the subtropical Atlantic, in better agreement with paleoclimatic data from that region. In the Southern Hemisphere the effect of D/O cycles is weak. This model suggests that the D/O events are a Greenland phenomenon, occasionally producing big enough events to be detected in the Southern Hemisphere. Therefore, even if these events are anti-phased their trigger is not in the Southern Hemisphere according to this study. Elliot et al. (2002) suggest that there is an amplifying mechanism needed to generate the widespread imprint and the amplitude of the climatic changes associated with D/O events, questioning the role of the THC as the only explanation. Furthermore, Wunsch (2006), along with Carter and Gammon (2004) contend the theory that the abrupt climate shifts are generated by changes in the North Atlantic Ocean circulation, and instead call for wind shifts as generated by ice sheet fluctuations as a more likely scenario to change the ocean circulation.

A true seesaw behavior, where the weakening of the Southern Hemisphere THC causes North Atlantic THC to strengthen has not yet been clearly shown in an atmosphere-ocean general circulation model (Seidov et al., 2005). Therefore, although the Northern Hemisphere trigger theory has gained the most attention, complete consensus has not been reached. There are also discrepancies between model simulations and the paleoclimate data, which according to de Boer et al. (2007), could result from a number of factors such as inaccuracies in the freshwater forcing estimates, inappropriate boundary conditions and uncertainties in the interpretation of the paleoclimate data. Furthermore, some models may be "predisposed" to a presumed seesaw behavior due to factors such as idealized topography overestimating the strength of Northern-Southern anti-correlation (de Boer et al., 2007). To compound the issue, recent work by Wunsch and Heimbach (2008) has shown that due to the response times and mechanisms of the oceans being far more complex than previously thought, some regions of the ocean respond to perturbations faster simply through their more efficient overturning circulation and not necessarily due to their close proximity to the perturbation itself.

Adkins et al. (2005) hypothesized of a "thermobaric" regulator of abrupt climate change events. During the last glacial the Southern Ocean deep water formation is thought to have resulted in a deep ocean filled with cold salty waters from the south. Northern source overturning was still active at the Last Glacial Maximum (LGM), but it was fresher and less dense. Uniform geothermal heating of $50 W/m^2$ at the ocean bottom

leads to a 25% increase in Antarctic Bottom Water (AABW) overturning strength and heats the Pacific by ~0.5°C (Adkins et al., 2005). Most of the geothermal heat radiates to the atmosphere in the Southern Ocean as this is the area where most of the world's abyssal isopycnals intersect at the surface. In the deep ocean temperature differences between waters masses have a larger effect than density differences. Therefore an early warming in Antarctica (~1000-3000 yrs before Greenland) could be the natural result of heating the deep isopycnals that outcrop in the Southern Ocean with leakage of some geothermal heat, but enough heat remains in the deep to charge the thermobaric capacitor.

As the Antarctic temperature changes were interpreted to lead those in Greenland by 1000-2000 years, an alternative theory is that the trigger lies in the Southern Hemisphere through changes in the strength of westerly winds and the circumpolar current and changes in Southern Ocean density structure. In their 1996 paper Charles et al. studied a Southern Ocean deep sea core RC11-83 located at 41°S, 9°E where changes in the isotopic composition of benthic and planktonic foraminifera match those of the Greenland and Antarctic ice cores respectively. From this they inferred that both hemispheric signals are represented in a single core and, as stated previously, that the $\delta^{18}O$ (planktonic, Antarctica) is found to lead the $\delta^{13}C$ (benthic, Greenland) by 1500years, which equates to a 20-40cm offset within the core. The suggested explanation to this southern hemisphere lead was tropical temperature

variability. Work by Clement et al. (1999, 2001) was among those suggesting the tropics could be the driver of millennial-scale climate changes.

As summed up by Wunsch (2006) the more widely accepted view of the ocean as the primary stimulus of the major climatic shifts has yet to be proven or disproven. The presence in other proxies of signals, even convincingly corresponding to remote manifestations of D/O events, needs to be interpreted with caution as they may be no more than measurable signals not corresponding to important local climatic shifts. Therefore even if a signal can be detected, it may not be an important one.

1-5. Planktonic and benthic records from the western tropical Pacific

The issue with all the climate records originating from outside of Greenland is whether the events in the records are actually a manifestation of the Greenland D/O signal or some more local phenomena. This is also the case for those recorded in Antarctica. Are the Northern and Southern Hemisphere ice core signals related and if so, is the Southern Ocean merely passively responding to Greenland and the Northern Hemisphere climate forcing? The question also remains of whether we are correct in drawing lead/lag relationships between climate records, or as Burns et al. (2003) suggested, this offset is just a shortcoming of the chronologies of these climate records. There is also a possibility that the current resolution of many records as well as these potential (and very probable) local forcings mask some of the climate variability. As presented by Raisbeck et al. (2007), more detail is continuously appearing in the

Antarctic records bringing to light more "counterparts" to the Greenland oscillations. Antarctica and Greenland have very different temporal characteristics. Even if the isotopic record of Antarctica mirrors that in Greenland, if they are too weak/short they may not be distinguished from the regional short-term climate signals that also influence the isotopic records. If these climate signals appear of a lesser magnitude in the southern hemisphere records compared to the northern ones, does this mean they must originate and be triggered in the northern hemisphere? The approach seems to have been on finding the single forcing, whether it is the northern or southern high latitudes or the tropics, to explain all the global records of abrupt climate change. However among all the differing conclusions, the evidence so far does not exclude the possibility that abrupt climate change events (D/O events in the north and Antarctic Isotope Maximum, AIM events, in the south) are each in fact the result of localized forcing in the Northern and Southern high latitudes.

This study presents a new dataset from the western tropical Pacific and addresses the question of the extent and probable source of abrupt climate change events during MIS3. The unique position of this marine core in the western equatorial Pacific Ocean provides both a northern and southern hemispheric climate record on the same chronology. This therefore removes the complications which face studies attempting to align northern and southern hemisphere climate records as they are usually by definition geographically far apart. High resolution oxygen isotope records for benthic and planktonic foraminifera, as well as a Mg/Ca paleotemperature record for

planktonic foraminifera are presented. Stott et al. (2002) presented a late Pleistocene history of seawater surface temperature and salinity variability from the western tropical Pacific warm pool that appeared to vary in accord with these millennial-scale stadial-interstadial cycles (Dansgaard/Oeschger cycles) over Greenland. Positive excursions in $\delta^{18}O_{SW}$ derived from a deconvolution of temperature and sea water $\delta^{18}O$ contributions in the planktonic records showed that tropical salinities in the Pacific warm pool increased during high latitude stadials whereas during interstadials surface salinities decreased (Stott et al., 20002). The SST and salinity variability in the western tropical Pacific during MIS3 was interpreted to reflect shifting atmospheric moisture akin to the modern ENSO (Stott et al., 2002). Yet, despite a growing number high resolution paleoclimate records of millennial climate variability within the northern hemisphere, there still remains relatively few high resolution marine or terrestrial records from the southern hemisphere. Consequently, it is not clear if the entire southern hemisphere participated in the anti-phased climate swings that are reflected in ice core reconstructions. In particular, it is not known how deep water temperatures within the Pacific were affected by these high latitude temperature variations.

In a recent study of deep water temperature change during the last deglaciation Stott et al. (2007) found that deep waters within the Pacific began to warm ~1000 years earlier than tropical surface waters. This lead-lag relationship was interpreted to reflect an earlier warming in the Southern Ocean at the location where Pacific Deep Water acquires its temperature. This deep water lead was interpreted to reflect a Southern

Ocean response to increased spring season insolation that influenced sea ice (Timmermann et al., in press). The present study expands on these findings and attempts to evaluate the timing of deep sea and tropical surface water temperature changes during the last glacial period and determine whether the anti-phased relationship between Southern Hemisphere (Deep Pacific) and Northern Hemisphere (tropical surface water) is evident.

Chapter 2: Regional setting and oceanography

2-1. Marine sediment core location

Marine core MD98-2181, from here on referred to as 'MD81', was collected aboard the *Marion Dufrense* in 1998 as part of the IMAGES coring program. At 6.3°N, 125.83°E MD81 is located in the Morotai Basin in the western tropical Pacific at a water depth of 2114m (Figure 2-1).

2-2. Western Pacific warm pool and equatorial circulation

The western Pacific warm pool (WPWP) is an important center of atmospheric convection with surface temperatures within the warm pool today in excess of 28°C that give rise to the strong atmospheric convection over the region that drives large scale atmospheric circulation between the tropics and subtropics. Westward currents and the trade winds funnel seawater warmed by long exposure to tropical sunlight into the WPWP region. As the western Pacific is very warm and sea surface temperatures on the eastern end of the Pacific are relatively cool (~20^{o}C) for such low latitudes, a large sea surface temperature (SST) gradient exists along the equatorial Pacific (Figures 2-3a to c). The SST gradient reflects how the ocean sequesters heat and this heat is then dispersed both by the atmosphere and through the oceans. (Pichat et al., 2004).

During the northern summer SSTs in the western Pacific warm pool average 29° to 30°C and the sea surface salinities (SSS) range between 33.8-34.0psu. In winter, SSTs cool to 26-27°C. Precipitation is highest in summer, with roughly 80% of annual

rainfall occurring between June and October. Rainfall averages between 300 and 400 mm/month during summer and between 50 and 100 mm/month during winter. This precipitation pattern causes a seasonal variation in the sea surface salinities of about 1.5‰. The annual precipitation pattern is tied to the migration of the Intertropical Convergence Zone (ITCZ) over the site and the timing of the northern monsoon. During El Niño and La Niña, the western tropical Pacific experiences dramatic differences in precipitation. Because of its great topographic relief and active tectonics, this region contributes large amounts of water, solutes, and sediment to the coastal ocean (Nittrouer et al., 1995).

The three major ocean currents in the region are the North Equatorial Current (NEC), the North Equatorial Counter Current (NECC), and the South Equatorial Current (SEC) (Figure 2-1). The SEC flows along the northern coast of New Guinea and turns to the north to join the NECC. When the west-bound NEC reaches the western end of the Pacific, the NEC divides into two branches around the Philippines. One branch turns to the south and feeds the east-bound NECC, while the northern extension of the northward-turning NEC forms the Kuroshio Current.

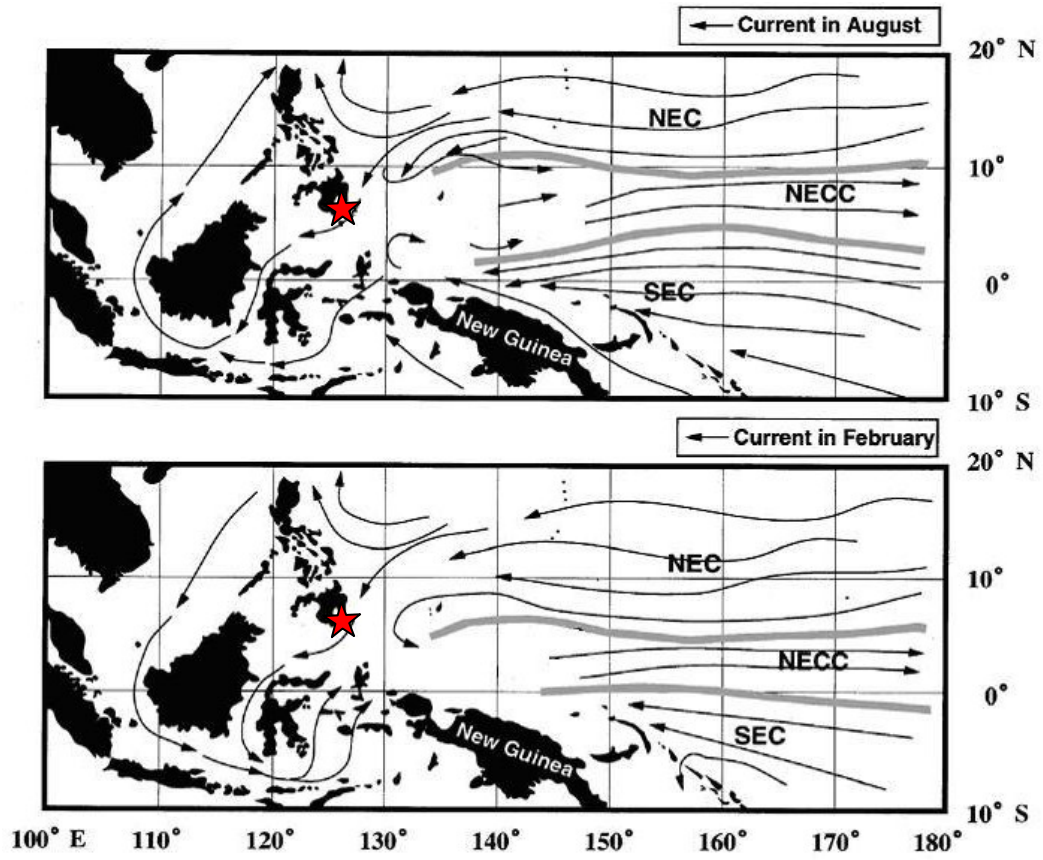

Figure 2-1: Western Equatorial Pacific surface circulation. NEC: North Equatorial Current, NECC: North Equatorial Counter Current, SEC: South Equatorial Current. Top panel shows currents in August and bottom panel in February. Location of MD81 is denoted by red star. Modified from Kawahata et al. (2002).

2-3. Monsoon

A monsoon-type climate strongly affects the western equatorial Pacific warm pool. During the northwest monsoon period (December–February), surface ocean currents passing from the South China Sea through the Indonesian Maritime Continent partly join the NECC, whereas during the southeast monsoon period (June–August) a part of the SEC flows into the South China Sea (Figure 2-1). The Monsoons are important because they transport heat and moisture from the warmest part of the tropical ocean (WTP) across the equator and to higher latitudes. Mindanao and MD81

are located in the northern part of the Asian-Australian monsoon region where increased precipitation during the summer months is the result of the increased influence of the ITCZ as part of the East Asian Monsoon (EAM). The East Asian monsoon results from the difference in potential heating between the Warm Pool and the Asian continent. During the boreal winter, the main heating source is located in the ocean and during the summer the continent is the location of the low pressure center. The latent heat release associated with intense convective precipitation fuels meridional circulation. Tropical convection in the western equatorial Pacific is connected to the descending branch over the Siberian region, forming a strong local Hadley cell in the East Asian region (Zhang et al., 1997).

Today, the summer monsoon humidity dynamics are strongly modulated by ENSO where the strength of the summer monsoon is reduced and rains are extremely weak during El Nino. Wang et al. (2001) established a teleconnection pattern between warm (cold) events in the eastern Pacific and the weak (strong) EAWM. Long-term variations of the WPWP SST related to the ENSO-like cycles may have had a strong influence on the East Asian monsoon. The dynamics of the winter monsoon for the last 380 ka have been linked with the glacial-interglacial cycles, implying a teleconnection between low and high latitudes (Beaufort et al., 2003). The strengthening and weakening of the Siberian high level pressure cell in the cold northern continent during the glacial, contrasting with the relatively warm tropical Indo-Pacific Ocean and thereby enforcing the winter monsoon, has been suggested to explain such a relationship between the North Atlantic and EAWM, a relationship that has also been found in

Chinese loess records (Porter, 2001; Porter and Zhisheng, 1995) and in marine records from the South China Sea (Wang et al., 1999).

2-4. Deep Pacific circulation and the Southern Ocean

The main water masses present in the Pacific Ocean basin are the northward flowing Antarctic Intermediate Water (AAIW) and Antarctic Bottom Water (AABW) and the southward flowing Upper and Lower Circumpolar Deep Water (UCDW and LCDW) or Pacific Deep Water (PDW) (Figure 2-2b). North Atlantic Deep Water (NADW) is warmer than the cold bottom water formed around Antarctica. NADW therefore carries heat to the Southern Ocean. It mixes with recirculated deep water from the Indian and Pacific Oceans, forming a relatively warm deep water mass, the Circumpolar Deep Water (CDW), characterized by a temperature maximum of ~+2°C around 600m depth and overlying the cold AABW. Today the main export pathway of CDW and modified AABW from the Antarctic Circumpolar Current (ACC) to the Pacific is the 550 km-wide Deep Western Boundary Current (DWBC) (van de Flierdt et al., 2004). The DWBC passes along the Tonga-Kermadec trench, up the western Pacific island arc, turning clockwise north of the equator and filling the entire deep North Pacific. During this northward course the water mass becomes warmer, fresher, depleted in oxygen and enriched in nutrients. Eventually, balancing this net northward flow, this modified water mass returns southward at mid-depth as UCDW identified by an oxygen minimum at 2-3km depth and LCDW which is marked by a faint salinity maximum (Figures 2-2a to c).

Located in the western tropical Pacific site MD81 is bathed in the southward returning UCDW or Pacific Deep Water. The present-day depths of intermediate and deep water propagation from the Southern Ocean to the western tropical Pacific are shown in Figures 2-2b and 2-3b. The neutral density surface σ_θ=27.9 kg/m^3 (relative to the 0m reference level) outcrops in the Southern Ocean near the Polar Front and attains a depth of about 2000m near the MD81 core location. The UCDW flows between σ_θ=27.4-28.0 (Rintoul et al., 2001). Therefore the benthic foraminifera at MD81 record southern source waters, and in combination with the Northern Hemisphere record from the planktonic foraminifera, provide both hemispheric climate signals in a single location.

The modern-day tracer properties at the MD81 site were analyzed in an ocean age model. According to the model results the site is bathed in Pacific Deep Water and it is estimated that 65% originates from AABW, 25% from AAIW, and 10% from NADW (errors in the estimates are ±20%) (G. Gebbie, 2008, personal communication).

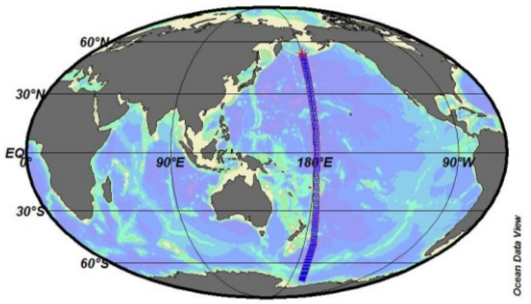

Figure 2-2a: Location of north-south hydrographic transect

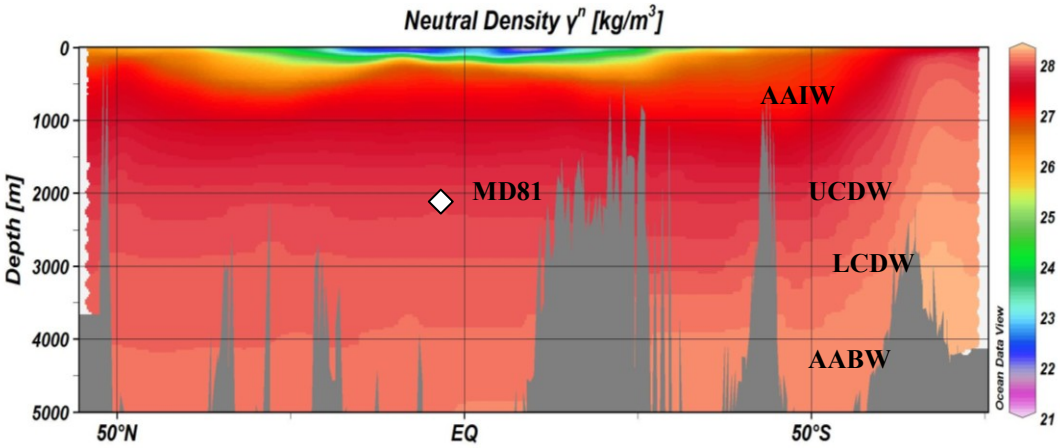

Figure 2-2b: Neutral density surfaces across the north-south transect. White diamond denotes location of MD81. Water masses Antarctic Intermediate Water (AAIW), Upper Circumpolar Deep Water (UCDW), Lower Circumpolar Deep Water (LCDW) and Antarctic Bottom Water (AABW) are shown at their appropriate depths.

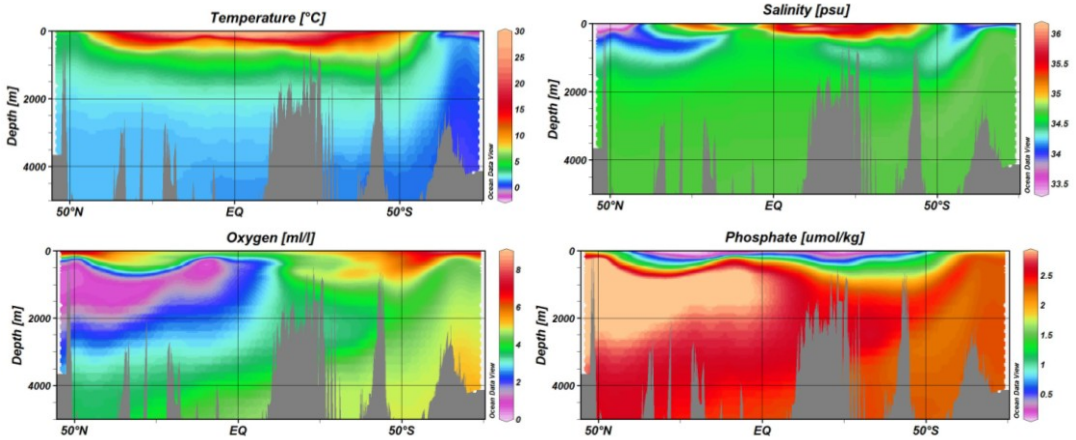

Figure 2-2c: Temperature, salinity, oxygen and phosphate structure across the north-south transect.

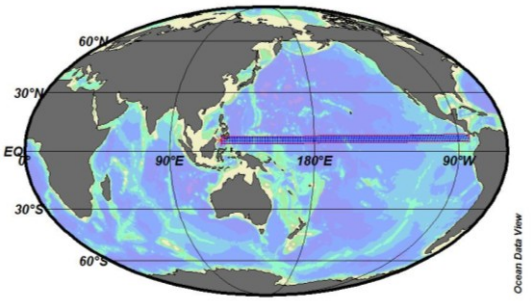

Figure 2-3a: Location of east-west transect from the western to the eastern tropical Pacific

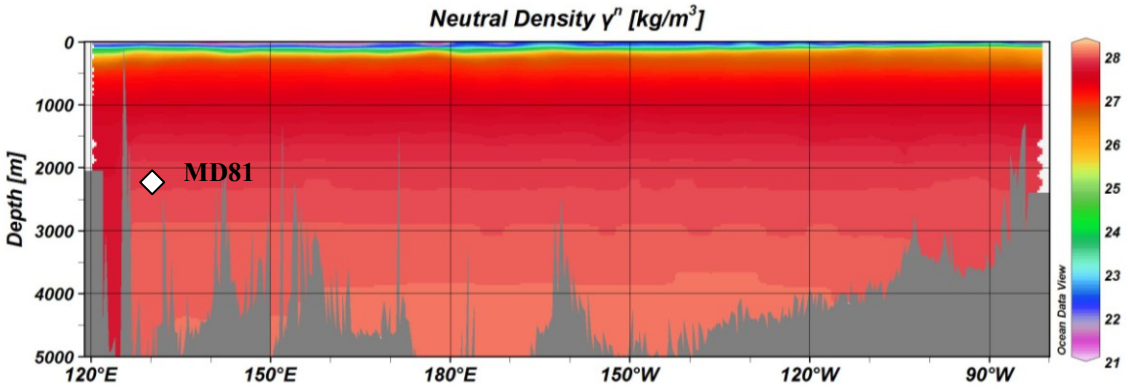

Figure 2-3b: Neutral density surfaces across the east-west transect. White diamond denotes location of MD81.

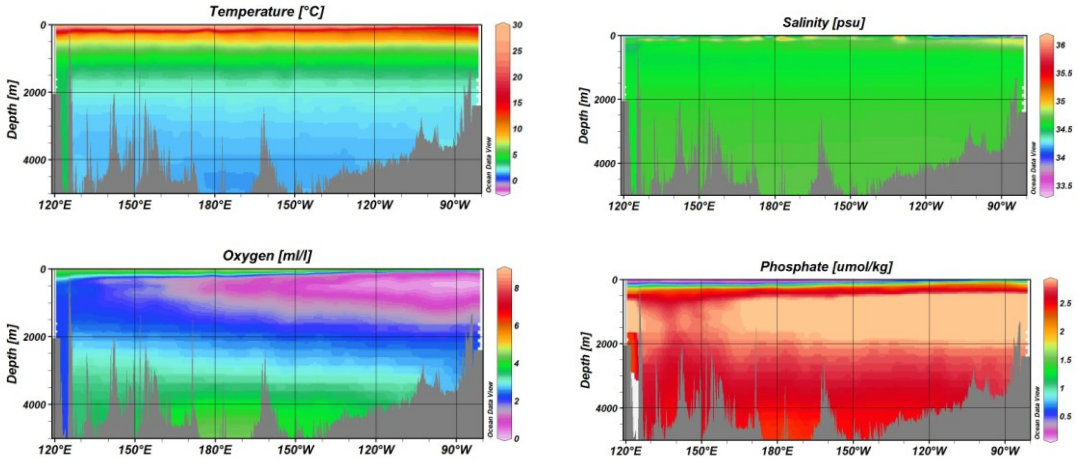

Figure 2-3c: Temperature, salinity, oxygen and phosphate structure across the east-west transect.

Chapter 3: Materials and methods

3-1. Foraminifera: *Globigerinoides ruber*, *Uvigerina hispida* and *Cibicidoides wuellerstorfi*

Globigerinoides ruber (white) is a surface dwelling planktonic foraminifera which is abundant in the warm summer surface waters of the Western Tropical Pacific that can reach up to 30°C (Kawahata, 2005). *G. ruber* exploits dinoflagellate or prymnesiophyte endosymbionts, which substantially supply nutrients to their hosts. *G. ruber* has two morphotypes which can be differentiated based on taxonomic criteria at species and/or subspecies level. *G. ruber sensu stricto* (s.s.) refers to specimens with spherical chambers sitting symmetrically over previous sutures with a wide high-arched aperture over the suture; *G. ruber sensu lato* (s.l.) refers to more compact tests with compressed chambers sitting asymmetrically over the previous sutures, with a round or medium-arched and relatively small aperture over the suture (Wang, 2000). Stable isotope differences between *G. ruber* s.l. and *G. ruber* s.s. are 0.21±0.21‰ and −0.28±0.29‰ for $\delta^{18}O$ and $\delta^{13}C$ respectively. This suggests a different depth habitat for these two morphotypes, with *G. ruber* s.s. living in the upper 30 m of the water column and *G. ruber* s.l. living at depths of 30-50 m (Kawahata, 2005, Wang, 2000). The estimated species-specific calcification depth for *G. ruber* is in good agreement with the depth range for living species by plankton tow and trap specimens from the South China Sea (Huang et al., 2008).

No differentiation was made between the two morphotypes in this study and as a result the planktonic signal is a record of the changes in the upper 50 m of the water column. MD81 resolution is approximately 25 years (2cm sample interval thickness with an average sedimentation rate of 80cm/1kyr), resulting in a homogenized sample of this time period, which therefore smoothes out any seasonal differences between the two morphotypes.

Uvigerina hispida is an open ocean, intermediate to deep water species which is rarely found in marginal basin sediments and has a shallow infaunal habitat (Boersma, 1984). *U. hispida* is common in areas of high surface productivity and very little detrital sedimentary input. It can tolerate a very broad temperature range occurring from 1000m at low latitudes to near 4000m in Antarctic seas. *U. hispida* has been found to peak in abundance between 1000-2000m depth during episodes of high sediment accumulation rates and upwelling which suggest high surface productivity over the area. (Boersma, 1984)

Cibicidoides or *Planulina wuellerstorfi* is an epifaunal species that prefers an epibenthic microhabitat (Lutze and Thiel, 1989), attached to rocks, spicules, etc., above the seafloor. This species typically has $\delta^{13}C$ values close to the $\delta^{13}C$ of bottom water dissolved inorganic carbon (McCorkle and Keigwin, 1994), although negative offsets have been reported in highly productive regions (Mackensen et al., 1993). These studies demonstrated that epifaunal taxa are closest to equilibrium of the overlying bottom water and therefore are the most reliable for reconstructing $\delta^{13}C$ conditions in the deep ocean.

3-2. Systematics of $\delta^{18}O$ and Mg/Ca in planktonic foraminifera

3-2-1 Planktonic oxygen isotope ratio, $\delta^{18}O$

The use of an oxygen isotope ratio for paleoclimatology is based on the fractionation of ^{16}O ("lighter" isotope) and ^{18}O ("heavier" isotope) that is observed in carbonate that precipitate in isotopic equilibrium. This fractionation is temperature dependent. To measure the ratio of ^{16}O to ^{18}O from a carbonate sample, the CO_2 gas evolved from the dissolution of the carbonate in acid is introduced to a stable isotope ratio mass spectrometer, which measures the relative beam sizes (number of ions/unit time) of mass 44 ($^{12}C^{16}O_2$), mass 45 ($^{13}C^{16}O_2$ or $^{12}C^{17}O^{16}O$) and mass 46 ($^{12}C^{16}O^{18}O$) (Clark and Fritz, 1997). As the $\delta^{18}O$ (or δR) is measured from the 46/44 mass ratio peak,

$$\delta^{18}O = [(^{18/16}O_{sample}/^{18/16}O_{standard})-1] * 1000‰ \text{ standard}$$

a correction (Clark and Fritz, 1997) is applied for the contribution ^{17}O in $^{12}C^{17}O^{17}O$ and $^{13}C^{17}O^{16}O$.

$$\delta^{18}O = 1.0010\ \delta^{46}R - 0.0021\ \delta^{45}R \text{ ‰ VPDB.}$$

The results from carbonates are typically reported with respect to an internationally agreed upon standard, the Vienna Pee Dee Belemnite, a calcium carbonate.

There is an uncertainty associated with the use of oxygen isotopes to derive paleotemperatures from carbonate archives due to the fact that the $\delta^{18}O$ of carbonate reflects both the temperature-dependent fractionation of ^{16}O and ^{18}O and also the $\delta^{18}O$ of the seawater from which the carbonate was precipitated. Both of these variables determine the isotopic ratio of the carbonate. The $\delta^{18}O$ of seawater in turn reflects the mean $\delta^{18}O$ of seawater that is influenced by the amount of continental ice, and the evaporation-precipitation balance for a particular part of the ocean.

Furthermore, the direct application of isotope thermometry using stable oxygen isotope ratios can be complicated by the biological influences on the $\delta^{18}O$. A number of studies have documented the non-equilibrium fractionation of oxygen isotopes by marine organisms that produce a carbonate shell or test. Bemis et al. (1998) demonstrated distinct deviations with respect to isotopic equilibrium among foraminifera. These deviations are presumably influenced by life processes including calcification rate (Ortiz et al., 1996), photosynthesis (Spero and Lea, 1993), and respiration (Wolf-Gladrow et al., 1999), the so-called vital effects, and the carbonate ion concentration or pH of calcification (Zeebe, 1999). However, a number of species of foraminifera do secrete calcite in isotopic equilibrium or appear to secrete calcite with a persistent isotopic offset with respect to the expected equilibrium value. This includes the species used in the present study.

3-2-2 Mg/Ca-paleothermometry

The basis for magnesium/calcium paleothermometry is that the substitution of magnesium in the calcite lattice is endothermic and is therefore favored at higher temperatures (Barker et al., 2005). Studies based on laboratory and field work have demonstrated that uptake of Mg by planktonic foraminifers from ambient seawater is positively correlated with water temperature (~9 ±1%, per °C) (Rosenthal et al., 1997, Lea et al., 1999, Rosenthal and Lohmann, 2002, Martin et al., 2002, Anand et al., 2003). Planktonic species have been calibrated based both on culture experiments (Lea et al., 1999) and core top specimens (Rosenthal et al., 2000; Dekens et al., 2002) and their Mg/Ca fit to equations that take the form:

$$\text{Mg/Ca (mmol mol}^{-1}) = be^{mT}$$

where b is the pre-exponential constant, m the exponential constant and T the temperature in °C (Lea et al., 1999). The exponential constant determines the magnitude of the temperature change calculated from down-core variations in Mg/Ca and the pre-exponential constant determines the absolute temperature. A six-year sediment trap time series from the Sargasso Sea shows that there is both interannual and seasonal variability in the Mg/Ca values of *G. ruber* (Anand et al., 2003). Values varied at this site between 2.99±0.14 and 4.74±0.26 mmol/mol. However, due to time-averaging over 100 years at this location, these signals are averaged. Core-top calibration studies that have used a sample of marine sediment are in general agreement with culturing results.

The Anand et al. (2003) Mg/Ca equation is specific to the planktonic foraminifera including *G. ruber* (white) and has an estimated accuracy of ±1.2°C. This equation will be used to calculated sea surface paleotemperatures in the present study:

$$Mg/Ca = 0.38 \pm 0.02 \exp (0.090 \pm 0.003 \times SST)$$

Besides temperature effects, foraminiferal Mg/Ca can be altered by post-depositional dissolution (Rosenthal and Lohmann, 2002) and physiological processes (Rosenthal et al., 1997). Salinity, pH and addition of gametogenic calcite at subsurface depths can also change the magnesium in the shells and therefore species-specific calibrations are necessary (Anand et al., 2003). Post-depositional dissolution could significantly alter foraminiferal Mg/Ca through preferential removal of Mg-enriched calcites (Brown and Elderfield, 1996). A study by Bemis et al. (1998) that compared the foraminiferal Mg/Ca and $\delta^{18}O$ calcification temperatures showed that higher Mg/Ca is not always related to shallow depth, indicating that in addition to seawater temperature and partial dissolution, other environmental variables, including lateral transport could also significantly modify the primary foraminiferal Mg/Ca ratio. The three dominant planktonic species used in paleothermometry are *Neogloboquadrina dutertrei*, *Globigerinoides sacculifer* and *G. ruber*. Huang et al. (2008) studied the dissolution sensitivity of these species in the South China Sea. The most sensitive species to dissolution are the deeper dwelling species, including *N. dutertrei* (up to 12% per km) and the two surface-dwelling species of *G. ruber* and *G. sacculifer* were found to be relatively resistant (~4–5%/km). This is consistent with results from previous core top

studies in Atlantic and Pacific. Non-equilibrium processes (or kinetic effects) and salinity were not found to have a major influence on shell Mg/Ca, but could not be completely excluded (Huang et al., 2008).

3-2-3 Stable oxygen isotope composition of surface water, $\delta^{18}O_W$

In the western tropical Pacific, sea surface salinity (SSS) and the stable oxygen isotope composition of surface water ($\delta^{18}O_W$ or δ_W) are correlated, reflecting the balance between the freshwater flux (evaporation - precipitation) and salt flux by means of ocean transport. $\delta^{18}O_W$ is incorporated into $CaCO_3$ shells of planktonic foraminifers that inhabit the surface ocean. To estimate how $\delta^{18}O_W$ and salinity varied during the last glacial, the difference in the $\delta^{18}O$ and Mg/Ca of the calcium carbonate produced by the surface-dwelling *G. ruber* estimates are transformed to an isotopic difference between modern and glacial seawater $\delta^{18}O_W$ by dividing the difference between the $\delta^{18}O$-derived and the Mg/Ca-derived paleotemperature by the temperature-dependent fractionation of 0.21‰/°C (Shackleton, 1974, Bemis et al., 1998, Lear et al., 2000, Anand et al., 2003), reflecting the change in surface water isotopic composition relative to the modern value.

$$\delta^{18}O_W = \delta^{18}O + ((SST-16.5)/4.8)$$ (Bemis et al., 1998)

A positive excursion in $\delta^{18}O_W$ is interpreted to reflect higher (higher surface water $\delta^{18}O$) and a negative lower (lower surface water $\delta^{18}O$) surface salinities at MD81.

3-2-4 Salinity

Ferguson et al. (2008) calibrated the Mg/Ca of *G. ruber* (white) against temperature in a number of regions, each with a slightly different salinity. A general trend to greater Mg/Ca ratios with increasing salinity was observed, implying that part of the scatter observed in the results can be accounted for by differing salinity. A response of foraminiferal Mg/Ca to salinity has significant implications for the application of Mg/Ca as a paleothermometer and for deriving estimates of $\delta^{18}O$ of sea water from $\delta^{18}Oc$. During the Last Glacial Maximum (~20,000 yrsBP) the oceans had an average salinity of 1psu higher than today (Adkins and Schrag, 2001) due to the large amounts of freshwater sequestered in land ice. This increase in salinity would result in higher foraminiferal Mg/Ca ratios and lead to overestimates of LGM temperatures, at least in areas where salinities are higher than 36.5 psu, such as the subtropical gyres in the Atlantic, parts of the Caribbean, the Red Sea, parts of the Persian Gulf and Arabian Sea. Therefore the salinity of the environment in question appears to be a strong factor in the significance of the salinity impact on Mg/Ca. However, studies (Lea et al., 1999; Rosenthal et al., 2000) suggest that such environmental factors as salinity are generally overwhelmed by the effects of temperature, particularly over the range of salinity and pH that may be reasonably expected in the marine environment. Modern salinities at MD81 are 33.8-34.0 psu and the glacial increase in salinity is estimated to be less than 2 psu, with site MD81 therefore remaining below 36 psu. As a result, for this study the control of salinity on Mg/Ca ratios is considered to be minimal and temperature is assumed to be the dominant control on Mg/Ca variability in *G. ruber*.

Based on observed coral data from the tropics, the oxygen isotope ratio within carbonate shells has been found to vary in a linear relationship with salinity (Figure 3-1, Fairbanks et al., 1997; Morimoto et al., 2002). However, the slope of the $\delta^{18}O_{SW}$ - SSS relationship is dependent on E-P conditions and cannot be assumed constant throughout the tropics. Therefore some difference in the SSS vs. $\delta^{18}O_{SW}$ slopes between different sites may exist. However, at any one site, $\delta^{18}O_{SW}$ and SSS have a strongly linear relationship that is independent of $\delta^{18}O_{precipitation}$ and evaporation changes (Morimoto et al., 2002, Fairbanks et al., 1997). According to the modern δ^{18}Osw-salinity relationship in the tropical Pacific a decrease in $\delta^{18}O_{SW}$ of ~0.5‰ signifies a decrease in sea surface salinity of ~1-1.5psu (Morimoto et al., 2002; Fairbanks et al., 1997).

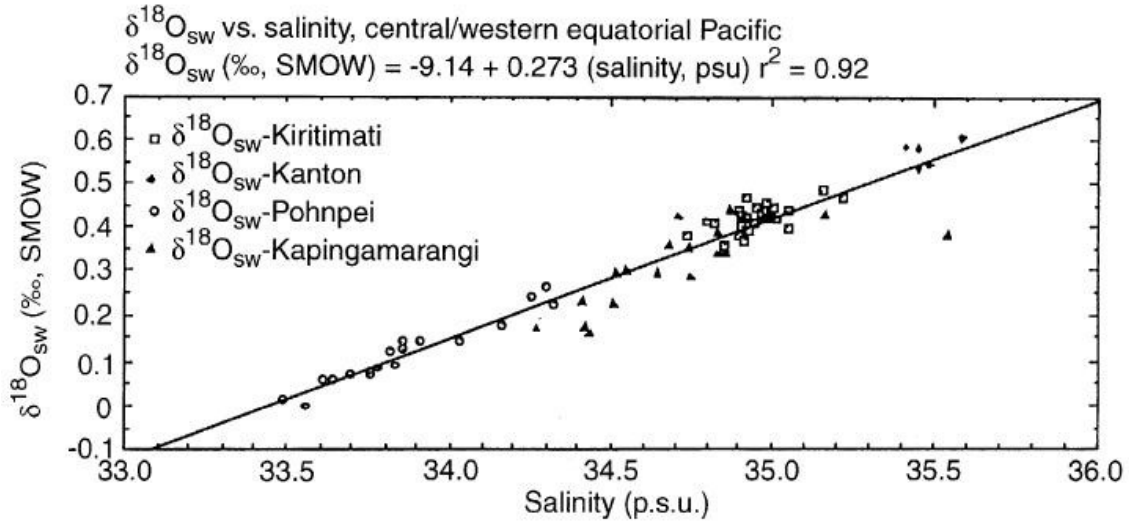

Figure 3-1: δ^{18}Osw vs. sea surface salinity for the central and western Pacific. From Fairbanks et al., 1997.

3-3. Systematics of $\delta^{13}C$ and $\delta^{18}O$ in benthic foraminifera

Studies of stable oxygen and carbon isotopes of live benthic foraminifera demonstrate that the $\delta^{13}C$ and $\delta^{18}O$ of deep-sea foraminifera are constrained by several

biological parameters (e.g., microhabitat, growth) and by the physicochemical properties of bottom and pore water (e.g., temperature, oxygenation, organic matter deposits, methane) (Fontanier et al., 2008). On the one hand, it is commonly accepted that infaunal benthic foraminifera calcify in the pore water from the sediment interval in which they preferentially live and, therefore, record the ambient pore water $\delta^{13}C$, following a so-called microhabitat effect (McCorkle et al., 1997; Corliss et al., 2002, Rathburn et al., 2003, Schmiedl et al., 2004).

The ambient pore-water $\delta^{13}C$ is largely influenced by the introduction of isotopically light carbon due to the aerobic and/or anaerobic degradation of organic matter in the sediment. Therefore, the carbon isotopic composition of foraminiferal tests would ultimately be controlled by the organic carbon flux at the sediment water interface and the oxygenation in the benthic environment (McCorkle et al., 1997, Eberwein and Mackensen, 2006). The $\delta^{13}C$ of foraminiferal taxa is strongly constrained by their microhabitat preferences. The deeper in the sediment the microhabitat is the lower the $\delta^{13}C$ values are. The isotopic gradient results from the progressive degradation of organic matter buried in deeper sediments and the related release of isotopically light carbon. Such observations are in agreement with numerous studies that showed that foraminifera might record the pore water $\delta^{13}C_{DIC}$ of the sediment interval where they preferentially live (Rathburn et al., 2003, Schmiedl et al., 2004, Fontanier et al., 2006). Only *Cibicidoides wuellerstorfi*, a very shallow and epifaunal species, seems to record the $\delta^{13}C_{DIC}$ of bottom water (McCorkle and Keigwin, 1994; McCorkle et al., 1997; Eberwein and Mackensen, 2006, Fontanier 2006).

Since the work of Shackleton and Opdyke (1973) and Shackleton (1974), *Uvigerina* has been considered the species that is most consistently found to secrete calcite in oxygen isotopic equilibrium with bottom waters. Core-top studies utilizing live-stained foraminifera consistently find *U. peregrina* and *Uvigerina* spp. $\delta^{18}O$ values very close to, if slightly lower than equilibrium calcite values (McCorkle et al., 1997, Rathburn et al., 2003, Fontanier et al., 2006). As demonstrated by Rathburn et al. (2003), McCorkle et al. (1997) and Fontanier et al. (2006), the $\delta^{18}O$ of taxa is not controlled by microhabitat preferences. *Cibicidoides* $\delta^{18}O$ are adjusted by +0.64% to account for an observed systematic species offset relative to *Uvigerina* (Shackleton and Opdyke, 1973).

3-4. Sample preservation at MD81

The main diagenetic concern with foraminifera is partial shell dissolution. Diagenetic dissolution would be expected to reduce the Mg/Ca of foraminiferal calcite as well as the average foram shell weight, and would be expected to have a greater effect on planktonic species, both because benthics are more resistant to dissolution and because the planktonic life cycle results in an uneven distribution of Mg in planktonic tests, with Mg-rich calcite being more prone to dissolution (Brown and Elderfield, 1996). Fragments also dissolve faster if the foraminifera are broken up.

During the picking of foraminifera from core MD81 the foraminifera did not fragment on contact. Also, the cleaning procedure caused only minimal fragmentation.

Careful visual examination using microscopy indicates the site contains well preserved biogenic carbonate. MD81 at a depth of 2114m is above the lysocline and has a high sediment accumulation rate; therefore dissolution effects are considered to be minimal.

3-5. Sample preparation and analysis

All MD81 planktonic and benthic data presented in the Results and Discussion sections was newly generated for this study. Marine sediment samples were disaggregated using Sodium Hexameta Phosphate in solution. Once disaggregated, the sediments were wet-sieved through a 63μm mesh to remove the clay fraction. The >63 μm fraction is then dry-sieved at >180μm size fraction and picked for foraminifera. The foraminifera were cleaned according to the following protocol designed to remove clays and other impurities. The foraminiferal shells were cracked between two glass plates under the microscope to open the tests. The tests were then rinsed with DIW, Methanol, hot alkaline oxidative cleaning using buffered hydrogen peroxide and a leach with 0.001 M nitric acid. During each of the rinses the vials were sonified to dislodge debris from the shells.

The cleaned *G. ruber* samples were split for isotope and Mg/Ca measurements. This ensured that isotopic and minor element measurements were made on the same samples of cleaned calcite, and eliminated potential discrepancies due to the effects of different cleaning methods on measured Mg/Ca and $\delta^{18}O$. For Mg/Ca the sample is dissolved in 500 μL of 1M nitric acid and analyzed on a Jobin Yvon ICP AES. Each sample measurement was bracketed with a standard that is made gravimetrically from solid Mg and reagent grade $CaCO_3$ in an elemental ratio of 5.62 mmol/mol and the

observed sample value is adjusted by the standard deviation of the two bracketing standards to correct for within and between run instrument drift.

Where $x = (Mg/Ca)_{meas.}$, $y = (Mg/Ca)_{sample}$, for bracketing standards x_1 and x_2; $x_{std} = (x_1+x_2)/2$, $y_i = (x_i/x_{std})(5.62)$. The average sample-standard deviation was 0.05mmol/mol.

For stable isotopic measurements the samples were analyzed on a VG Prism II stable isotope ratio mass spectrometer equipped with a common acid bath acidification system. Approximately 30 foraminiferal samples are run sequentially on the mass spectrometer along with approximately 10 Ultissima marble standards that are used to monitor the analytical precision. The precision of the Ultissima standard $\delta^{18}O$ is 0.06‰ for the present study with a 1σ of 0.068‰ over 17 runs.

3-5-1 Cleaning test for Mg/Ca

Ratios of Fe/Ca, Mn/Ca and Al/Ca serve as indicators of potential contamination of Mg/Ca measurements by Mg-bearing clays and/or authigenic encrustations. The amount and composition of terrigenous input and the presence of authigenic phases (such as Mn-Fe-oxides, pyrite, and secondary minerals such as ferric oxyhydroxides) affect the Mg/Ca paleothermometry. Two cleaning tests were therefore performed on *G. ruber* to check if the MD81 results were being affected by Fe or Mn contamination.

Test 1.

Six samples of *G. ruber* were picked from a single sample depth of 2140cm. The samples were cleaned in three different ways, as shown in Table 3-1 below; samples 1 and 2 were only rinsed with DIW three times, samples 3 and 4 were cleaned according to the standard procedure outlined above, but without any repeat rinses, and samples 5 and 6 were cleaned according to the complete standard procedure. All six samples were then analyzed for Mg/Ca. The results are plotted in Figure 3-2.

Sample number	Procedure	Corrected Mg/Ca (mmol/mol)	Mn (ppb)	Fe (ppb)
1	Sample rinsed 3xDIW	4.8	204	184
2	Sample rinsed 3xDIW	5.1	175	632
3	Normal procedure without repeat rinses	4.6	143	98
4	Normal procedure without repeat rinses	4.5	205	148
5	Normal cleaning procedure	4.6	183	132
6	Normal cleaning procedure	4.4	161	115
	Mean of 3-6	4.5	173	123

Table 3-1: Procedures and results for *G. ruber* Cleaning Test 1.

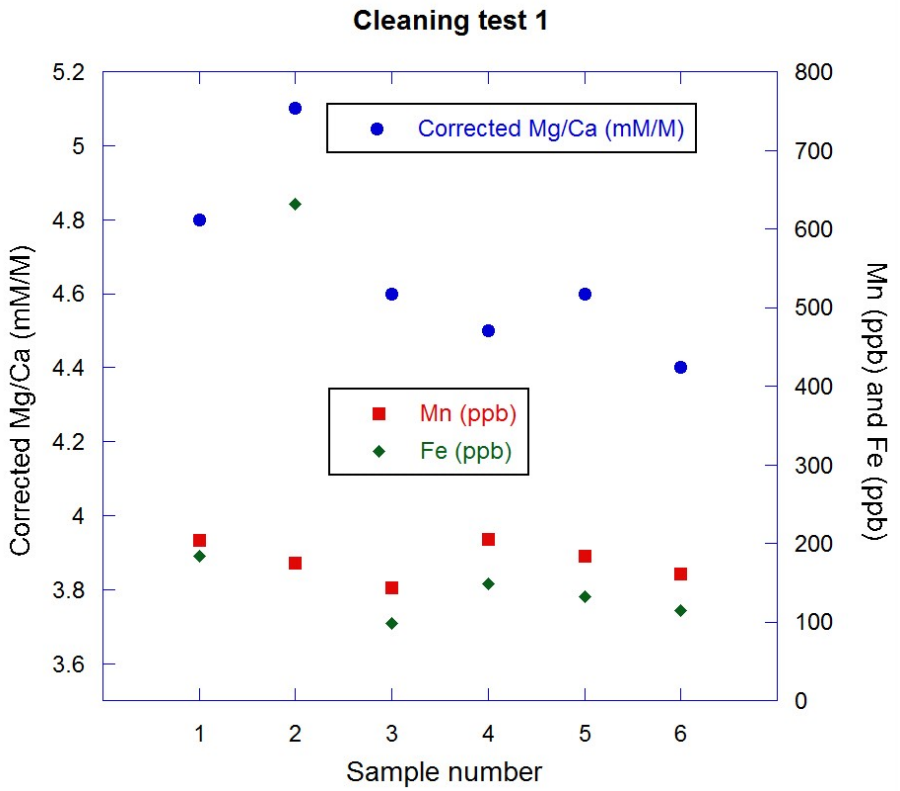

Figure 3-2: Results of Cleaning Test 1. Corrected Mg/Ca (mmol/mol) plotted in blue, Mn (ppb) in red and Fe (ppb) in green.

The corrected Mg/Ca (mmol/mol) values for the six samples ranged between 4.4 and 5.1mmol/mol. The two samples which received only the minimal cleaning had the highest values. The standard deviation among the remaining four samples was 0.09mmol/mol. This translates to ~0.5°C error in the temperature estimates which is within the calibration margin of error ±1.2°C (Anand et al., 2003). All six samples show similar Mn (ppb) and Fe (ppb) values except for sample #2.

Test 2.

The efficacy of our cleaning procedure was evaluated continuously by measuring Fe and Mn in all *G. ruber* samples analyzed. Fe (ppb) and Mn (ppb) values for 100 randomly chosen Mg/Ca data points between core depths of 1836-3102cm were plotted to check for any correlation between the Fe and Mn and Mg/Ca values. Mn and Fe exhibit no positive correlation with Mg/Ca measured in *G. ruber* suggesting that contamination is not a significant influence on Mg/Ca variability (Figure 3-3.).

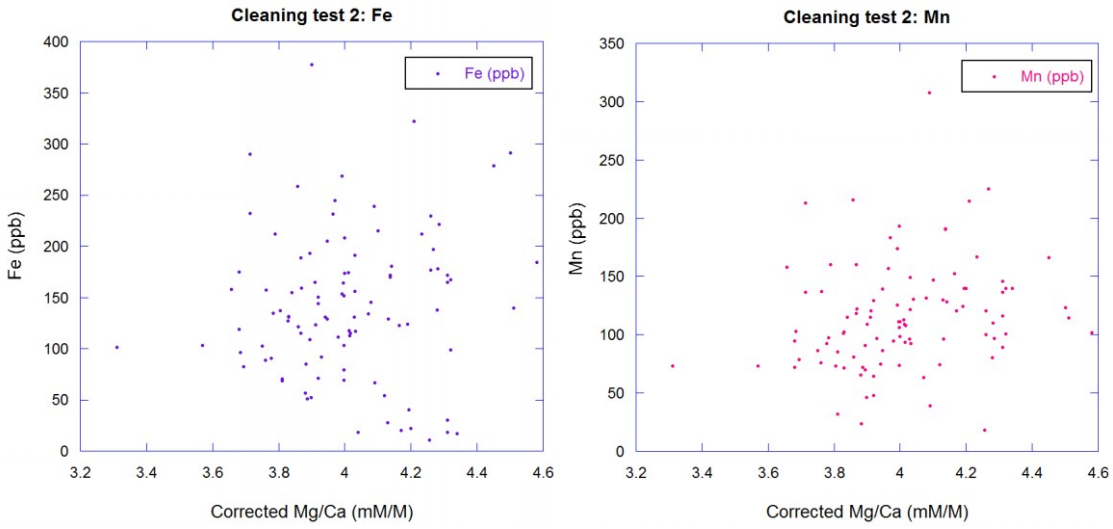

Figure 3-3: Results of Cleaning Test 2. Corrected Mg/Ca (mmol/mol) plotted against Fe (ppb) on the left and Mn (ppb) on the right.

Contamination and dissolution artifacts have therefore been ruled out as major controls on the Mg/Ca variability observed in MD81 by reference to Fe and Mn concentrations, none of which show a consistent positive correlation with planktonic Mg/Ca.

3-6. Age models

The Holocene age model for the MD81 core based on AMS dates has been previously published down to 1711cm (Stott et al., 2007). This age model for the MD98-2181 core is derived from the planktonic ^{14}C ages using the CALIB 5.0.2 routine with the Marine04 calibration data set. The reservoir age correction for tropical surface waters was to add 480 years for samples younger than 13,000 years BP and 630 years for older samples. This correction includes effects of gas exchange ratio, vertical mixing and atmospheric ^{14}C production change. The ^{14}C age for the 12cm interval is 580 years and indicates the top of this core has a 0 kyrBP age. An age/depth plot of these calibrated ages indicates a continuous and linear sediment accumulation rate through the glacial transition. The Stage 3 *G. ruber* $\delta^{18}O$ of MD81 was visually matched to GISP2 $\delta^{18}O$ record (Blunier and Brook, 2001) based on the synchrony of temperature variations recorded in planktonic $\delta^{18}O$ and Greenland $\delta^{18}O_{ice}$ with tie-points selected at the maximum and the preceding minimum of each stadial-interstadial transition for D/O-events 5-17, excluding D/O 9, 13 and 14 where only the maxima have been used. This allowed the transferal of GISP2 ages to MD81 and linearly interpolating between the tie-points, assuming constant sedimentation rates between the tie points. This placement of the D/O-events in the *G. ruber* $\delta^{18}O$ record was independently confirmed

by their placement according to the paleomagnetic record of MD81 with an accuracy of ±300 yrs (S. Lund, personal communication, 2008, not shown).

MD81 planktonic $\delta^{18}O$ was also matched to Greenland NGRIP and Hulu Cave speleothem $\delta^{18}O_{VPDB}$. *G. ruber* $\delta^{18}O$ fits all three age models with minor differences (Figure 3-4), which demonstrates that *G. ruber* $\delta^{18}O$ at the MD81 site reflects isotopic variability over the Northern Hemisphere. There is good correlation to 40kyr. Older ages lack precise agreement in chronologies of Hulu with GISP2 due to the increased uncertainties associated with older dates. Further support for the MD81 age model is given by the agreement with the paleomagnetic record (S. Lund, personal communication).

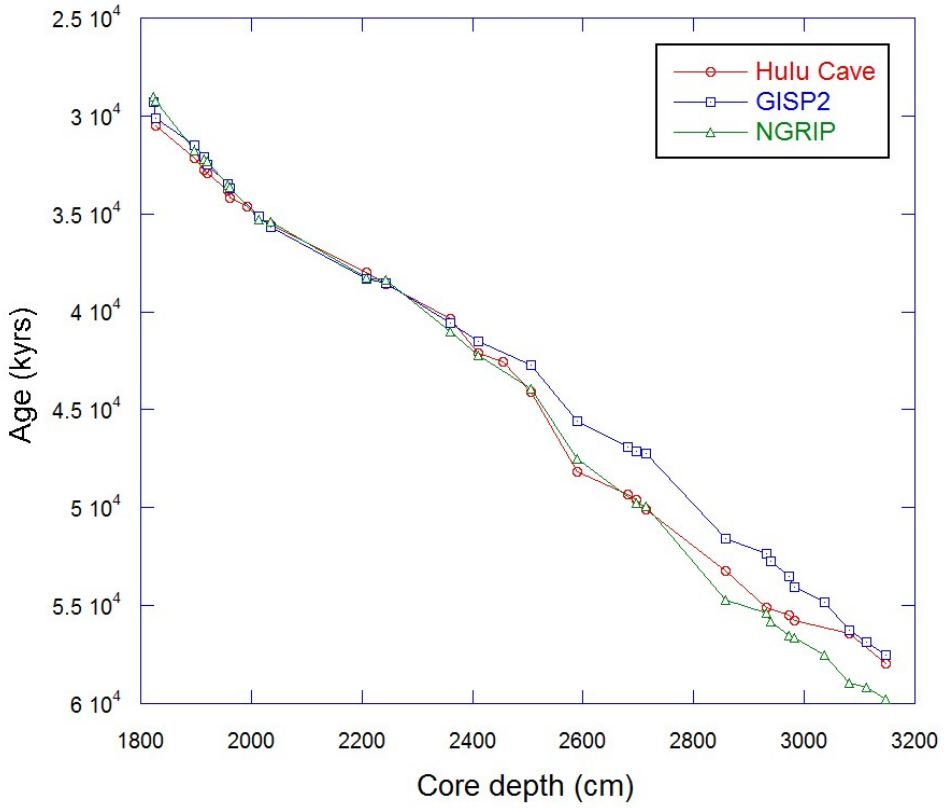

Figure 3-4: MD81 core depth plotted against the different Greenland ice core NGRIP (in green), GISP2 (in blue) and Hulu Cave stalagmite (in red) chronologies. Symbols denote tie-points.

The Greenland Ice Sheet Project 2 (GISP2) depth-age scale is based on a multi-parameter continuous count approach, to a depth of 2800 m, dated at 110,000 years B.P. with an estimated error ranging from 1 to 10% in the top 2500 m (57,500 yrs BP) of the core and averaging 20% between 2500 and 2800 m. Age dating of the GISP2 ice core was done by identifying and counting annual layers using a number of physical and chemical parameters that included measurements of visual stratigraphy, electrical conductivity method (ECM), oxygen isotopic ratios of the ice and the analysis of glass shards and ash from volcanic eruptions (Meese et al. 1997). North Greenland Ice Core Project (NGRIP) is also absolutely dated using the annual layer counted Greenland Ice Core Chronology (GICC05). The highest resolution record is from NGRIP. So far this record only covers the time period 48-38 kyr BP. After 38 kyr BP GRIP data is used and before 48 kyr BP GRIP and GISP data. The maximum counting error of the chronology ranges from 4% in the warm interstadial periods to 7% in the cold stadials (EPICA Community Members, 2006).

The Wang et al. (2001) Hulu Cave speleothem $\delta^{18}O_{VPDB}$ dataset is made up of five stalagmites from 35 m depth in Hulu Cave (32°309N, 119°109E). Fifty-nine 230Th dates, all in stratigraphic order, have analytical errors equivalent to about ±150 years at 10,000 years and ±400 years at 60,000 years. The oldest age is 74,875 ±1,010 yr. B.P. (relative to 1950 A.D.) and the youngest is 10,933 ±160 yr. B.P., with at least one stalagmite active during all intervening times. These speleothem records have been shown to match GISP2 (Wang et al., 2001).

3-7. Planktonic-benthic offset

Obtaining the rate of deep water flow requires a ‘‘clock’’ such as radiocarbon. Its entry from the atmosphere, where it is produced, into the deep ocean is reasonably well understood, and its radioactive decay rate or half-life is well established. In theory this means that water parcels, once in the ocean interior and isolated from the atmosphere, will have no source of ^{14}C, but only loss by decay at a known rate. Therefore the amount of ^{14}C that has decayed within the ocean is a measure of time since losing contact with the atmosphere. The typical residence time of waters at the surface is less than the roughly 10-year period that is required for full carbon isotopic equilibration to become established (Broecker and Peng, 1982). This means that the surface ocean does not have the same ^{14}C age as the atmosphere (i.e. not zero age), therefore giving rise to a so-called ‘‘reservoir age.’’ When surface waters are transformed into deep waters and become isolated from the atmosphere, the radiocarbon clock begins, but the ^{14}C age is already a few hundred years old (Matsumoto, 2007).

Propagation time is defined as the time it takes for a change occurring in, for example, Antarctic source water to propagate to a location in the deep oceans, which is different from the traditional ^{14}C age (age of the water itself, reservoir age, ventilation age). Stott et al. (2007) estimated the propagation time of deep water from its source region near the Southern Ocean to MD81 in the western tropical Pacific to have remained relatively constant throughout the previous glacial termination. For this study, it is assumed that this offset also remained unchanged for Marine Isotope Stage 3.

A reservoir age correction for tropical surface waters of 630 years was added to samples older than 13,000 years BP (Stott et al., 2007). A reservoir age for glacial sub-polar surface waters within the Southern Ocean, the source region for Pacific Deep Water, is estimated to be 560 ±40 years (Sikes et al., 2000). The tropical surface water to upper Pacific Deep Water ^{14}C age difference today is approximately 1400 years and was ~1500 years (1482 +/- 367 years) during the late glacial and termination, based on AMS dates on coexisting planktonic-benthic foraminifera from MD81 (Stott et al., 2007). It is possible that the ^{14}C age of Pacific deep water was somewhat older during the glacial compared to today. However, work by Broecker et al. (2004) suggests that at the LGM deep waters at MD81 were no older with respect to surface waters than today. Furthermore, work by Butzin et al. (2005) with ocean model sensitivity experiments showed that the surface-to-deep water ^{14}C age difference in the western tropical Pacific was not significantly changed (1000±100 years) by glacial/interglacial climate changes such as changing winds, brine release in the Southern Ocean and North Atlantic melt water pulses. Stott et al. (2007) estimated the propagation time of deep water from its source region near the Southern Ocean to MD81 in the western tropical Pacific to have remained relatively constant throughout the previous glacial termination based on the constant benthic-planktonic ^{14}C differences. The present-day propagation time of deep waters from their source region to the tropical Pacific can be roughly estimated from the prebomb-^{14}C distribution in the Pacific using the GLODAP carbon isotope climatology (Key et al., 2004). Eddy mixing, convection and Ekman transport mix deeper and older ocean waters with surface waters south of 50°N, which enhances the reservoir age of the Pacific deep waters. Between the Antarctic and the northern equatorial Pacific the

^{14}C age of Pacific deep water increases from ~800-1000 years to about ~1900 years at 10°N, suggesting a propagation time of between 900-1100 years (Stott et al., 2007). It should be noted however, that ^{14}C is not a pure advective tracer because it is subject to ocean interior mixing. The estimated time required for deep waters to travel between the Southern Ocean to the north equatorial Pacific based on the ^{14}C gradients depicted in modern observational data set is also consistent with ocean model estimates of a transit time of ~800-1000 years (Broecker et al., 2004).

Combining the modern observational data, paleo-proxy data and model estimates for modern circulation in the Pacific, the transit time from the Southern Ocean to MD81 is estimated to be ~1000 years (±300 years) during the glacial, the same as it is today. This study therefore applies a 1000 year lead in benthic (deep water) $\delta^{18}O_c$ record to the planktonic $\delta^{18}O_c$ record.

To provide an independent estimate of transit times of deep water masses in the Pacific an ocean dynamical model is used, which incorporates a nutrient and radiocarbon mixing model. The model estimates the age of water at MD81 to be 1056 years, in very close agreement with the propagation estimate of ~1000 years (±300 years) (G. Gebbie, 2008, personal communication).

3-8. Reworked depth intervals

Although the integrity of the MD81 sediment core is not in doubt, there are discrete intervals that on closer examination were suspected to be reworked. The coarse- and silt-fraction sample size of these intervals is much larger than that of

neighboring intervals, which may indicate the presence of coarser, reworked material. The majority of samples used in the present study are composed primarily of fine clay and small fraction of silt size sediment, including foraminifera. The sieving process eliminates the clay fraction, leaving only small silt fraction for use. In some intervals especially the silt fraction was very small and in these intervals it was a challenge to find enough material to allow for both isotope and Mg/Ca-measurements. Along with the larger overall sample size, these suspected reworked intervals also appeared to consist of two populations of foraminifera present; a more clean population and a population that consists of dirty and/or cracked specimens. Some of these suspected intervals were chosen for AMS dating of concurrent planktonic (*G. ruber* and *G. sacculifer*) and mixed benthic species at the Keck Carbon Cycle AMS Facility, Earth System Science Dept., UC Irvine. Wood fragments were found in several depth intervals and these were also dated, both as wood and as cellulose. The results are shown below in Table 3-2 and Figure 3-5. As can be seen from Figure 3-5, in some of the tested intervals the two co-existing planktonic foraminifera species (*G. ruber* and *G. sacculifer*) gave different ^{14}C ages and was in one interval older than the co-existing mixed benthic sample. These intervals were therefore confirmed to be reworked and were removed from the data set and are not included in any of the isotope or Mg/Ca data presented in this study.

UCIAMS #	Sample name	^{14}C age (BP)	±	Calibrated age (BP)
46226	MD81 1868 G. ruber	35350	350	40948
46227	MD81 1868 G. sacculifer	36740	410	42171
46228	MD81 1868 Mixed benthics	33370	230	38761
46229	MD81 2134 G. ruber	31320	180	36999
46230	MD81 2134 G. sacculifer	32980	230	38676
46231	MD81 2134 Mixed benthics	33950	240	39321
46232	MD81 2234 G. ruber .46mgC	36010	460	41535
46233	MD81 2234 Mixed benthics	36320	320	41544
46234	MD81 2520 G. ruber	43370	930	47879
46235	MD81 2520 Mixed benthics	44190	830	48292
46243	MD98-2181 2134 wood ABA	32530	260	37926
46244	MD98-2181 2234 wood ABA	34540	260	39904
46245	MD98-2181 2520 wood ABA .40mgC	36300	620	41522
46249	MD98-2181 2234 .46mgC hollocellulose chunks	33700	830	39078
46250	MD98-2181 2234 hollocellulose after grinding	32610	490	38004

Table 3-2: AMS results for selected MD81 planktonic, mixed benthic and wood samples analyzed at the Keck Carbon Cycle AMS Facility, Earth System Science Dept., UC Irvine.

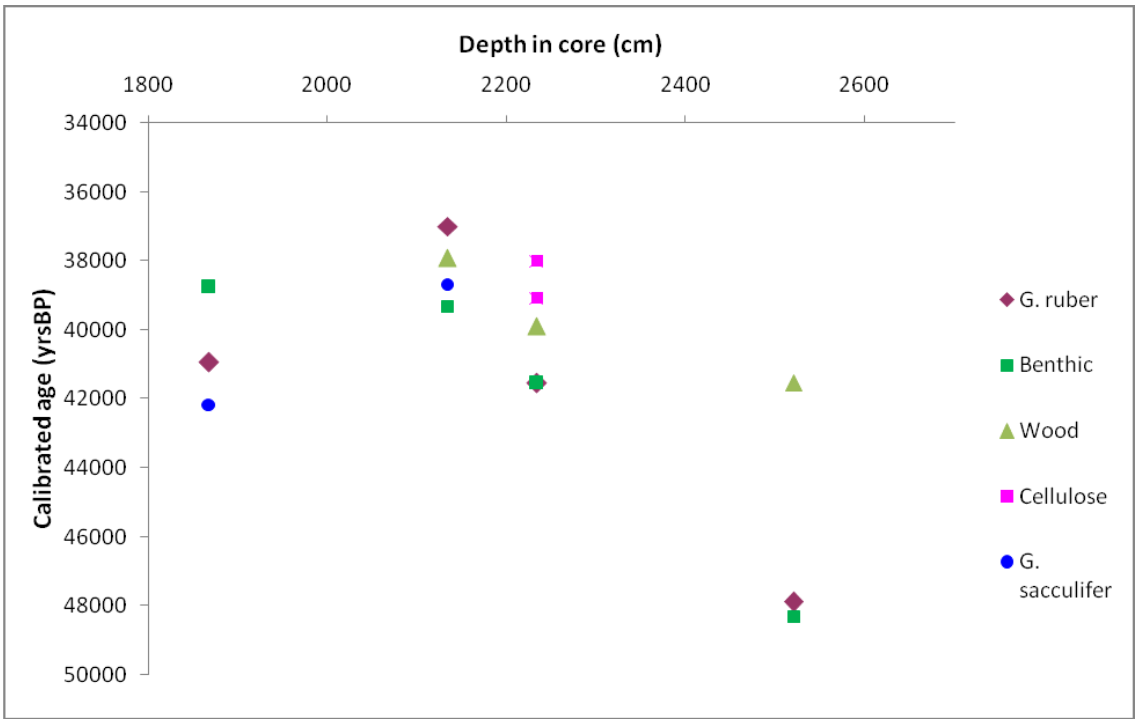

Figure 3-5: Calibrated ages (yrs BP) of planktonic (*G. ruber* and *G. sacculifer*), mixed benthic and wood samples. All are disturbed intervals. Older samples have larger errors associated with them.

Chapter 4: Results

The oxygen isotope and Mg/Ca paleothermometry results for planktonic *G. ruber* and oxygen isotope results for benthic *U. hispida* are shown in Figures 4-1, 4-2 and 4-3 below plotted against depth in core. Section 4.1 describes the planktonic and 4.2 the benthic record.

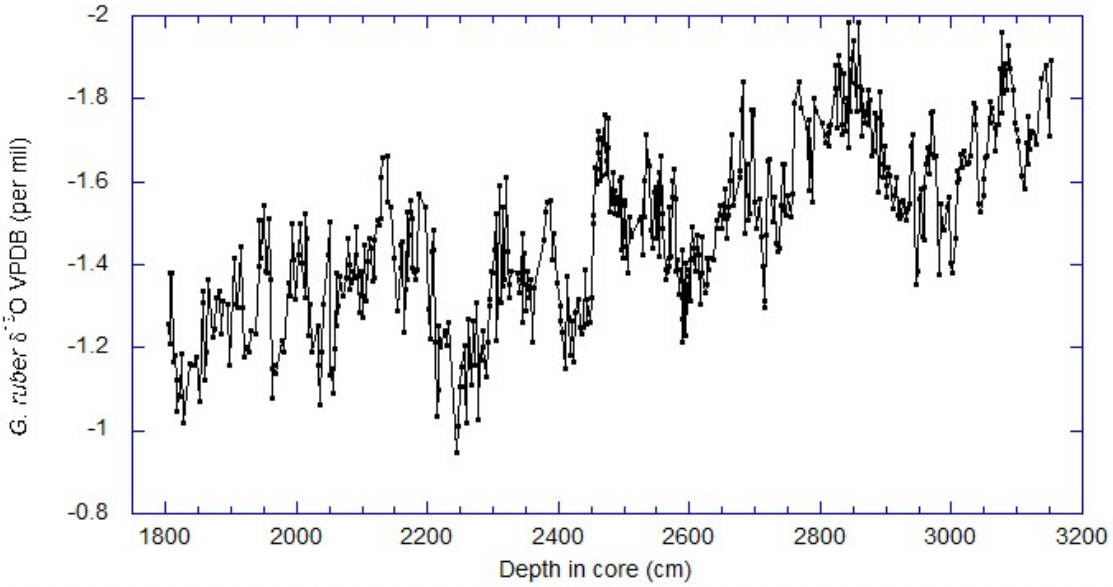

Figure 4-1: MD81 *G. ruber* $\delta^{18}O$ VPDB plotted with respect to depth in core.

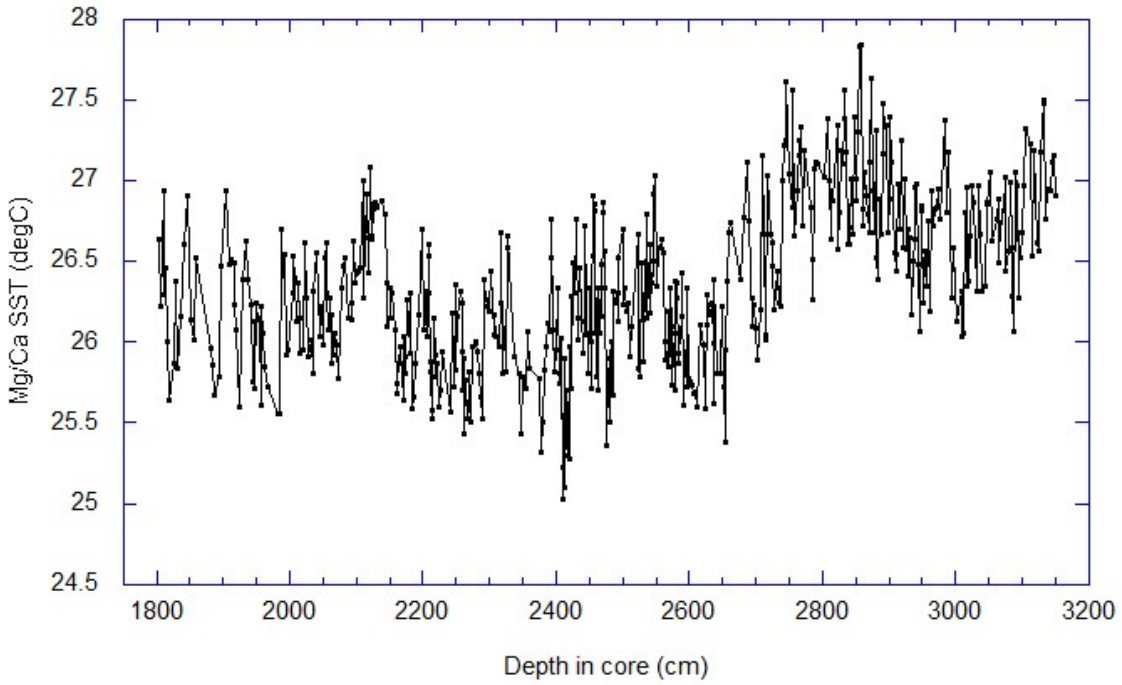

Figure 4-2: MD81 *G. ruber* Mg/Ca Sea surface temperature (SST, °C) plotted with respect to depth in core.

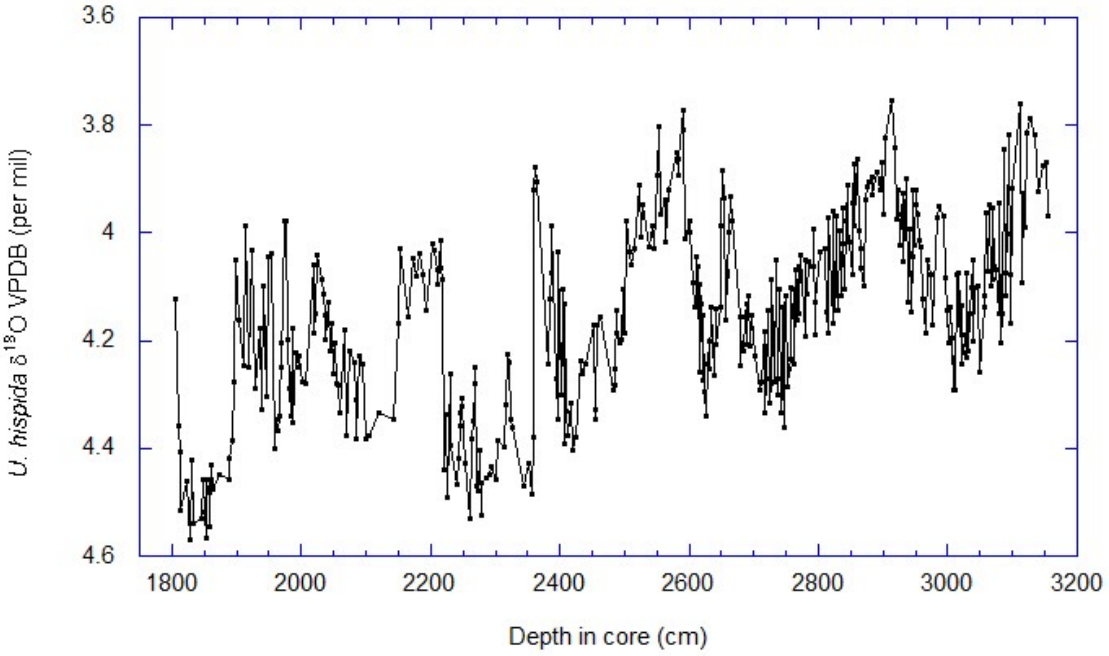

Figure 4-3: MD81 *U. hispida* $\delta^{18}O$ VPDB plotted with respect to depth in core.

4-1. MD81 planktonic record

The planktonic foraminiferal Mg/Ca SST and $\delta^{18}O$ records from MD81 are compared to the Hulu Cave stalagmite (Wang et al., 2001) and the GISP2 Greenland ice core (Blunier and Brook, 2001; Ahn and Brook, 2007) records in Figure 4-4. Planktonic *G. ruber* $\delta^{18}Oc$ and SSTs in the western tropical Pacific varied by up to 0.8‰ (-1 to -1.8‰) and 2°C, respectively, throughout the D/O-events of Stage 3. These variations coincide closely with the shifting monsoon rainfall over Asia as reflected in the Hulu Cave isotope reconstruction and with the atmospheric temperature changes over Greenland (Figure 4-4). Estimates of surface water $\delta^{18}O_{SW}$ derived from the G. ruber $\delta^{18}Oc$ and SST data also follow the millennial-scale oscillations. According to the modern $\delta^{18}Osw$-salinity relationship in the tropical Pacific a decrease in $\delta^{18}O_{SW}$ of ~0.5‰ signifies a decrease in sea surface salinity of ~1-1.5psu (Morimoto et al., 2002; Fairbanks et al., 1997). The MD81 western tropical Pacific SST record documents a long-term cooling between 60 and 38ka (Figure 4-4). This sustained downward trend in SSTs appears to have leveled off by ~38ka when SSTs reached their lowest values during MIS3 record. The D/O-events in the Greenland ice core record, and the approximate timing of the Heinrich (H) -events H3 at ~31ka, H4 at ~38ka and H5 at ~45ka (Hemming, 2004) are indicated in the figure.

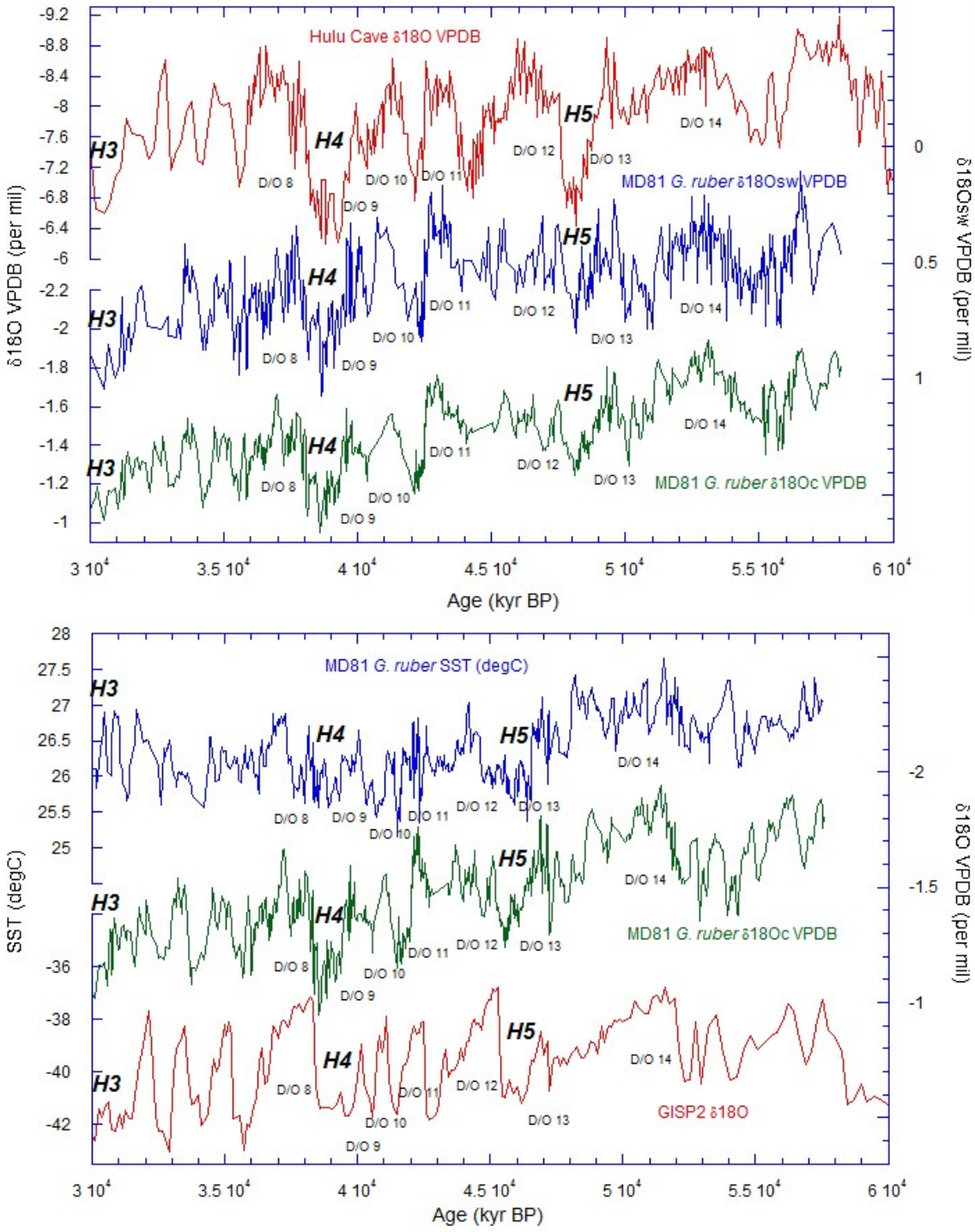

Figure 4-4: Top – Hulu Cave $\delta^{18}O$ VPDB in red, *G. ruber* $\delta^{18}O_{SW}$ in blue and $\delta^{18}O$ VPDB in green plotted with respect to the Hulu stalagmite age scale. Bottom – GISP2 $\delta^{18}O$ in red, G. ruber SST (°C) in blue and $\delta^{18}O$ VPDB in green plotted with respect to the GISP2 age scale.

The western tropical Pacific and the East Asian Monsoon region are linked by the seasonal migration of the Intertropical Convergence Zone (ITCZ). During boreal summer (July to September) the northward movement of the ITCZ brings southerly/southeasterly winds across the Indonesian maritime continent and East Asia. It is during this season that the western tropical Pacific receives the greatest rainfall, as much as 300 and 400 mm/month during summer (Stott et al., 2002). The boreal winter season is characterized by a reversal in the winds across the maritime continents of the western Pacific (Gordon, 2005). These seasonal wind patterns are associated with marked changes in surface water properties including temperature and salinity. In the region of Mindanao, during the northern summer SSTs in the western Pacific warm pool average 29° to 30°C and in winter, SSTs cool to 26-27°C (Gordon, 2005). The sea surface salinities (SSS) annually range between 33.8-34.0‰ (Gordon, 2005). In plankton tow studies, *G. ruber* (white) is abundant in the warm summer surface waters of the western tropical Pacific and hence this species is most sensitive to summer season changes (Troelstra and Kroon, 1989).

The distinctive pattern that is evident in both the surface water variables at MD81 (Figure 4-4) and the Asian monsoon speleothem records implies there was a close temporal coupling between the tropical Pacific ocean/atmospheric changes and the high northern latitude temperatures variability. However, there are also notable differences between the low and high latitudes in the rate of temperature change at the beginning of millennial warm events during MIS 3. This is particularly evident at the beginning of D/O 14 and D/O 12 in the Greenland ice core record. In the North Atlantic, interstadial warming was abrupt whereas in Asia and the tropical Pacific,

higher precipitation and SST warming was more gradual and may have begun to change earlier (Figure 4-4). This is not an artifact of the way the MD81 age model was constructed.

4-2. MD81 benthic record

The MD81 benthic $\delta^{18}O$ record documents millennial-scale variations of 0.3-0.5‰, with rapid shifts from more depleted to more isotopically enriched values throughout MIS3 (Figure 4-5). If these $\delta^{18}O$ shifts were due entirely to temperature change in the deep Pacific they would translate to ~1-2°C (0.21‰ per °C, Shackleton, 1974). The abruptness of some of these events is especially striking. For example, between ~32-42ka there were changes of 0.3-0.5‰ over approximately a century. At a depth of 2114m, the benthic foraminifera are recording changes in Southern Ocean-sourced waters. The timing of these events in the MD81 record must therefore take into account the transit time between the Southern Ocean and the location of MD81. A 1ka-offset is applied to the MD81 benthic data with respect to the MD81 planktonic data to account for this transit time. With this time adjustment the MD81 benthic $\delta^{18}O$ record is compared to the Antarctic Dome Fuji, EDML and Byrd ice core $\delta^{18}O_{VSMOW}$ to assess how the timing of events in the deep Pacific compare to those reflected in the Antarctic ice core records (Figure 4-5). The MD81 benthic $\delta^{18}O$ record exhibits strong resemblance to the pattern of Antarctic $\delta^{18}O$ variability during the last glacial.

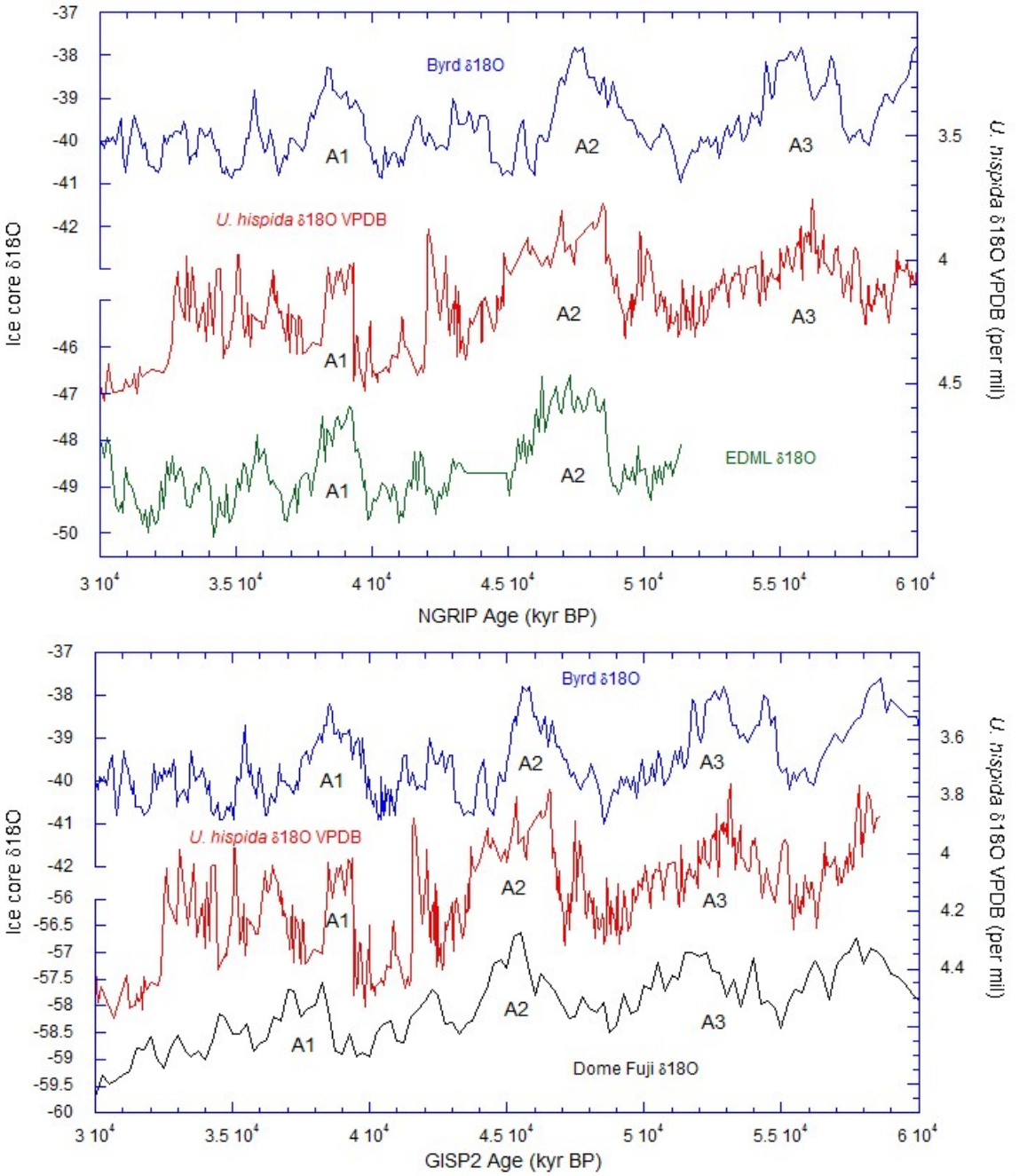

Figure 4-5: *U. hispida* $\delta^{18}O$ VPDB in red plotted against Antarctic ice core $\delta^{18}O$ from Byrd ice core in blue (top and bottom panel), EDML ice core in green (top panel) and Dome Fuji in black (bottom panel) with respect to the GISP2 age scale.

The gradual warmings evident in the millennial temperature swings over Antarctica that are evident in the Dome Fuji, EDML and Byrd ice cores between ~35-60ka (such as events A1, A2 and A3) are also seen in the MD81 benthic $\delta^{18}O$ record.

This is in marked contrast to the more rapid oscillations in surface water variables in the MD81 record that are typical of Northern Hemisphere millennial-scale changes during MIS 3. During late MIS3 the Antarctic warming excursions in the Dome Fuji and EDML records are box- shaped, such as event A1, reflecting both rapid warming at their onset and similarly abrupt cooling at their terminations. This pattern is also evident in the MD81 benthic record. The degree of correspondence between the MD81 record and the Antarctic ice core record is not as clear between 30-40ka.

Chapter 5: Discussion

5-1. Planktonic record - Northern Hemisphere and Monsoon variability

Planktonic *G. ruber* $\delta^{18}O$ and Mg/Ca SST changes of up to 0.8‰ (-1 to -1.8‰) and 2°C, respectively, occurred in the western tropical Pacific during MIS3. These temperature changes were accompanied by shifting surface water $\delta^{18}Osw$. The planktonic calcite $\delta^{18}O$ record contains components of ice volume variability as well as changes in local salinity and temperature. The glacio-eustatic component is expressed as a longer-term increase (Chappell, 2002) in $\delta^{18}O$ of both sea water and calcite. Chappell (2002) identified sea level cycles as recorded by coral terraces at Huon Peninsula in Papua New Guinea with peaks at 33, 38, 44.5, 52 and 58–60 ka where the timing is fixed by U-series dates. Each cycle of 6000–7000 years ended with a sea level rise of 10–15m and lasting 1000–2000 years. These were associated with a shift in oceanic $\delta^{18}O$ of 0.008‰/m. More recent estimates of global sea level change are 35±12m (Siddall et al., 2003) and 25m (Arz et al., 2007). Therefore, glacio-eustatic contributions to the MD81 $\delta^{18}Oc$ variations during MIS 3 account for ~0.12-0.28‰ of the total change. The close correspondence between the MD81 $\delta^{18}Oc$, SST and $\delta^{18}Osw$ variations, and Hulu Cave stalagmite records, relative to millennial-oscillations seen in the Greenland ice core history implies a strong northern hemisphere influence on the hydroclimate in the tropical Pacific. The Hulu Cave speleothem record of Wang et al. (2001) was interpreted to reflect variations in monsoon rainfall over China during the last glacial; lower $\delta^{18}O$ values in the speleothem calcite as signifying more intense

summer monsoon (June-September) precipitation. Greenland temperature increases correlates positively with greater summer (June-September) precipitation in eastern China. On the basis of their own independent time scale, it appears that increased summer monsoon precipitation was synchronous with atmospheric warming over the northern high latitudes (Wang et al., 2001). The stronger summer monsoon and increased summer precipitation (more depleted δ^{18}OVPDB) at Hulu Cave coincided with fresher (lower δ^{18}Osw) and warmer conditions in the western Pacific warm pool.

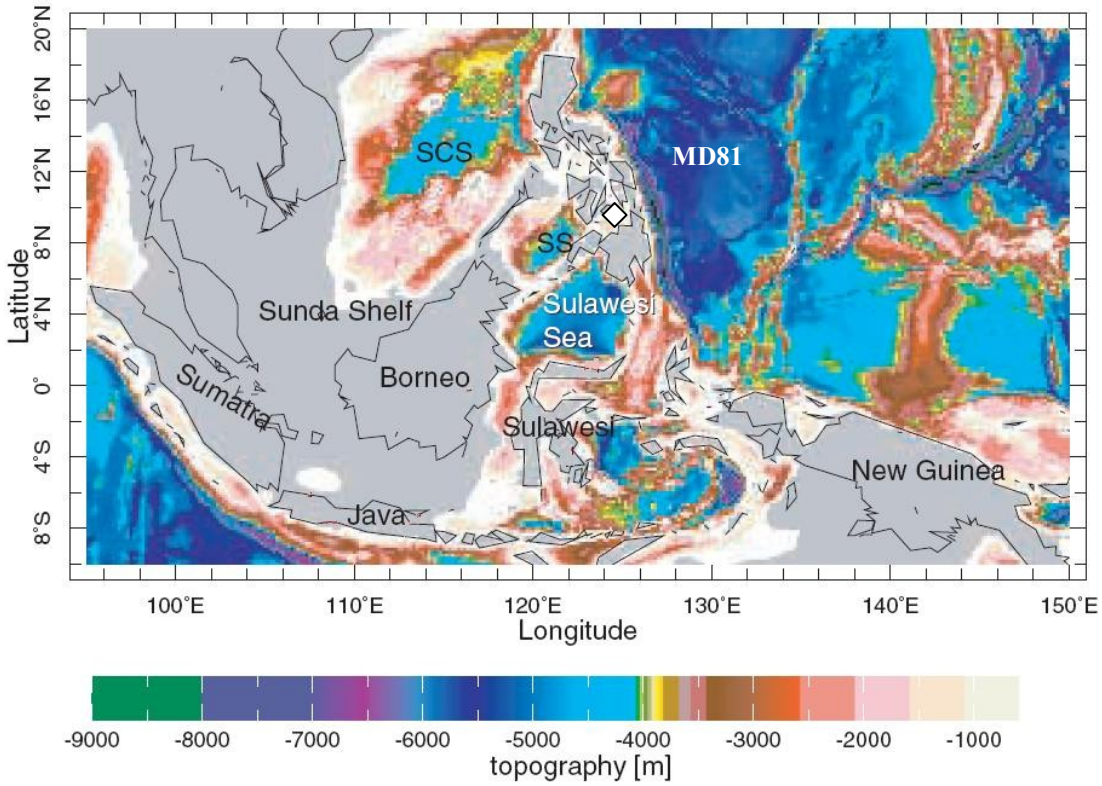

Figure 5-1: Map of the western tropical Pacific. SCS: South China Sea, SS: Sulu Sea. Location of MD81 indicated by white diamond. Image modified from Oppo et al. (2003).

Other cores from the strong atmospheric convection region of the western Pacific also show large sea surface temperature and salinity changes interpreted to reflect hydrologic response to the changes in the monsoon circulation (Beaufort et al.,

2003, Dannemann et al., 2003, Oppo et al., 2003), further evidence of a strong atmospheric teleconnection of the East Asian monsoon circulation and the western tropical Pacific. However, there are regional differences in climate responses between the South China Sea, the Sulu Sea and the Warm Pool (Figure 5-1). For example, while the WPWP warms and receives more rainfall during La Nina events, the southern South China Sea cools and receives less rainfall (Dannemann et al., 2003). During El Nino the Sulu Sea appears to register a mixed SST and precipitation response from both the South China Sea and the WPWP (Dannemann et al., 2003). Dannemann et al. (2003) reported suborbital-scale $\delta^{18}O$ changes in marine core MD97-2141 in the Sulu Sea during MIS3 with amplitudes (0.4 to 0.7%), similar to those seen in MD81. SST variations were estimated at a warming and subsequent cooling of 1 to 1.5°C which was not in phase with $\delta^{18}O$. This estimate is comparable with the Mg/Ca, and U-Th –based estimates of ~2°C cooling during MIS3 from the Ontong Java Plateau (Lea et al., 2000) and southern South China Sea (Pelejero et al., 1999). Approximately 0.1 to 0.3‰ of the 0.5‰ MIS3 $\delta^{18}O_{SW}$ variations may be due to suborbital changes in sea level leaving 0.2-0.4‰ sea surface salinity signal. Due to the effects of lower sea level, a generally weaker summer monsoon and a stronger winter monsoon, there was an increase in the input of lower salinity South China Sea surface water to the Sulu Sea over the saltier WPWP surface water during MIS3 (Oppo et al., 2003). The MIS3 millennial $\delta^{18}O$ events in the Sulu Sea were primarily the result of changes in surface water salinity, which today is directly related to the EAM and its influence on the balance between surface water contributions from the South China Sea and WPWP (Dannemann et al., 2003). As with MD81 during MIS3, relatively fresh surface waters in the Sulu Sea

coincided with a greater summer/winter precipitation ratio in the EAM, and also with the warm phases of suborbital cycles in the North Atlantic. Dannemann et al. (2003) suggest that the suborbital climate variability during MIS3 in the Northern Hemisphere and in the low latitudes maybe connected via the WPWP (and Indian Ocean) to the North Atlantic, placing WPWP in a central role.

5-1-1 ITCZ Movement

The position of the ITCZ is controlled by the seasonal pole-to-equator temperature gradient. The seasonal motion of the ITCZ is accompanied by large changes in seasonal rainfall across the tropics. In the tropical Atlantic, negative rainfall anomalies occur in northeastern Brazil in response to negative SST anomalies in the southern tropical Atlantic and positive anomalies in the northern tropical Atlantic (Wang et al., 2004); a pattern that is associated with a northward displacement of the ITCZ during boreal summer. Temperature anomalies in the opposite direction strengthen the northeast trade winds and cause a southward shift in the ITCZ. This is accompanied by enhanced rainfall over northeastern Brazil (Wang et al., 2004). In their study of the rainfall patterns during MIS3, Wang et al. (2004) found that wet periods in NE Brazil were synchronous with periods of weaker East Asian summer monsoons, cold stadials in Greenland and Heinrich events in the North Atlantic. MD81 results indicate that these conditions were also associated with a more saline and cooler western tropical Pacific. The SST and SSS changes documented in the MD81 record appear to reflect similar north-south shifts in the tropical Pacific ITCZ during MIS3. New terrestrial records from the southern hemisphere from Lynch's Crater, Australia

(Muller et al., 2008) further corroborates this interpretation of the MD81 results where proxies for precipitation/wetness indicate enhanced rainfall due to a southern-deflection of the ITCZ in the region during Heinrich events (H events 1–3) (Muller et al., 2008). A fully coupled atmosphere/ocean climate model simulating a 1 Sv freshwater influx to the North Atlantic Ocean produces a scenario which agrees with the climate changes shown by the Lynch's Crater record (Muller et al., 2008). The model shows precipitation anomalies that include a southward migration of the ITCZ and a zonal shift in mid-latitude storm tracks over the Southern Hemisphere equatorial region. These data indicate large-scale shifts of the austral summer ITCZ position that is known to control monsoonal precipitation in NE Australia.

In addition to the reduction in precipitation locally at MD81, an ITCZ shift would have also influenced surface salinities in the western tropical Pacific by modulating the transport of water vapor between the Atlantic and Pacific basins. Today there is a net export of water vapor from the Atlantic Basin to the Pacific Basin across central America during boreal summer and this contributes to the lower salinities in the Pacific Basin (Leduc et al., 2007). During Greenland stadials, increased salinities were recorded in the EEP (Leduc et al., 2007), which coincide with those documented here in WEP (this study), attributed to the southward migration of the tropical ITCZ. Due to the prevailing westward ocean currents and trade winds, the salinity of the western Pacific would have increased further due to greater advection of salt into the region from the EEP. Model simulations agree with paleodata suggesting that the mean salinity of the Pacific was higher because less water vapor was transported from the Atlantic Ocean (Xie et al., 2008). A high-resolution regional ocean–atmosphere model (ROAM) of the

eastern tropical Pacific was used to investigate key processes of the Isthmus of Panama conduit by examining the response to a sea surface temperature (SST) cooling over the North Atlantic (Xie et al., 2008). The Atlantic cooling was found to increase sea level pressure, driving northeasterly wind anomalies across the Isthmus of Panama year-round and advecting anomalously cool and dry air from the North Atlantic (Xie et al., 2008). The anomalous northeasterly winds across Central America appear as a robust feature in water-hosing experiments across models, in response to the SST cooling and increased atmospheric pressure over the tropical North Atlantic and in particular the Caribbean (Xie et al., 2008). Although focusing on the Holocene instead of the last glacial, similar mechanisms have also been found in other studies of water vapor transport across the Isthmus. Simulations from the Goddard Institute of Space Studies Model E-R, a coupled ocean-atmosphere general circulation model that tracks water isotope tracers throughout the hydrologic cycle, showed the decrease in water vapor transport from the Atlantic Ocean and the increase in water vapor transport to the Indian Ocean raising the mean salinity of the Pacific Ocean (Xie et al., 2008). In response to stronger winds, tropical surface ocean currents are stronger further, enhancing the transport of salt into the region by surface currents (Oppo et al., 2007).

5-1-2 Forcing mechanisms

A global picture of ITCZ migration is now emerging with cold periods in Greenland and Heinrich events in N. Atlantic corresponding to a weak East Asian Monsoon, a wetter eastern Brazil (Wang et al., 2004) and northern Australia (Muller et al., 2008), and a colder and more saline western tropical Pacific as the ITCZ migrates

south. Records of such migrations as recorded by MD81 show the importance and role of the equatorial region in global climate dynamics. Specifically, these results demonstrate unequivocally that changes in the East Asian Monsoon and the hydrology of the tropics are linked on millennial timescales via atmospheric and oceanic circulation pathways to the northern high latitudes. However, the important question that arises from this opposing pattern of precipitation between the northern and southern tropics is whether these changes are in response to high latitude forcing originating with dynamics of freshwater pulses and ice extent at the poles, or instead the result of tropical forcing.

Modeling studies by Cane and Clement (Cane and Clement, 1999; Clement et al., 2001) illustrate how the impact associated with changing ENSO variability on millennial time scales would influence both temperature and rainfall over the tropics. When forced with the smoothly varying solar forcing, the models have shown that ENSO can abruptly ‘‘shut down’’ for several centuries. Clement et al. (2001) argued that such a change in ENSO is caused by solar forcing modulating the strength of the seasonal cycle. Timmermann et al. (2007) found similar results with a coupled general circulation ECHO-G model where a smoothly varying modulation of the strength of the seasonal cycle leads to regime shifts in ENSO. During warm El Nino events, upwelling of cold subsurface waters in the eastern equatorial Pacific is reduced and the temperature structure of the region becomes more symmetric about the equator. As a result, warm El Nino events are characterized by a mean southward shift of the ITCZ in the Pacific basin (Fedorov and Philander, 2000). A more southerly position of the ITZC would shift the rain belt south and increase the salinity in the Warm Pool, creating

modern ENSO-like conditions at MD81 with atmospheric convection shifting away from the site (Stott et al., 2002; Timmermann et al., in press). It is therefore possible that abrupt climate events may have been triggered by temperature shifts in climate systems that originated in the low latitudes.

The alternative hypothesis is that the cooling and freezing of the northern Atlantic would cause a southward displacement of the tropical rain belt, the effects of which would then have been transmitted via the atmosphere-ocean bridge between the tropical Atlantic and Pacific across the Central American Isthmus. In model simulations, extratropical oceanic cooling strengthens the northeasterly trade winds, reducing the tropical North Pacific SSTs and shifting the Pacific ITCZ southward through the wind-evaporation-SST feedback. When coupled GCMs are forced with a 1 Sv freshwater flux anomaly in the subarctic North Atlantic, the Atlantic Meridional Overturning Circulation (AMOC) nearly shuts down and the North Atlantic cools significantly (Okumura et al., 2008). At the same time, the South Atlantic warms slightly, shifting the Atlantic ITCZ southward. The atmospheric response to the Atlantic cooling, as measured by the atmospheric pressure increase and anomalous cross-isthmus winds, is much stronger during boreal summer than winter because the North Atlantic is warmer and more conducive to deep convection in summer (Okumura et al., 2008; Xie et al., 2008). The Atlantic ITCZ position during the last glacial has also been found to be sensitive to changes in land ice and sea ice extent, with sea ice extent potentially controlled by variations in ocean meridional heat transport (Chiang et al., 2003). Therefore more sea ice following colder Heinrich-events, compared to a D/O-stadial, would mean a larger southward push of the tropical rain belt.

5-2. Benthic record - High southern latitudes

A 1ka-offset has been applied to the MD81 benthic data from the MD81 planktonic data to account for the deep water travel time from the Southern Ocean to the western tropical Pacific and to evaluate the timing of change at the source region where the deep waters obtain their temperature and salinity. With no other modification applied, the benthic data exhibits remarkable correlation with the Antarctic surface temperature history as recorded by the Byrd, EDML and Dome Fuji $\delta^{18}O$ (Figure 4-5). The MD81 benthic $\delta^{18}O$ record documents millennial-scale oscillations of 0.3-0.5‰ signifying changes in temperature with a potential added salinity and/or sea level component. If the entire $\delta^{18}O$ shift was due to a temperature changes it would translate to Pacific deepwater changes of between ~1-2°C (~0.21‰ per °C, Shackleton, 1974). Skinner and Elderfield (2007) found temperature excursions of up to 1.5°C in North Atlantic deep water as measured from benthic foraminifera occurring during Heinrich-events in Stage 3. Maximum sea level variation estimates during Stage 3 range from ~0.12-0.28‰ (Arz et al., 2007; Chappell, 2002; Rohling et al., 2004; Siddall et al., 2003), therefore the millennial variations in benthic $\delta^{18}Oc$ are not accounted for by global ice-volume fluctuations alone, and must therefore reflect local hydrographic changes in temperature and salinity. According to Skinner and Shackleton (2005) the large volume of the deep Pacific combined with the relatively small lateral gradient of temperature/$\delta^{18}Odw$ would mean that large changes in local deep-water characteristics are most likely driven by changes in temperature and/or $\delta^{18}O$ at the source region where deep Pacific water is formed in the Southern Ocean. Also recent work by McCave et al.

(2008) on cores from the Deep Western Boundary Current in the Southwest Pacific demonstrated that the structure of Lower Circumpolar Deep Water–Upper Circumpolar Deep Water/North Pacific Deep Water–Antarctic Intermediate Water has remained constant over the past 160ka with no apparent changes in the depths of water mass boundaries between glacial and interglacial states. Therefore our MD81 results suggest that the Pacific Deep Water/UCDW is rapidly responding to climate perturbations on short timescales and with large magnitudes.

5-3. North-South Phasing at MD81

The high resolution (~50yr/sample) $\delta^{18}O$ and Mg/Ca results for MD81 have been 3-point smoothed for both *G. ruber* and *U. hispida* and are presented on the GISP2 timescale (Figure 5-2).

The correlation of planktonic marine records to Greenland ice cores is via an atmospheric teleconnection. The atmospheric mixing time is of the order of a year and therefore, within the error inherent in proxy records, is considered instantaneous. The benthic $\delta^{18}O$ record combines a glacioeustatic 'reservoir' component, a non-glacioeustatic component due to local deep-water $\delta^{18}O$ variability, which may vary significantly between ocean basins, and a component due to deep-water temperature. Therefore, the signal in itself represents changes in water mass composition and temperature, as well as sourcing (i.e. source mixture). The MD81 benthic record has been offset from the planktonic by 1ka, to account for the deep water travel time from the Southern Ocean to MD81. Therefore MD81 is among the few marine locations in

the world oceans that are uniquely positioned to allow the study of phasing of hemispheric climate signals on a single time-scale. Both MD81 planktonic and benthic records show the long-term change from an interglacial towards the LGM, a trend towards a heavier oceanic $\delta^{18}O$ value due to the sequestration of ^{16}O in continental ice and cooling temperatures. These planktonic and benthic records each exhibit similar long-term changes that reflect the progressive cooling and ice buildup in the northern hemisphere throughout the glacial. However, what is most striking about the comparison is the phase shift of ~1500yrs relative to SST between the surface and deep water record on shorter, millennial time scales. Shifts towards colder and/or more saline (more enriched) surface waters corresponded to warming and/or freshening (more depleted) in the Southern Ocean, the source region of Pacific Deep Water.

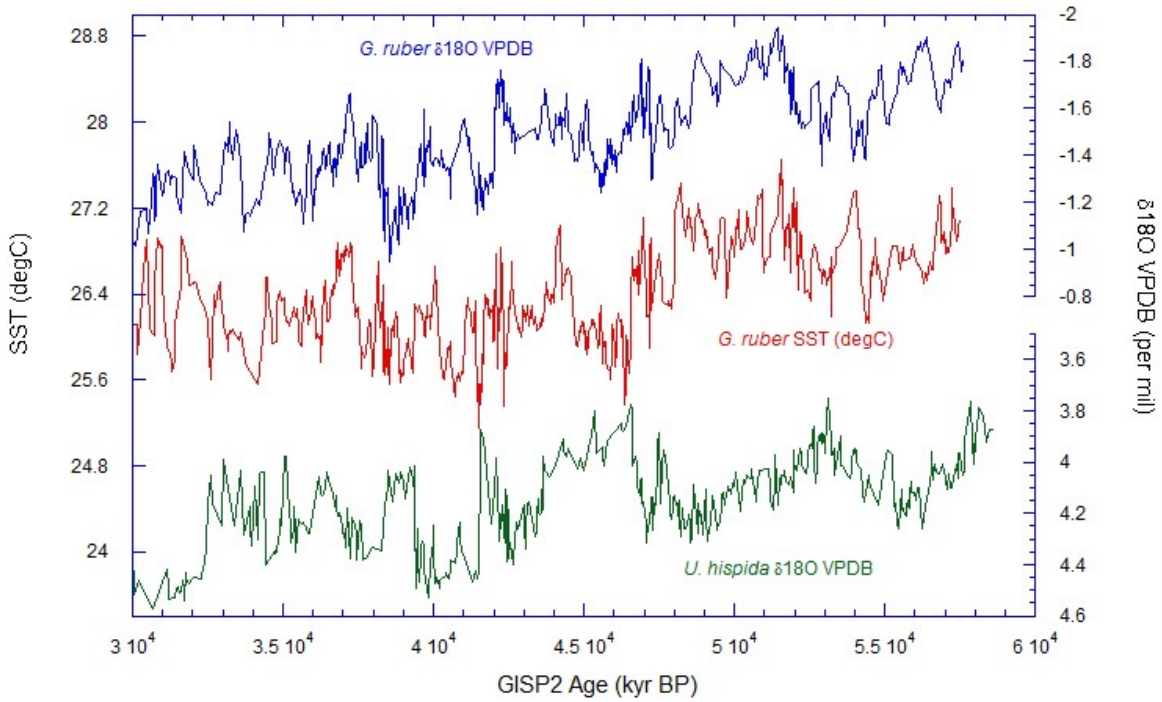

Figure 5-2: MD81 *G. ruber* SST and $\delta^{18}O$ VPDB and *U. hispida* $\delta^{18}O$ VPDB plotted on the GISP2 age model. The benthic record is offset from the planktonic by 1000yrs.

5-4. Evidence for a bipolar seesaw in the Pacific?

5-4-1 MD81 compared to polar ice cores

The ice core records of Greenland and Antarctic were anti-phased during the last glacial period (Blunier et al., 1998; Blunier et al., 1997; Jouzel et al., 1995; Labracherie et al., 1989; Sowers and Bender, 1995). These differences in the timing of millennial scale temperature variations between the two hemispheres were a persistent characteristic of the last glacial period and were maintained throughout the glacial despite the changing background state of the climate system (Blunier and Brook, 2001). Climate model studies have suggested that North Atlantic Deep water variations could have played an important role in modulating the anti-phasing of climate change between the northern and southern hemispheres. As North Atlantic Deep Water (NADW) formation switched on or intensified, heat would have been extracted from the Southern Hemisphere, leading to reduced temperatures in the south. This north-south heat transfer has been termed the 'bi-polar seesaw' (Broecker, 1998; Stocker, 1998; Stocker and Johnsen, 2003; Stocker et al., 1992).

The MD81 benthic and planktonic data plotted against GISP2 and Byrd ice core $\delta^{18}O$ (Blunier and Brook, 2001) in Figure 5-3 suggests a similar northern and southern hemispheric anti-phased relationship, consistent with observations that have been made in the Atlantic (Martrat et al., 2007). While the Antarctic temperature is increasing, Greenland is cooling. The Antarctic temperature rise is interrupted once Greenland temperature jumps to an interstadial state within a few decades. The temperatures then decrease in both hemispheres to full glacial levels, but Antarctica reaches this level

before Greenland. This is also in agreement with previous results from the deep northeast Pacific Ocean, where the benthic foraminiferal $\delta^{18}O$ signal showed warming roughly in unison with the Southern Ocean temperatures, out of phase with the planktonic record in that core (Mix et al., 1999).

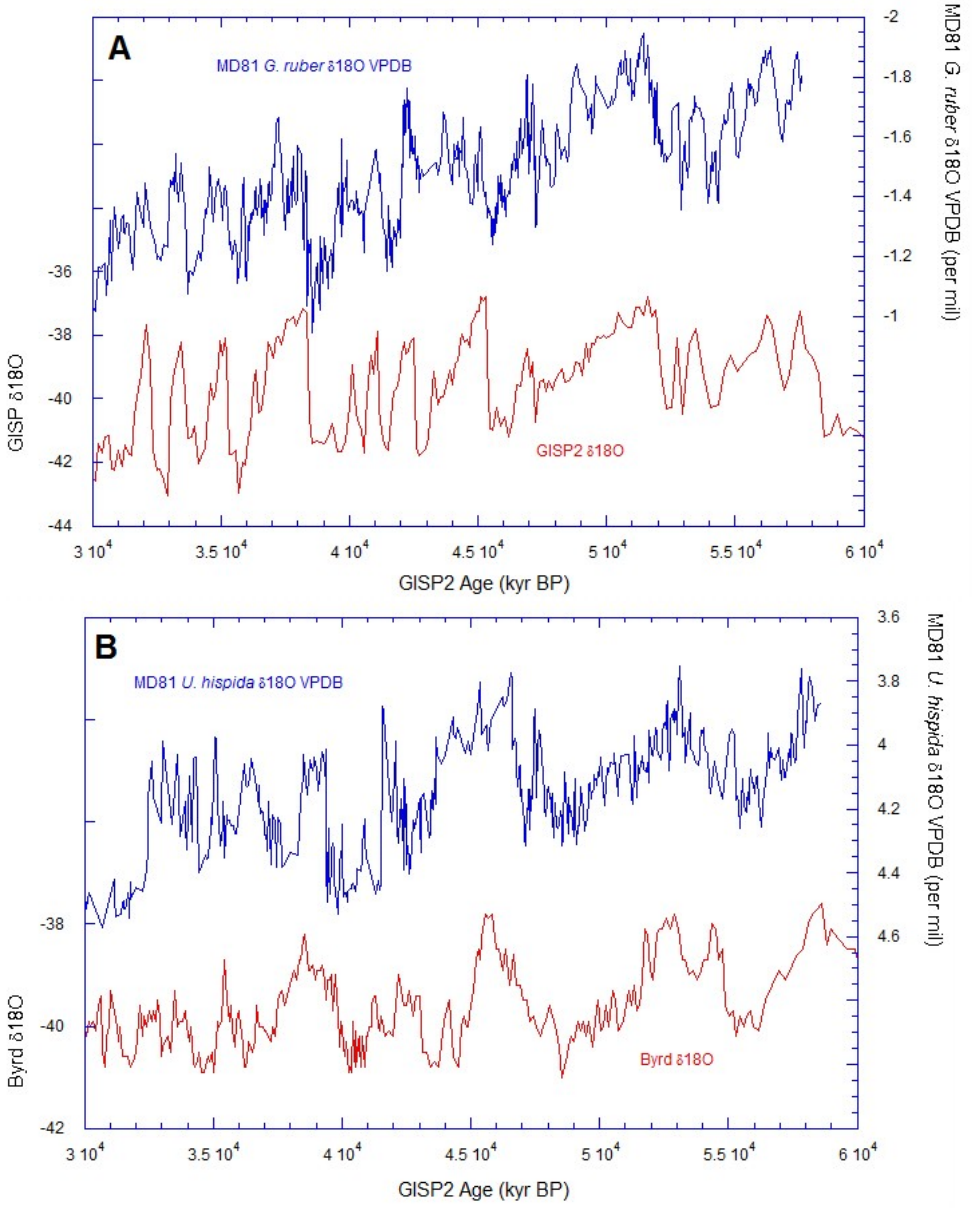

Figure 5-3: A) GISP2 $\delta^{18}O$ and MD81 *G. ruber* $\delta^{18}O$ VPDB data B) Byrd $\delta^{18}O$ and MD81 *U hispida* $\delta^{18}O$ plotted with respect to the GISP2 age scale of Blunier and Brook (2001).

5-4-2 Millennial-scale atmospheric and oceanographic climate fluctuation

The synchrony of millennial-scale climate change recorded in the Greenland ice cores and North Atlantic marine sediments (Broecker, 1994) contrasts with asynchrony that has been identified between planktonic and benthic foraminiferal calcite $\delta^{18}O$ in the North Atlantic during MIS3 (Shackleton et al., 2000), which in turn is set to the phasing of Greenland and Antarctic millennial-scale temperature change (Blunier et al., 1998, Blunier and Brook, 2001). The coupling of Greenland and North Atlantic temperatures has long been proposed to involve perturbations to the thermohaline circulation system, which may behave in an ‘‘oscillatory’’ manner alternating between the dominance of either northern- or southern sourced deep-water in the deep Atlantic (Duplessy et al., 1988, Charles et al., 1996, Boyle, 2000), and potentially responding to internal instabilities and/or external forcing (such as ice dynamics and/or ice-volume fluctuations) initiated in either hemisphere (Stocker et al., 1992, Broecker, 1994, Kanfoush et al., 2000, Seidov and Maslin, 2001, Weaver et al., 2003). Computer simulations suggest that the imbalances between northern- and southern-sourced water masses are the primary agent for these abrupt climate oscillations (Stocker et al., 1992), but there is no consensus yet. Some models suggest that the interaction between these two water masses is driven by changes in AABW (Toggweiler and Samuels, 1995, Knorr and Lohmann, 2003) and others by NADW (Stocker and Johnsen, 2003, Knutti et al., 2004). Instead of any major changes in the overall velocity of MOC during MIS3, many studies (Charles et al., 1996, Ninnemann and Charles, 2002, Skinner et al., 2003, Pahnke and Zahn, 2005, Martrat et al., 2007) have interpreted benthic $\delta^{18}O$ and $\delta^{13}C$ oscillations from the North Atlantic and South Atlantic and the southwest Pacific as

changes in the dominance of the AAIW and AABW versus NADW (Figure 5-4). Millennial deep water temperature and $\delta^{18}O_{dw}$ variations recorded from the Iberian Margin describe an alternation between two relatively invariant deep-water end-members; colder, low- $\delta^{18}O_{dw}$ and warmer, high $\delta^{18}O_{dw}$ conditions, which suggests the changing local dominance of northern-sourced NADW versus southern-sourced AABW (Skinner and Shackleton, 2004). The benthic $\delta^{18}O$ results of Martrat et al. (2007) from other Iberian Margin cores are consistent with this view and correlate with the air temperature profiles in Antarctica. Depleted $\delta^{13}C$ values in the North Atlantic documenting entrances of AABW in the North Atlantic were found not only during glacials, but within the short-term cooling stages of interglacials. The $\delta^{13}C$ records of Pahnke and Zahn (2005) from the southwest Pacific are interpreted by the authors as showing swings between northern and southern source water influence at the site with enriched values showing enhanced AAIW production. Pahnke and Zahn (2005) interpret the relationship between the Iberian Margin $\delta^{13}C$ record (AABW influence represented by depleted $\delta^{13}C$) and the southwest Pacific $\delta^{13}C$ record (enhanced AAIW represented by enriched $\delta^{13}C$) as anti-phased. In two South Atlantic cores, TN057-21 and RC11-83, depleted $\delta^{13}C$ interpreted as decreased NADW influence at the sites which correlates with the Iberian Margin records. The eastern Pacific record E11-2 appears as a boundary site where there are no clear swings between north-south influence (Ninnemann and Charles, 2002).

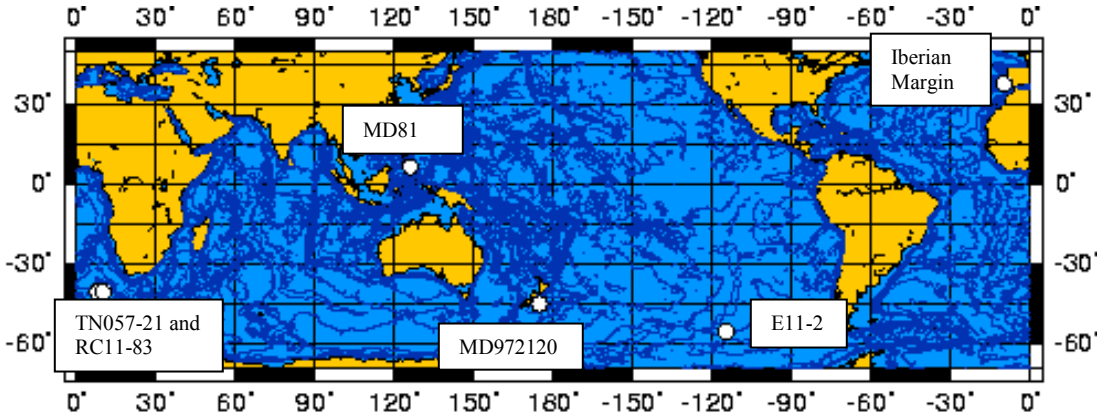

Figure 5-4: Locations of south Atlantic cores TN057-21 (Ninnemann and Charles, 2002) and RC11-83 (Charles et al., 1996), south Pacific cores E11-2 (Ninnemann and Charles, 2002) and MD972120 (Pahnke and Zahn, 2005), Iberian Margin cores and MD81 in the western tropical Pacific.

The western tropical Pacific now also fits this global picture. MD81 $\delta^{18}O$ benthic oscillations recorded in the western Pacific MD81 show warming of the Pacific Deep Water with a potential reduction of salinity coinciding with warming over the Antarctic continent and enhanced AAIW and AABW production. Colder/more saline Pacific Deep Water and Antarctic air temperatures appear to coincide with increased influence of NADW in the southern hemisphere. There are still some chronological uncertainties, but a growing number of studies now link the oceanographic changes seen in the Atlantic and the Pacific to the ice core records of swings in air temperature over Greenland and Antarctica. The MD81 planktonic and benthic data display the anti-phased relationship associated with a bi-polar seesaw oceanographic behavior throughout MIS3. The planktonic $\delta^{18}O$ and SST record Northern Hemisphere and monsoon climate shifts. The benthic $\delta^{18}O$ excursions appear concurrent with changes in conditions over the Antarctic continent as recorded by ice cores and, in combination with other marine records, form a coherent pattern of deep and intermediate water shifts in the Southern Ocean that now also includes the western Pacific warm pool.

5-5. Southern Ocean origin of abrupt climate change?

Ahn and Brook (2007) found that CO_2 concentrations and Antarctic temperatures were positively correlated over millennial-scale climate cycles, implying a strong connection to Southern Ocean processes. Atmospheric CO_2 concentrations are influenced by oceanic dynamical and biological processes in the Southern Ocean (Russell et al., 2006). Figure 5-5 shows a comparison of the MD81 benthic $\delta^{18}O$ with the Antarctic atmospheric temperature and CO_2 history from Byrd Station.

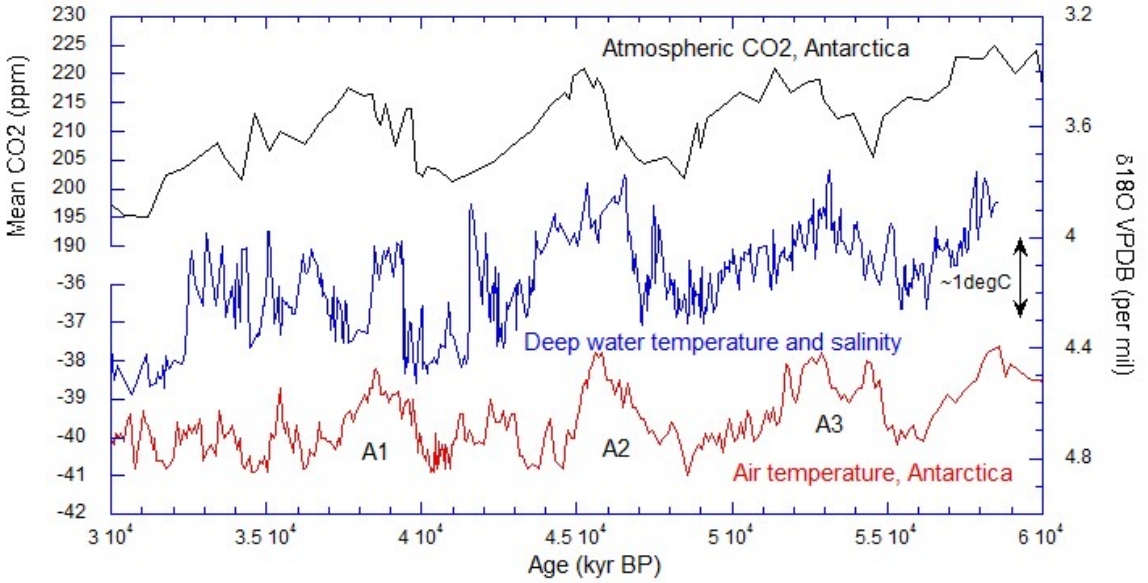

Figure 5-5: Byrd $\delta^{18}O$, Byrd atmospheric CO2 and MD81 *U hispida* $\delta^{18}O$ plotted with respect to the GISP2 age scale of Blunier and Brook (2001) and Ahn and Brook (2008).

The atmospheric and deep water temperatures for events A3 and A2 appear to begin warming and reach peak values in advance of rising CO_2. However, this observation is dependent upon the accuracy of the deep sea and Antarctic age models and, for example, does not appear to hold for event A1, where the correlation between the MD81 benthic record and Antarctic air temperature is also poorer. If these age models are correct it would imply that changing temperatures in the Southern Ocean

were involved in producing the observed CO_2 changes. The Southern Ocean is the meeting point for the Pacific, Atlantic and Indian Oceans. The strong westerly winds drive the Antarctic Circumpolar current and the resulting divergence drives upwelling. Due to the sloping isopycnals and the tendency for water masses to mix along these isopycnals, water at depths of up to 2-3km can be ventilated to the surface (Russell et al., 2006). Therefore climate signals originating in the Southern Ocean can be amplified and transmitted globally via the ACC and the atmosphere. More details of the extent of regional variability within Antarctica are now beginning to appear. Fischer et al. (2007) presented evidence for large changes in the flux of non-sea salt Ca, a proxy for the strength of winds carrying dust from Patagonian to the EDML site. There is a strong correlation between the EDML air temperatures and the dust source wind strength during Antarctic warm/cold events. The large changes in dust indicate changes in the westerly winds strength just before the air temperatures began to increase. Regional changes in the westerly wind strength and corresponding changes in sea ice extent may have resulted in reduced stratification of the Southern Ocean and greater exchange of CO_2 from the ocean to the atmosphere. Against a background of increasingly glacial climate on the way towards the LGM and of changing orbital and solar forcing, regional changes such as wind strength around Antarctica may be significant to the onset of abrupt climate change events on these millennial-timescales.

Chapter 6: Conclusions

There was close temporal correspondence between the MD81 planktonic $\delta^{18}O$, Mg/Ca SST and $\delta^{18}O_{water}$ variations and temperature changes over Greenland during MIS 3. Sea surface temperatures and salinities in the western Pacific also corresponded to a record of varying strength of the Asian Monsoon. The MD81 results indicate higher salinities and colder SSTs in the WPWP during the Greenland stadials of MIS3. This tropical behavior appears to reflect a southerly migration of the ITCZ together with a weakened East Asian summer monsoon and decreased summer precipitation.

In contrast to the planktonic record from MD81, the benthic $\delta^{18}O$ record from this core documents large millennial-scale oscillations that correlate closely with the Antarctic surface temperature history and reflect shifting deep water temperatures and perhaps salinity and minor glacial-eustatic changes. Such changes in deepwater properties are interpreted to reflect changes in the source water temperatures (and perhaps salinity) at the site where Upper Circumpolar Deep Water forms in the Antarctic Ocean.

The surface and the deep water climate signals (adjusted for travel time) in the MD81 are out of phase during MIS3. These combined planktonic and benthic records from MD81 thus provide both northern and southern hemispheric climate records and verify the anti-phased relationship associated with a bi-polar seesaw oceanographic behavior throughout MIS3. There are still some chronological issues to be resolved, but a growing number of studies link oceanographic changes seen in the Atlantic and the Pacific to the swings in air temperature over Greenland and Antarctica and the data

from MD81 fit this interpretation. The origin of abrupt climate swings during MIS3 remains unclear but the fact that the deep Pacific was undergoing contemporaneous changes in temperature with those in Antarctica implicates the Pacific as a major factor in the large scale climate oscillations during the last glacial.

Chapter 7: Introduction

Project II is a record covering the past two millennia of Mg/Ca and $\delta^{18}O$ measurements on planktonic, and $\delta^{18}O$ measurements on benthic foraminifera from two continuous marine cores taken from high sedimentation sites in the Western Pacific Warm Pool.

7-1. Western Pacific Warm Pool and teleconnections

The Western Pacific Warm Pool (WPWP) is one of the warmest regions in the world oceans and an important center of atmospheric convection which impacts global heat and water vapor exchange between the ocean and atmosphere. Changes in sea surface temperatures and convection in this region create interannual to decadal climate variability, such as El Nino Southern Oscillation (ENSO), Indian Ocean Dipole (IOD) and Pacific Decadal Oscillation (PDO) (Ashok and Saji, 2007, Cane, 1998, D'Arrigo and Wilson, 2006, Hoerling et al., 2001, Sun et al., 2003). ENSO is a global coupled ocean-atmosphere phenomenon associated with floods, droughts, and other disturbances in a range of locations around the world. The Indian Ocean Dipole (IOD) is a coupled ocean-atmosphere phenomenon in the Indian Ocean and is normally characterized by anomalous cooling of SST in the south eastern equatorial Indian Ocean and anomalous warming of SST in the western equatorial Indian Ocean (negative dipole mode). Associated with the positive dipole mode, the normal convection situated over the eastern Indian Ocean warm pool shifts to the west and brings heavy rainfall over the east Africa and severe droughts/forest fires over the Indonesian region. The anomalous

SSTs are found to be closely associated with changes in surface winds, and positive IOD events have been found to amplify the ENSO-induced dryness over the Indonesian region (Ashok et al., 2001, Ashok et al., 2004). The Pacific Decadal Oscillation (PDO) is a pattern of Pacific climate variability that shifts phases on at least inter-decadal time scales, usually ~20-30 years. The PDO is detected as warm or cool surface waters in the Pacific Ocean, north of 20° N. During a "warm", or "positive", phase, the west Pacific becomes cool and part of the eastern ocean warms; during a "cool" or "negative" phase, the opposite pattern occurs. The teleconnections of the western tropical Pacific to other regions around the globe are also enhanced through climate components such as the East Asian Monsoon (EAM) and the Intertropical Convergence Zone (ITCZ). Mindanao and the Sulawesi Sea are located in the northern part of the Asian-Australian monsoon region where increased precipitation during the summer months is the result of the increased influence of the ITCZ as part of the East Asian Monsoon (EAM) (Gordon, 2005).

7-2. Climate of the past two millennia

Prominent climate events which occurred during the past 1,000 years were the Medieval Warm Period (MWP), which can broadly be defined as the time period between ~800 to ~1170 A.D., followed by the Little Ice Age (LIA; ~1300 to ~1850 A.D). MWP was a time when radiative forcing was high, whereas the LIA epoch includes the Maunder Minimum of anomalously low solar activity (~1645-1715) (Lean et al., 1995). Both events have been well documented in mid to high latitude historical records (Lamb, 1995) and there is now also a coherent picture of a cooler Northern

Hemisphere during the LIA from mid-to high latitudes from marine core, tree ring, and historical data, records of glacial advances and Greenland cooling (Bradley and Jones, 1993, Broecker, 2001, Hoffmann et al., 2001, Hughes and Diaz, 1994, Kreutz et al., 1997, Mann and Bradley, 1999). The northern subtropical sea surface temperatures were an estimated -0.7C lower during the LIA and ~0.6C warmer during the short warm period in the medieval (Hoffmann et al., 2001). For the southern hemisphere, ice cores from Siple Dome, West Antarctica, showed increased atmospheric circulation intensity in the polar South Pacific at ~1400 A.D., the beginning of LIA, corresponding with cooler temperatures in the North Atlantic and central Greenland (Kreutz et al., 1997). The LIA was characterized by substantial meridional circulation strength variability (Kreutz et al., 1997). Results from the study of several East Antarctic ice cores (Talos Dome, Dome C EPICA, South Pole and Taylor Dome) suggest cooler climate conditions between the middle of 16th and the beginning of 19th centuries, which might be related to the LIA cold period. The strongest LIA cooling was not temporally synchronous over East Antarctica due to the high degree of geographical variability observed there (Stenni et al., 2002). A marine stable isotope record from the nearshore Antarctic continental shelf showed rapid (<20 years) Palmer Deep bottom water temperature fluctuations of 1-1.5°C associated with oscillations between a warmer, stable Upper Circumpolar Deep Water (UCDW) state and a cooler, variable shelf water state between 3.6 and 0.05 ka (Shevenell and Kennett, 2002). Cool shelf water intervals correlate with the Little Ice Age (Shevenell and Kennett, 2002). The authors interpreted this as sensitivity of the western Antarctic Peninsula hydrography to westerly wind strength and/or position of the Southern Hemisphere westerly wind field, suggesting

this as the control mechanism over thermohaline reorganization. Similar results were found from Lago Guanaco, located directly east of the southern margin of the South Patagonian Ice field, showing the LIA as a period dominated by intense westerly flow, increased precipitation, and highly evaporative conditions indicating regional climate changes due to the intensification of the westerlies during the LIA, accompanied by a poleward shift in the southern margin of the wind field (Moy et al., 2008).

The manifestation of the LIA in the tropics is interpreted to be a southern displacement of the Inter-tropical Convergence Zone due to a cooler Northern Hemisphere, with drier conditions north and wetter conditions south of the equator. The East Asian and Asian Monsoon have also been found to fit this picture, with the summer monsoon strength decreasing with decreased Northern Hemisphere temperature and Alpine glacial advance (Zhang et al., 2008). The Asian summer monsoon was strong during Europe's MWP and weak during Europe's LIA (Zhang et al., 2008). Calibrated rainfall records from the East Asian Monsoon region show multi-centennial variability, with notable dry periods occurred at 1.4–1.0 ka and during the Little Ice Age (Hu et al., 2008). Cariaco Basin sediments suggest increased aridity during the LIA (Haug et al., 2001) along with decreased sea surface temperatures and higher salinities in the Caribbean Sea (Watanabe et al., 2001). Lake Titicaca in South America (Baker et al., 2001) records enhanced precipitation that coincides with a maximum in lake levels occurring at Lake Naivasha, Kenya during the LIA (Verschuren et al., 2000). A 1,000-year sea surface temperature and salinity record from WPWP showed a long-term cooling and freshening trend during the Little Ice Age, with more arid conditions in the northern tropics and wetter conditions in the southern tropics (Newton et al., 2006).

This study continues the work on the decadal to centennial–scale variability in this climatically important region with a 2,000 year-long climate record from two cores in the Western Pacific Warm Pool, placing the more abrupt climate changes of the last millennia in the context of a longer record. $\delta^{18}O$ measurements for planktonic and benthic foraminifera, and Mg/Ca for planktonic foraminifera are presented from continuous marine cores taken from high sedimentation sites in the WPWP.

The question has also remained of whether the abrupt anti-phased climate oscillations, known as the bipolar seesaw, recorded during the Last Glacial period (see Project I, Chapters 1-6) carried on into the Holocene as well, with the Little Ice Age and the Medieval Warm Period as potential manifestations of the bipolar seesaw in the Holocene (Denton and Broecker, 2008). On the basis of Northern Hemisphere records such as the ratio of iron-stained to clean grains in ice-rafted debris in North Atlantic deep-sea sediments, Bond et al. (2001) argue that climatic conditions have oscillated steadily over the past 100,000 years with an average period close to 1500 years. However, the spatial variability in Antarctic ice core records obscures any evidence of seesaw behavior. Due to the ideal location of marine core MD81, where both northern and southern hemisphere climate signals are present, it is possible to investigate if a bipolar seesaw existed during the Holocene.

Chapter 8: Regional setting and oceanography

Marine cores MD98-2181 (MD81) and MD98-2177 (MD77) (Figure 8-1, 8-2) were collected aboard the *Marion Dufrense* in 1998 as part of the IMAGES coring program. At 6.3°N, 125.83°E MD81 is located in the Morotai Basin in the western tropical Pacific at a water depth of 2114m. MD77 was cored from 968m water depth on the edge of the Sulawesi Sea (also known as Celebes Sea) at the entrance to the Makassar Strait (1.4°N, 119°E).

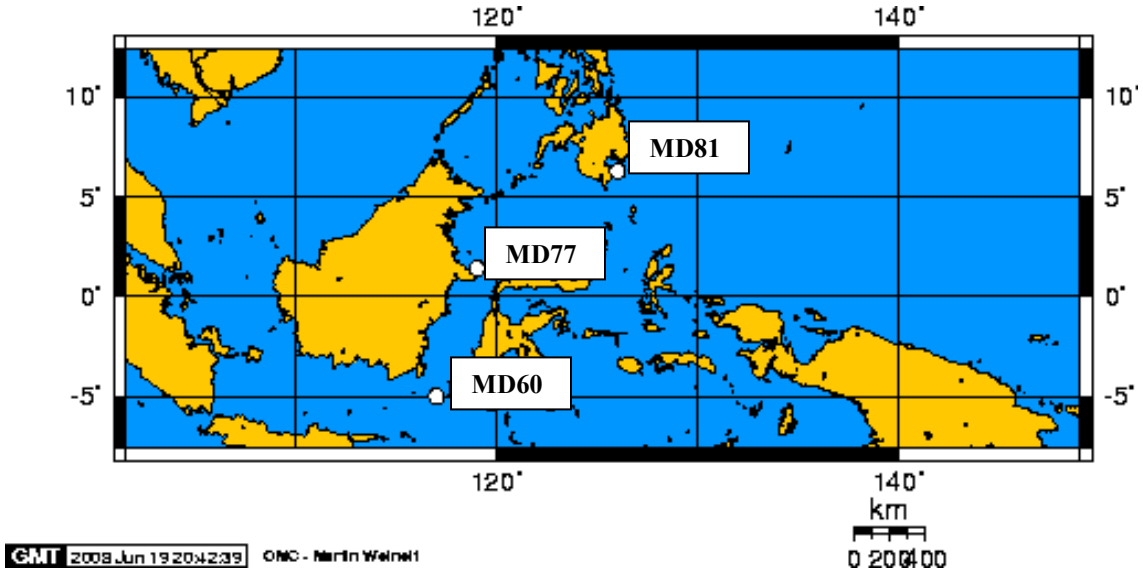

Figure 8-1: Map showing study area with locations of *Marion Dufrense* cores MD81 and MD77 (this study) and MD60 (Newton et al., 2006, see Chapter 10: Results).

Surface temperatures within the warm pool today are in excess of 28°C giving rise to the strong atmospheric convection over the region that drives large scale atmospheric circulation between the tropics and subtropics. Westward currents and the trade winds funnel seawater warmed by exposure to tropical sunlight into the WPWP region. As the western Pacific is very warm and sea surface temperatures on the eastern

end of the Pacific are relatively cool (~20^{o}C) for such low latitudes, a large sea surface temperature (SST) gradient exists along the equatorial Pacific (Pichat et al., 2004). During the northern summer, SSTs in the western Pacific warm pool average 29° to 30°C and the sea surface salinities (SSS) range annually between 33.25-34.0‰ (Gordon, 2005). In winter, SSTs cool to 27° to 26°C. Precipitation is highest in summer, with roughly 80% of annual rainfall occurring between June and October. Rainfall averages between 300 and 400 mm/month during summer and between 50 and 100 mm/month during winter. The annual precipitation pattern is tied to the migration of the Intertropical Convergence Zone (ITCZ) over the site, and the timing of the northern monsoon. The winds over the Indonesian maritime continent are directed towards Asia in the boreal summer (July to September) and towards Australia in the boreal winter (January to March) (Gordon, 2005). During El Niño and La Niña, the western tropical Pacific experiences dramatic differences in precipitation. Because of its great topographic relief and active tectonics, this region contributes large amounts of water, solutes, and sediment to the coastal ocean (Nittrouer et al., 1995). The Luzon Strait (Figure 8-2) inflow delivers low salinity water into the surface layer of the Indonesian seas at Sulawesi Sea, with additional fresh water introduced through regional rainfall and river runoff (Gordon, 2005). Regional flow has complexities below the surface. The major surface currents in the western Pacific region are the North Equatorial Current (NEC), the North Equatorial Counter Current (NECC), and the South Equatorial Current (SEC). A branch from the Mindanao Current (an eddy, Figure 8-2) flows into the Sulawesi Sea and is among the currents supplying water to the Indonesian Seas (Fine et al., 1994). Water from the Sulawesi Sea then flows south into the Makassar

Strait, which is the primary pathway for surface flow from the Pacific to the Indian Ocean (Gordon and Fine, 1996). The sill depth of the Sangihe Ridge (Figure 8-2) between the Pacific and the Sulawesi Sea is 1350m (Gordon et al., 2003) compared to MD77 at 968m water depth. Therefore the flow reaching site MD77 is not affected by the sill. At a depth of 1350m the source water for the Throughflow is the low-salinity, well ventilated North Pacific Thermocline Water (NPTW) (Gordon and Fine, 1996) (Figure 8-2). NPTW is comprised of North Pacific Tropical Water, (Remnant) North Pacific Subtropical Mode Water from the western subtropical gyre (~28°N), and North Pacific Intermediate Water (Fine et al., 1994).

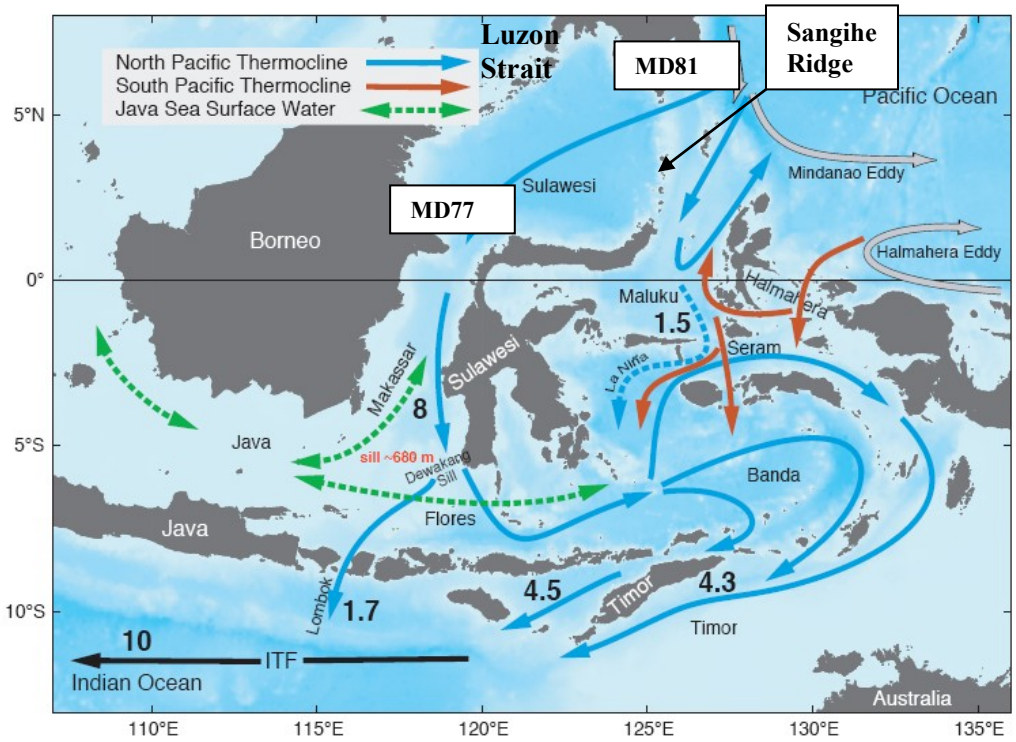

Figure 8-2: Map showing the Indonesian Throughflow circulation and locations of MD81, MD77, the Sangihe Ridge and the Luzon Strait in northern Sulawesi Sea. North Pacific Thermocline flows in blue, numbers indicate flow in Sv. Modified from Gordon, 2005.

Chapter 9: Materials and methods

This is a briefer description of the methodology as the procedure followed is identical for Projects I and II. For the more detailed description, please see Chapter 3.

Marine sediment samples were disaggregated using Sodium Hexameta Phosphate in solution. Once disaggregated, the sediments were wet-sieved through a 63µm mesh to remove the clay fraction. The >63µm fraction was then dry-sieved, and foraminifera were picked from the >180µm size fraction. *Globigerinoides ruber* (white) is a surface dwelling planktonic foraminifera which is abundant in the warm summer surface waters of the Western Tropical Pacific. The benthic foraminifera *Uvigerina hispida* and *costata* have a shallow infaunal and *Cibicidoides wuellerstorfi* an epifaunal habitat. The foraminifera were cleaned according to the following protocol designed to remove clays and other impurities. The foraminiferal shells were cracked between two glass plates under the microscope to open the tests. The tests were then rinsed with DIW, Methanol, hot alkaline oxidative cleaning using buffered hydrogen peroxide and a leach with 0.001 M nitric acid. During each of the rinses the vials were sonified to dislodge debris from the shells. The cleaned *G. ruber* samples were split for isotope and Mg/Ca measurements. This ensured that isotopic and minor element measurements were made on the same samples of cleaned calcite, and eliminated potential discrepancies due to the effects of different cleaning methods on measured Mg/Ca and $\delta^{18}O$. For Mg/Ca the sample is dissolved in 500 µL of 1M nitric acid and analyzed on a Jobin Yvon ICP AES. Each sample measurement was bracketed with a standard that is made from solid Mg and reagent grade $CaCO_3$ in an elemental ratio of 5.62mmol/mol,

and the sample value is adjusted by the standard deviation of the two bracketing standards to correct for within and between run instrument drift (see Chapter 3, Section 3-5 for equation). The average sample-standard deviation was 0.04mmol/mol. The Anand et al. (2003) equation based on planktonic foraminiferal species including *G. ruber* (white) with an accuracy of ±1.2°C was used to calculate sea surface paleotemperatures (SST). Ratios of Fe/Ca, Mn/Ca and Al/Ca serve as indicators of potential contamination of Mg/Ca measurements by Mg-bearing clays and/or authigenic encrustations. The amount and composition of terrigenous input and the presence of authigenic phases (such as Mn-Fe-oxides, pyrite, and secondary minerals such as ferric oxyhydroxides) affect the Mg/Ca paleothermometry. Contamination and dissolution artifacts have been ruled out as major controls on the Mg/Ca variability observed in MD81 and MD77 by reference to Fe and Mn concentrations, none of which show a consistent positive correlation with planktonic Mg/Ca. For stable isotopic measurements the samples were analyzed on a VG Prism II stable isotope ratio mass spectrometer equipped with a common acid bath acidification system. Approximately 30 foraminiferal samples are run sequentially on the mass spectrometer along with approximately 10 Ultissima marble standards that are used to monitor the analytical precision. The precision of the Ultissima standard $\delta^{18}O$ is 0.06‰ for the present study with a 1σ of 0.08‰ over 8 runs. For the $\delta^{18}O_{SW}$ calculations the equation of Bemis et al. (1998) is used. The age models for cores MD77 and MD81 are based on three and five AMS dates, respectively, of planktonic foraminifera *G. sacculifer* (see Table 9-1).

Sample code	Lab code	^{14}C age	+/-	Calibrated Age (BP)	Lower range	Upper Range	Calendar Age
MD77 12cm	os-38302	395	240	0			1950 A.D.
MD77 109cm	os-38335	1870	272	1360	1055	1646	590 A.D.
MD77 212cm	os-38373	3760	175	3607	3389	3817	1657 B.C.
MD81 12cm	os-36493	580	110	149	50	231	1801 A.D
MD81 55cm	os-37308	815	200	353	185	525	1597 A.D.
MD81 99cm	os-37292	1010	100	537	471	624	1413 A.D.
MD81 145cm	os-37306	1090	120	595	498	677	1355 A.D.
MD81 238cm	os-36485	1900	100	1376	1277	1478	574 A.D.

Table 9-1: AMS results for cores MD77 and MD81 on planktonic foraminifera *G. sacculifer*.

Chapter 10: Results

The oxygen isotope and Mg/Ca paleothermometry results for MD77 planktonic *G. ruber* and the oxygen isotope data for MD77 benthic *U. hispida* and *U. costata* are shown in Figures 10-1 and 10-2 below plotted against depth in core. The $\delta^{18}O$ and Mg/Ca data for MD81 *G. ruber* and oxygen and 13C isotope data for epifaunal benthic *C. wuellerstorfi* is shown in Figures 10-3 and 10-4 also with respect to depth in core. Section 10.1 discusses the planktonic, and section 10.2 the benthic records.

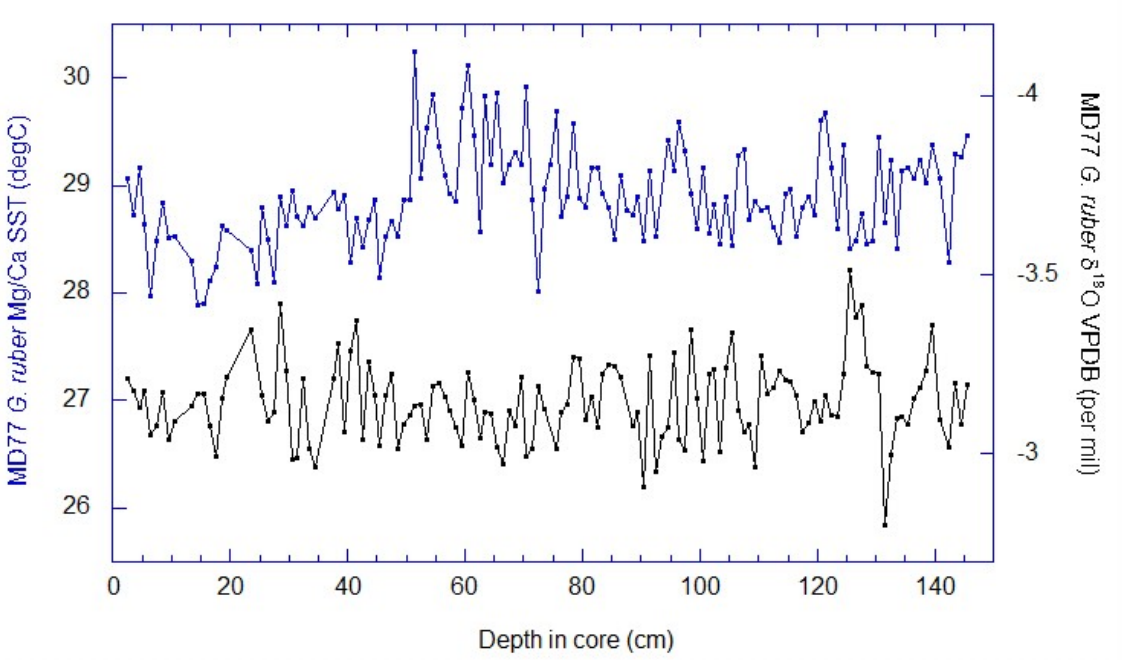

Figure 10-1: MD77 *G. ruber* Mg/Ca sea surface temperature and δ^{18}OVPDB plotted with respect to depth in core.

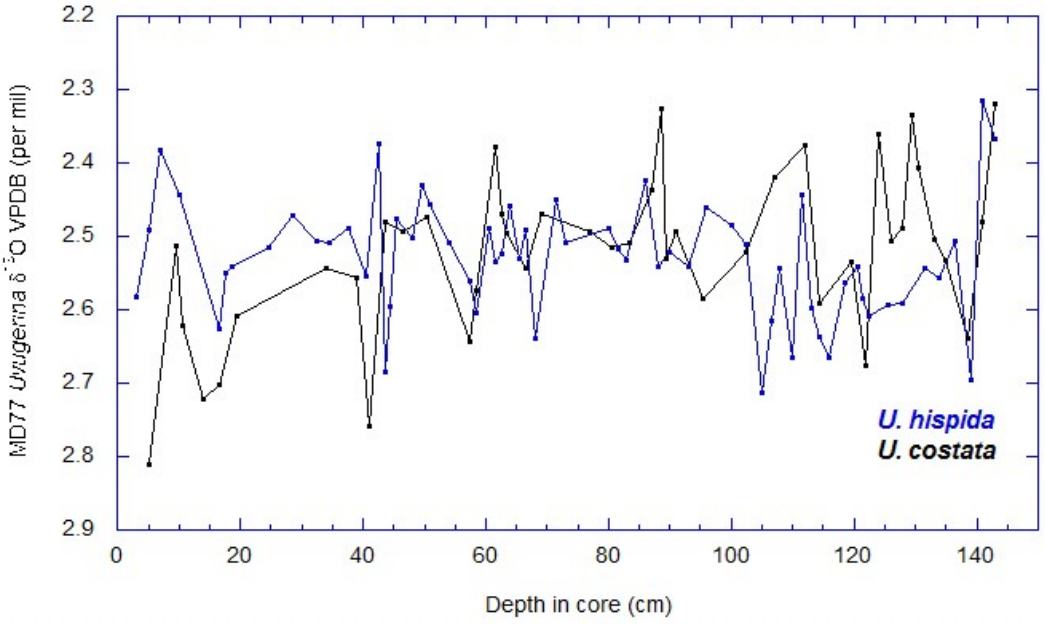

Figure 10-2: MD77 *U. hispida* and *U. costata* $\delta^{18}O$ VPDB plotted with respect to depth in core.

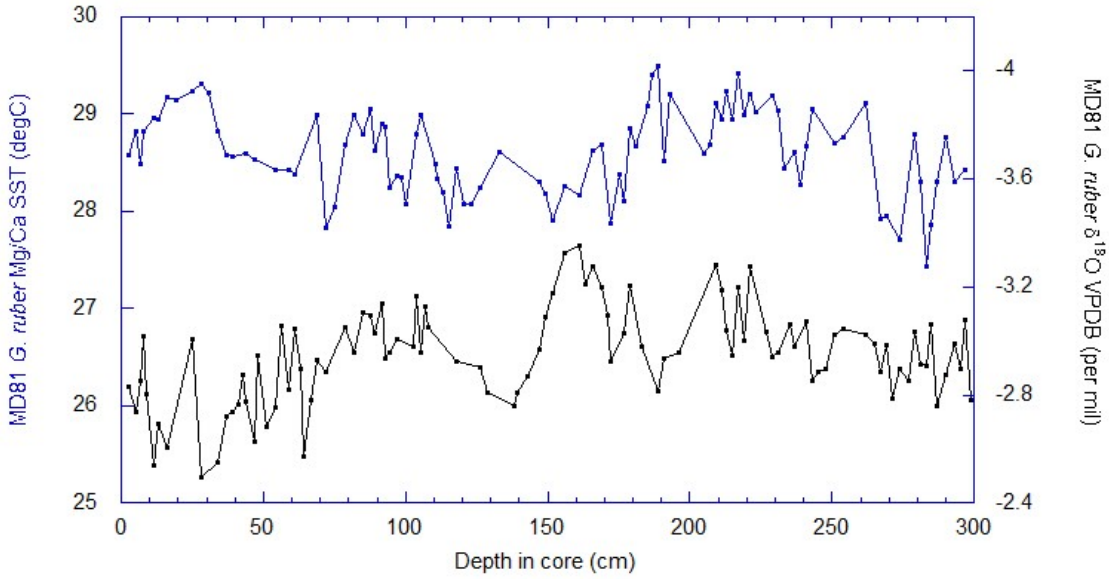

Figure 10-3: MD81 *G. ruber* Mg/Ca sea surface temperature and $\delta^{18}O$ VPDB plotted with respect to depth in core.

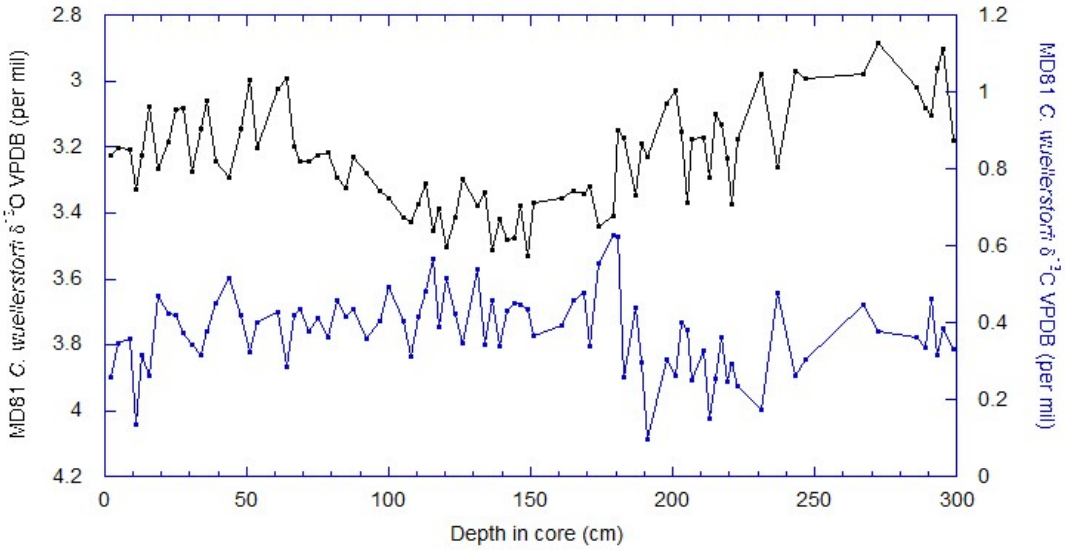

Figure 10-4: MD81 *C. wuellerstorfi* δ^{18}O VPDB δ^{13}C VPDB plotted with respect to depth in core.

10-1. Planktonic – Warm Pool surface changes

The surface water results for cores MD77 and MD81 are presented in Figure 10-5 on their respective age models. Data from core MD60 (Newton et al, 2006) is also included for comparison, and shows a close correlation with MD77 results. Centennial scale oscillations are evident in the SST and δ^{18}Oc records of both MD77 and MD81. For the time period of ~900-1800yrBP both cores record similar centennial scale oscillations about a mean sea surface temperature of ~29°C. Site MD81 records approximately 0.5°C cooler temperatures between ~1800-2200yrBP. For the last millennia the sites also differ in their sea surface temperature. Site MD81 appears to record lower SSTs by ~1°C during the time of Medieval Warm Period compared to MD77. Between 100-300 yrBP MD81 records warmer temperatures than MD77 by approximately 0.5°C. In the oxygen isotope records, the sites also differ with site MD81 tending towards more enriched values between 1500-2000yrBP by ~0.2‰.

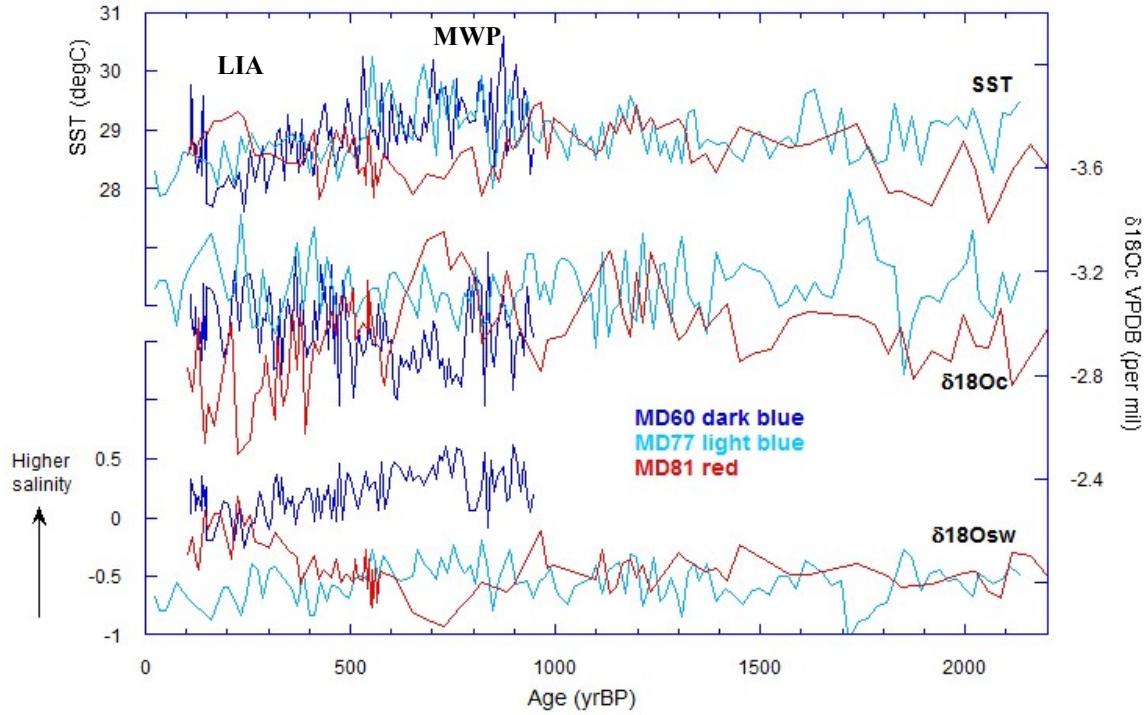

Figure 10-5: Surface records for cores MD81 and MD77 (this study) and MD60 (1kyrBP record, Newton et al., 2006) showing planktonic δ^{18}Oc, δ^{18}Ow and sea surface temperature changes for 2kyrBP.

For the δ^{18}Oc data, MD77 shows a large excursion of ~0.6‰ centered at 1800yrBP which is not evident in the MD81 record. The δ^{18}Oc of the two cores also differ during the last 800yrBP with a clear trend towards enriched isotope values at MD81 and a shift towards depleted values at MD77 resulting in an offset of ~0.4‰ between the sites. The δ^{18}Osw record is fairly constant for the time period 1000-2000yrBP for MD81, with no great changes in salinity observed. A trend implying a shift towards more saline conditions starts at 700yrBP. MD77 shows a more varied δ^{18}Osw record with a large excursion towards fresher conditions from 1900yrBP to 1700yrBP. In general due to the higher resolution of MD77 the higher frequency

variability in the salinity is apparent in the δ^{18}Osw record here. MD77 δ^{18}Osw shows a trend towards fresher conditions starting around 900yrBP.

The freshening and cooling trend over the past 1kyr seen in MD77 is also evident in MD60 (Newton et al., 2006) but MD81 appears to have an opposing trend. This new MD81 planktonic record also has several differences when compared to the previously published MD81 data of Stott et al. (2002) as shown in Figure 10-6. There is good correlation between the δ^{18}Oc records from 100-600yrBP with the new data appearing less noisy. However, the present study δ^{18}Oc record shows consistently more depleted values starting at ~600yrBP for the remainder of the overlapping section as compared to the record of Stott et al. (2002). For Mg/Ca, the records show good correlation from 100-600yrBP and 900-2000yrBP, but transitioning at 600yrBP as in the δ^{18}Oc record, the Mg/Ca-values are consistently lower for the new study than those in Stott et al. (2002) until 900yrBP. This coincides with the time of the Medieval Warm Period.

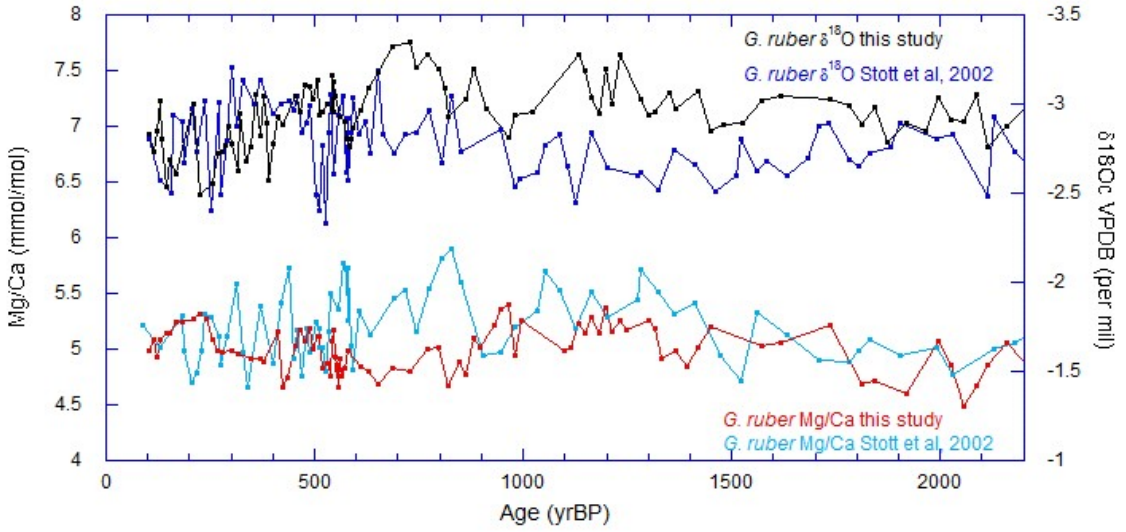

Figure 10-6: *G. ruber* δ^{18}Oc VPDB (per mil) and Mg/Ca (mmol/mol) for core MD81 from the present study and from Stott et al. (2002).

The reason for these discrepancies is not clear. The sample size for the present study was very small. Resolution of the new record was high from 100-600yrBP which is where these replicate records (the present study and Stott et al., 2002) agree, and low in the following 600-900yrBP (MWP) section. Therefore size bias may have been introduced through juvenile or morphotype effects due to the small sample size of the present study. Changes to the foraminifera cleaning method have also been introduced since the 2002-study; the foraminifera shells for the present study are cracked open during the cleaning procedure to more thoroughly check for and remove impurities. Since there was a failure to replicate the results, the Stott et al. (2002) record is considered to be more reliable for this section of the record due to a larger sample size.

10-2. Benthic – North Pacific Thermocline and Pacific Deep Water changes

The benthic results for MD77 and MD81 are presented in Figure 10-7 on their respective age models. MD77 benthic $\delta^{18}O$ from *U. hispida* and *U. costata* record multicentennial-scale oscillations on the order of ~0.2‰ and about a mean value of ~2.5‰ during the past 2000yrs. This reflects changes in the North Pacific Thermocline Water which flows into the Sulawesi Sea. MD81 shows a large, what appears to be a millennial-scale, oscillation spanning ~400-1400yrBP. The $\delta^{18}O$ of *C. wuellerstorfi* becomes enriched by ~0.4‰ reaching values of 3.5‰ at ~600yrBP suggesting a significant cooling or/and increase in salinity of the Pacific Deep Water reaching MD81. This trend then reverses and values reach back to ~3.1‰ by 400yrBP. Since ~400yrBP the trend appears to have once again reversed towards enriched values. There

is a moderate shift in the $\delta^{13}C$ of *C. wuellerstorfi* at ~1000yrBP, but overall there is little change in the $\delta^{13}C$ of the Pacific Deep Water reaching site MD81. Unadjusted MD81 benthic $\delta^{18}O$ values for *C. wuellerstorfi* cover a range of 2.3-2.9‰ with a mean value of ~2.5‰. This general range is in agreement with late Holocene values of ~2.5-2.91‰ recorded within a depth range of 1980-2335m in the North West Pacific (Keigwin et al., 1992, Keigwin, 1998).

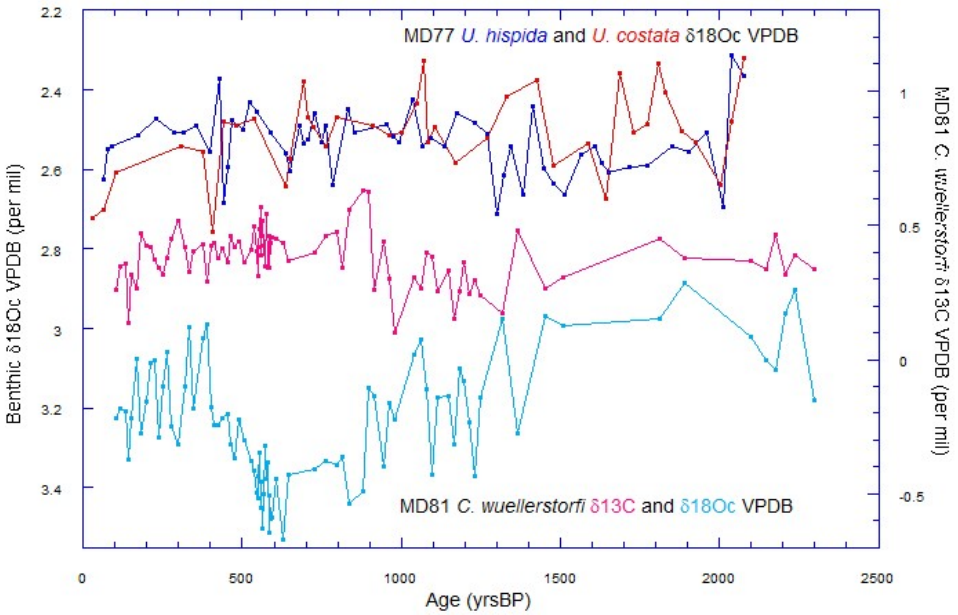

Figure 10-7: Record of North Pacific Thermocline Water (MD77) and Pacific Deep Water (MD81) changes for 2kyrBP. MD77 $\delta^{18}Oc$ data for *U. hispida* (dark blue) and *U. costata* (red), MD81 $\delta^{18}Oc$ (pink) and $\delta^{13}C$ (light blue) data for *C. wuellerstorfi*.

Chapter 11: Discussion

11-1. Planktonic - ITCZ migration and hydrologic changes

As shown by marine sediment records from MD77 and MD81, the climate of the western Pacific warm pool during the last two millennia exhibited centennial scale variability, potentially modulated by the decadal and interannual forcing mechanisms present in the tropics.

During 1000-2000yrBP, the MD77 planktonic $\delta^{18}O$ record shows a shift towards fresher conditions between 1700-1900yrBP which was not evident at site MD81 (Figure 10-5). As MD77 is located in the Sulawesi Sea near the Luzon Strait, which today supplies fresh water to the Sulawesi Sea (Gordon, 2005), it is possible that site MD77 is recording a large localized freshwater input episode.

Previous centennial-scale records from the Western Pacific Warm Pool at the southern end of the Makassar Straits have shown a shift towards fresher and cooler surface conditions during the last millennia (Newton et al., 2006, Stott et al., 2002). This was thought to occur due to the southerly migration of the ITCZ during the LIA, part of a global signal of dry conditions in the northern tropics and wetter conditions in the southern tropics. Core MD77, located at the entrance of the Makassar Straits, follows the sea surface temperature, $\delta^{18}O$ and $\delta^{18}Osw$ trends seen at MD60 (Figure 10-5). Therefore it would appear that MD77 was also influenced by higher precipitation and cooler surface temperatures due to the ITCZ shift.

Site MD81, however, appears to record an opposing shift in the $\delta^{18}O$, SST and therefore $\delta^{18}Osw$ to cores MD77 and MD60, showing a trend towards higher salinity conditions during the LIA (Figure 10-5). However, as discussed previously in Section 10-1, this new record from MD81 is in disagreement in parts over the last 1000yrBP with the previously published MD81 record of Stott et al. (2002). The reasons for this discrepancy are still not clear and therefore no definitive conclusions are made on this new MD81 planktonic record on the climate of the past millennia.

11-2. The Warm Pool and Northern Hemisphere climate

In Figure 11-1 an Indo-Pacific Warm Pool composite sea surface temperature record from cores MD60 (Newton et al., 2006), MD81 (Stott et al., 2002) and MD77 (this study) is plotted against a Northern Hemisphere temperature anomaly record (here 10-point smoothed, Moberg et al., 2005). The MD77 data points include an uncertainty of ~0.12%. The general trends of these temperature records are similar. However, there are also differences between the two records such as the times of peak warming and cooling associated with the LIA and MWP, which in the case of the LIA differs by ~200yrs. MWP appears as the warmest and LIA as the coolest sea surface temperatures recorded in the Warm Pool over the last 2ka (note the dataset is missing the last ~150yrBP).

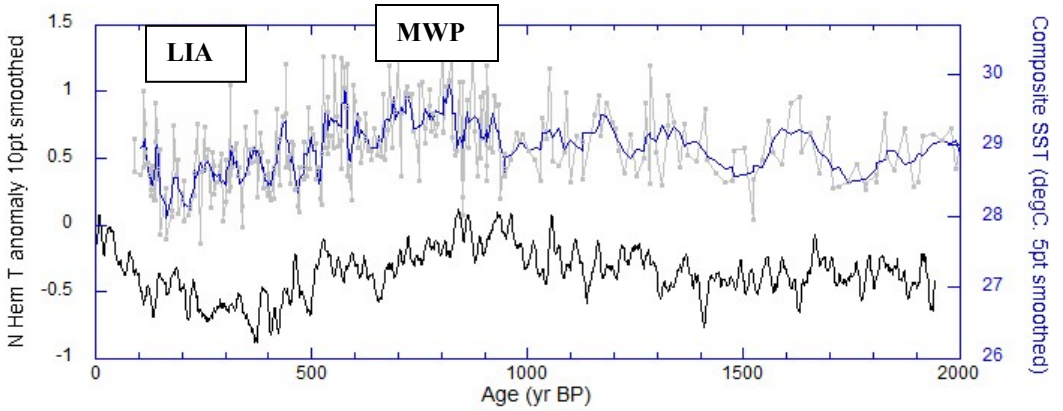

Figure 11-1: Composite 5-point running mean sea surface temperature record (°C) from MD81 (Stott et al., 2002), MD77 (this study) and MD60 (Newton et al., 2006) plotted against record of Northern Hemisphere temperature anomaly w.r.t. 1961–90 average (Moberg et al., 2005).

In Figure 11-2 δ^{18}Osw from core MD77 is plotted against stalagmite δ^{18}O records from Heshang Cave (recording the East Asian Monsoon variability, Hu et al., 2008) and Wanxiang Cave (recording Asian Monsoon variability, Zhang et al., 2008). The δ^{18}Osw of MD98-2177 shows large changes in sea surface salinity and hydrology over the past 2ka (where ~0.3-0.5‰ equals 1 psu), such as at 1.7-1.9kyrBP, compared to the present annual variation of <1psu (~33.25-34.0 psu, Gordon, 2005). There is an overall freshening trend over the last 1ka (as in core MD98-2160, Newton et al., 2006). No similar clear trend is apparent over last 1ka in the monsoon records (Hu et al., 2008 and Zhang et al., 2008). During the Holocene on shorter decadal- to centennial-timescales the clear warm pool-monsoon region connection seen during Marine Isotope Stage 3 (Project I) is no longer evident. Differences can also be seen between the monsoon records themselves (Figure 11-2).

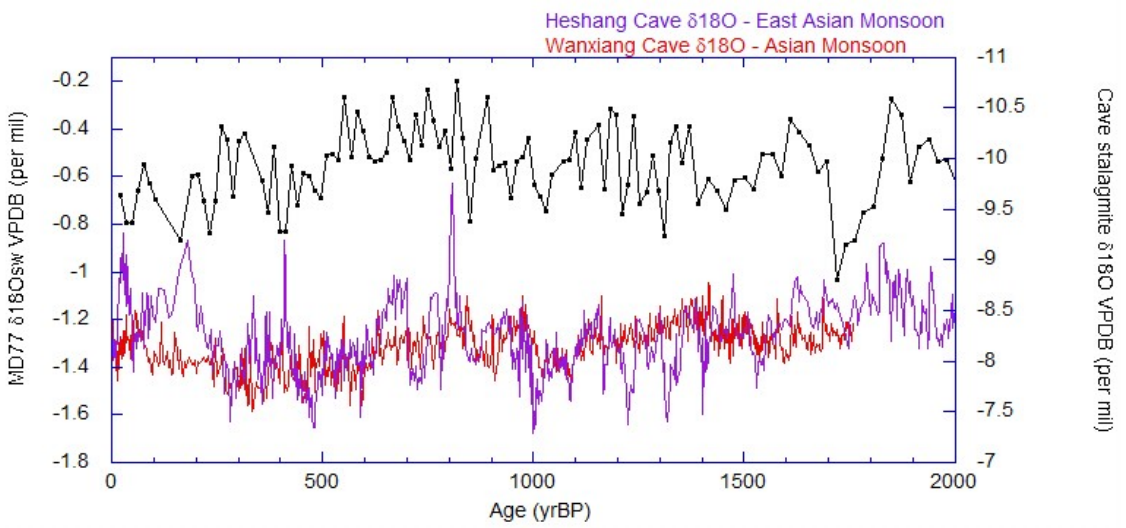

Figure 11-2: Speleothem δ^{18}Oc records from Heshang Cave (Hu et al., 2008, East Asian Monsoon variability) and Wanxiang Cave (Zhang et al., 2008, Asian Monsoon variability) and western tropical Pacific *G. ruber* δ^{18}Osw record at MD77.

11-3. Benthic record

11-3-1 MD77 – North Pacific Thermocline Water

The North Pacific Thermocline Water (which bathes site MD77) also exhibited centennial-scale variation which may have been due to changes in its source water conditions on these timescales (Figure 10-7). While today the water entering the Sulawesi Sea comes solely from the North Pacific Thermocline (Gordon and Fine, 1996), an alternative hypothesis for these oscillations in the MD77 benthic record may have been sporadic events of higher salinity South Pacific Thermocline Water input into the Sulawesi Sea.

11-3-2 MD81 – Bi-polar seesaw operating during the Holocene?

Located in the western tropical Pacific site MD81 is bathed in the southward returning Upper Circumpolar Deep Water (UCDW) or Pacific Deep Water. The UCDW flows between σ_θ=27.4-28.0 (Rintoul et al., 2001). The neutral density surface σ_θ =27.9 kg/m3 (relative to the 0m reference level) outcrops in the Southern Ocean near the Polar Front and attains a depth of about 2000m near the MD81 core location. Therefore the benthic foraminifera at MD81 record southern source waters, and in combination with the Northern Hemisphere record from the planktonic foraminifera, provide both hemispheric climate signals in a single location. During the last glacial period the Northern and Southern Hemispheres exhibited millennial-scale oscillations in temperature which were out of phase between the hemispheres (Blunier and Brook, 2001). A suggested explanation has been a weakening of deep-water formation in the north which was accompanied by a strengthening of deep-water formation in the south, commonly referred to as the bi-polar seesaw. Combined planktonic and benthic records from site MD81 during Marine Isotope Stage 3 (MIS3, ~30,000-60,000yrBP) provide northern and southern hemispheric climate signals which are out of phase as expected from the bi-polar seesaw behavior (Project I, chapters 1-6). However, an open question has remained about whether centennial scale oscillations observed during the Holocene (such as the Medieval Warm Period, ~1150-780yrBP, and the Little Ice Age, ~650-100yrBP) have been a continuation of this bipolar behavior. Most recently, Denton and Broecker (2008) discuss the possibility that the Atlantic's conveyor circulation varied on a millennial time scale also during the Holocene. Furthermore, this raises the important question of whether, as suggested by the bi-polar seesaw theory, these

Holocene events were anti-phased between the northern and southern high latitudes. However, to date there has been a scarcity of coherent records from the southern hemisphere. As with the MIS3 record from MD81, it is possible to address this pertinent question using this 2ka record and provide a glimpse of the phasing of the hemispheres during the Holocene. The water presently bathing site MD81 benthic foraminifera was last at the surface in the Southern Ocean approximately 1000 years ago (Stott et al., 2007). By offsetting the benthic (Southern Hemisphere signal) and planktonic (Northern Hemisphere signal) records by 1000 years we can assess if the tropics and Southern high latitudes were in or out of phase at this time.

In Figure 11-3 the MD81 benthic $\delta^{18}O$ record is plotted against the Vostok deuterium temperature anomaly (°C) (based on linear relationship between average annual surface T and snow deuterium content, slope $\delta D/T = 9‰/°C$, Lorius et al., 1985). From ~1600yrBP to 2100yrBP the MD81 benthic record becomes enriched by ~0.4‰ which is equivalent to a drop in temperature of over 1°C (~0.21‰ per °C) if the entire shift is due to temperature, but which may also include a salinity component. This is a significant change in the deep water properties, but in line with previous results from the Southern Ocean. Palmer Deep bottom water temperature fluctuations of 1-1.5°C were associated with oscillations between a warmer, stable Upper Circumpolar Deep Water (UCDW) state and a cooler, variable shelf water state (Shevenell and Kennett, 2002). This benthic $\delta^{18}O$ shift towards more enriched values (colder and/or more saline) beginning at ~2100yrBP coincides with a cooling in air Vostok temperature. Episodes of glacier and sea ice expansion are associated with spring-summer sea ice diatom assemblages in the Southern Ocean (Denis et al., QSR,

accepted). A shorter ice free season and more sea ice during spring-summer was recorded by diatom assemblages from 1.6-2.0kyr (Denis et al., QSR, accepted), outlined in red in Figure 11-3, at the time of cooling in the MD81 benthic $\delta^{18}O$. This MD81 benthic cooling event therefore appears to be a Southern Hemisphere-wide event.

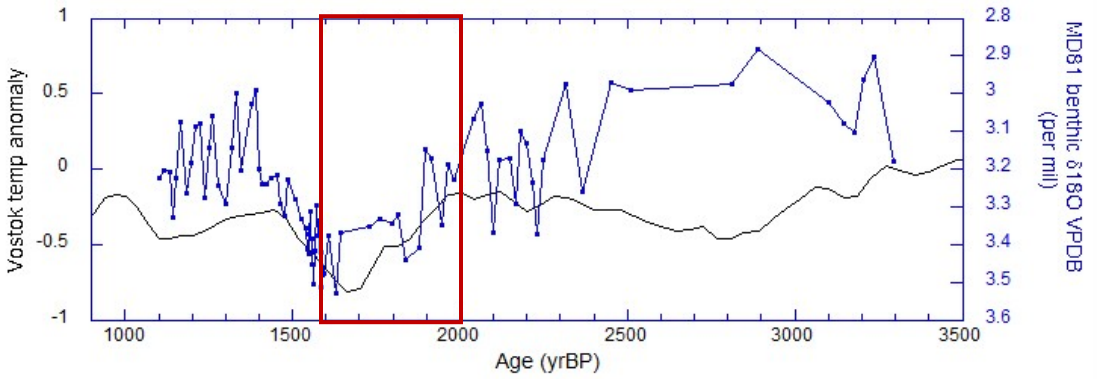

Figure 11-3: Vostok deuterium temperature anomaly (°C) in black (Lorius et al., 1985) and benthic $\delta^{18}Oc$ record at MD81 of Pacific Deep Water variability (offset from MD81 planktonic record by 1000yrs) in blue. Time period outlined in red corresponds to a shorter ice free season and more sea ice during spring-summer recorded by diatom assemblages (Denis et al., QSR, accepted).

The MD81 planktonic foraminifera record (from the present study and from Stott et al., 2002), on the other hand, shows oscillations towards more depleted values, signifying warmer/fresher conditions periodically from 1.1-2.4kyr (Figure 11-4). However, no single large millennial-scale oscillation is apparent in the present study or Stott et al., 2002 (Figure 11-4). This therefore suggests that bi-polar seesaw conditions did not exist between the tropics and Southern high latitudes during this time during the Holocene. Similarly no large anti-phased event is recorded in the N Hemisphere temperature anomaly (Moberg et al., 2005) or the monsoon record from Heshang (Hu et al., 2008) (Figure 11-4).

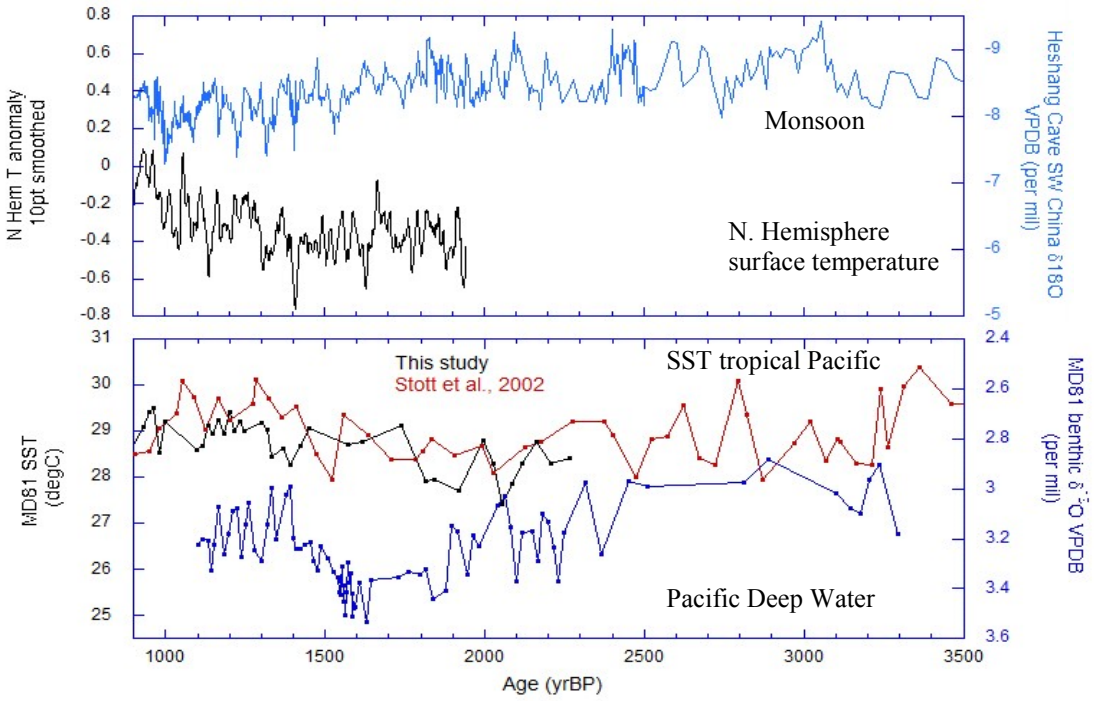

Figure 11-4: MD81 benthic Pacific Deep Water (*C. wuellerstorfi* δ^{18}Oc, dark blue curve) record compared to the monsoon climate record (Heshang Cave speleothem record in light blue, Hu et al., 2008), Northern Hemisphere surface temperature (anomaly record in black, Moberg et al., 2005) and western Pacific Warm Pool surface temperature from the present study (in black) and from Stott et al. (2002, in red). The benthic MD81 record is offset from planktonic by 1kyr to account for deep water travel time from the Southern Ocean source region to the core site in the western tropical Pacific.

Chapter 12: Conclusions

A 2000-year record from the western Pacific warm pool exhibits centennial scale variability, with larger, potentially millennial-scale oscillations present within the last 1000 years as recorded by two marine sediment cores. The Little Ice Age is recorded as the coldest and Medieval Warm Period as the warmest over last 2ka (data ends at 150yrBP)

The MD81 benthic record suggests a large drop in temperature of ~1°C occurred in the Southern Ocean source region centered at ~1.7kyrBP, which may also include a salinity component. This event correlates with other proxy records from the Southern Ocean confirming the event as Southern Hemisphere-wide.

Due to the ideal core location of MD81 it was also possible to address the question of phasing of the northern and southern climate records and whether the "bipolar seesaw" was still active during the Holocene. Based on available data there is no evidence for a bipolar seesaw operating during this benthic cooling event between the high southern latitudes represented by PDW variability and the surface waters of the tropics, the Northern Hemisphere surface temperature and Monsoon strength. The deep water that descended from the Southern Ocean surface during the ~550-duration of the Little Ice Age is not yet present at site MD81.

References

Adkins, J. F., and Schrag, D. P. (2001). Pore Fluid Constraints on Deep Ocean Temperature and Salinity During the Last Glacial Maximum. *Geophys. Res. Lett.* 28, 771-774.

Adkins, J. F., Ingersoll, A. P., and Pasquero, C. (2005). Rapid climate change and conditional instability of the glacial deep ocean from the thermobaric effect and geothermal heating *Quaternary Science Reviews* 24, 581-594.

Ahn, J. H., and Brook, E. J. (2007). Atmospheric CO2 and climate from 65 to 30 ka BP. *Geophysical Research Letters* 34, 4.

Altabet, M. A., Higginson, M. J., and Murray, D. W. (2002). The effect of millennial-scale changes in Arabian Sea denitrification on atmospheric CO2. *Nature* 415, 159-162.

Anand, P., Elderfield, H., and Conte, M. H. (2003). Calibration of Mg/Ca thermometry in planktonic foraminifera from a sediment trap time series. *Paleoceanography* 18.

Andersen, K. K., Azuma, N., Barnola, J. M., Bigler, M., Biscaye, P., Caillon, N., Chappellaz, J., Clausen, H. B., DahlJensen, D., Fischer, H., Fluckiger, J., Fritzsche, D., Fujii, Y., Goto-Azuma, K., Gronvold, K., Gundestrup, N. S., Hansson, M., Huber, C., Hvidberg, C. S., Johnsen, S. J., Jonsell, U., Jouzel, J., Kipfstuhl, S., Landais, A., Leuenberger, M., Lorrain, R., Masson-Delmotte, V., Miller, H., Motoyama, H., Narita, H., Popp, T., Rasmussen, S. O., Raynaud, D., Rothlisberger, R., Ruth, U., Samyn, D., Schwander, J., Shoji, H., Siggard-Andersen, M. L., Steffensen, J. P., Stocker, T., Sveinbjornsdottir, A. E., Svensson, A., Takata, M., Tison, J. L., Thorsteinsson, T., Watanabe, O., Wilhelms, F., and White, J. W. C. (2004). High-resolution record of Northern Hemisphere climate extending into the last interglacial period. *Nature* 431, 147-151.

Arz, H. W., Lamy, F., Ganopolski, A., Nowaczyk, N., and Pätzold, J. (2007). Dominant Northern Hemisphere climate control over millennial-scale glacial sea-level variability. *Quaternary Science Reviews* 26, 312-321.

Ashok, K., and Saji, N. H. (2007). On the impacts of ENSO and Indian Ocean dipole events on sub-regional Indian summer monsoon rainfall. *Natural Hazards* 42, 273-285.

Ashok, K., Guan, Z. Y., and Yamagata, T. (2001). Impact of the Indian Ocean Dipole on the relationship between the Indian monsoon rainfall and ENSO. *Geophysical Research Letters* 28, 4499-4502.

Ashok, K., Guan, Z. Y., Saji, N. H., and Yamagata, T. (2004). Individual and combined influences of ENSO and the Indian Ocean Dipole on the Indian summer monsoon. *Journal of Climate* 17, 3141-3155.

Baker, P. A., Seltzer, G. O., Fritz, S. C., Dunbar, R. B., Grove, M. J., Tapia, P. M., Cross, S. L., Rowe, H. D., and Broda, J. P. (2001). The History of South American Tropical Precipitation for the Past 25,000 Years. *Science* 291, 640-643.

Barbante, C., Barnola, J. M., Becagli, S., Beer, J., Bigler, M., Boutron, C., Blunier, T., Castellano, E., Cattani, O., Chappellaz, J., Dahl-Jensen, D., Debret, M., Delmonte, B., Dick, D., Falourd, S., Faria, S., Federer, U., Fischer, H., Freitag, J., Frenzel, A., Fritzsche, D., Fundel, F., Gabrielli, P., Gaspari, V., Gersonde, R., Graf, W., Grigoriev, D., Hamann, I., Hansson, M., Hoffmann, G., Hutterli, M. A., Huybrechts, P., Isaksson, E., Johnsen, S., Jouzel, J., Kaczmarska, M., Karlin, T., Kaufmann, P., Kipfstuhl, S., Kohno, M., Lambert, F., Lambrecht, A., Lambrecht, A., Landais, A., Lawer, G., Leuenberger, M., Littot, G., Loulergue, L., Luthi, D., Maggi, V., Marino, F., Masson-Delmotte, V., Meyer, H., Miller, H., Mulvaney, R., Narcisi, B., Oerlemans, J., Oerter, H., Parrenin, F., Petit, J. R., Raisbeck, G., Raynaud, D., Rothlisberger, R., Ruth, U., Rybak, O., Severi, M., Schmitt, J., Schwander, J., Siegenthaler, U., Siggaard-Andersen, M. L., Spahni, R., Steffensen, J. P., Stenni, B., Stocker, T. F., Tison, J. L., Traversi, R., Udisti, R., Valero-Delgado, F., van den Broeke, M. R., van de Wal, R. S. W., Wagenbach, D., Wegner, A., Weiler, K., Wilhelms, F., Winther, J. G., and Wolff, E. (2006). One-to-one coupling of glacial climate variability in Greenland and Antarctica. *Nature* 444, 195-198.

Barker, S., Cacho, I., Benway, H., and Tachikawa, K. (2005). Planktonic foraminiferal Mg/Ca as a proxy for past oceanic temperatures: a methodological overview and data compilation for the Last Glacial Maximum. *Quaternary Science Reviews* 24, 821-834.

Beaufort, L., de Garidel-Thoron, T., Linsley, B., Oppo, D. W., and Buchet, N. (2003). Biomass burning and oceanic primary production estimates in the Sulu Sea area over the last 380 kyr and the East Asian monsoon dynamics. *Marine Geology* 201, 53-65.

Behl, R. J., and Kennett, J. P. (1996). Brief interstadial events in the Santa Barbara basin, NE Pacific, during the past 60 kyr. *Nature* 379, 243-246.

Bemis, B. E., Spero, H. J., Bijma, J., and Lea, D. W. (1998). Reevaluation of the oxygen isotopic composition of planktonic foraminifera: Experimental results and revised paleotemperature equations. *Paleoceanography* 13, 150-160.

Benson, L., Lund, S., Negrini, R., Linsley, B., and Zic, M. (2003). Response of North American Great Basin Lakes to Dansgaard-Oeschger oscillations. *Quaternary Science Reviews* 22, 2239-2251.

Blunier, T., and Brook, E. J. (2001). Timing of millennial-scale climate change in Antarctica and Greenland during the last glacial period. *Science* 291, 109-112.

Blunier, T., Chappellaz, J., Schwander, J., Dallenbach, A., Stauffer, B., Stocker, T. F., Raynaud, D., Jouzel, J., Clausen, H. B., Hammer, C. U., and Johnsen, S. J. (1998). Asynchrony of Antarctic and Greenland climate change during the last glacial period. *Nature* 394, 739-743.

Blunier, T., Schwander, J., Stauffer, B., Stocker, T., Dallenbach, A., Indermuhle, A., Tschumi, J., Chappellaz, J., Raynaud, D., and Barnola, J. M. (1997). Timing of the Antarctic cold reversal and the atmospheric CO2 increase with respect to the Younger Dryas event. *Geophysical Research Letters* 24, 2683-2686.

Boersma, A. (1984). A Handbook of Common Tertiary Uvigerina

Bond, G., Broecker, W., Johnsen, S., McManus, J., Labeyrie, L., Jouzel, J., and Bonani, G. (1993). Correlations between climate records from North Atlantic sediments and Greenland ice. *Nature* 365, 143-147.

Bond, G., Kromer, B., Beer, J., Muscheler, R., Evans, M. N., Showers, W., Hoffmann, S., Lotti-Bond, R., Hajdas, I., and Bonani, G. (2001). Persistent Solar Influence on North Atlantic Climate During the Holocene. *Science* 294, 2130-2136.

Boyle, E. A. (2000). Is ocean thermohaline circulation linked to abrupt stadial/interstadial transitions? *Quaternary Science Reviews* 19, 255-272.

Bradley, R. S., and Jones, P. D. (1993). "Little Ice Age" summer temperature variations: their nature and relevance to recent global warming trends. *The Holocene* 3, 367-376.

Broecker, W. S. (1994). Massive iceberg discharges as triggers for global climate-change. *Nature* 372, 421-424.

Broecker, W. S. (1998). Paleocean circulation during the last deglaciation: A bipolar seesaw? *Paleoceanography* 13, 119-121.

Broecker, W. S. (2001). Paleoclimate: Was the Medieval Warm Period Global? *Science* 291, 1497-1499.

Broecker, W. S. (2006). Abrupt climate change revisited. *Global and Planetary Change* 54, 211-215.

Broecker, W., and Peng, T. H. (1982). "Tracers in the sea." Eldigio Press, Lamont Doherty Geological Observatory.

Broecker, W., Barker, S., Clark, E., Hajdas, I., Bonani, G., and Stott, L. (2004). Ventilation of the glacial deep Pacific Ocean. *Science* 306, 1169-1172.

Brook, E. J., White, J. W. C., Schilla, A. S. M., Bender, M. L., Barnett, B., Severinghaus, J. P., Taylor, K. C., Alley, R. B., and Steig, E. J. (2005). Timing of millennial-scale climate change at Siple Dome, West Antarctica, during the last glacial period. *Quaternary Science Reviews* 24, 1333-1343.

Brown, S. J., and Elderfield, H. (1996). Variations in Mg/Ca and Sr/Ca Ratios of Planktonic Foraminifera Caused by Postdepositional Dissolution: Evidence of Shallow Mg-Dependent Dissolution. *Paleoceanography* 11, 543-551.

Burns, S. J., Fleitmann, D., Matter, A., Kramers, J., and Al-Subbary, A. A. (2003). Indian Ocean climate and an absolute chronology over Dansgaard/Oeschger events 9 to 13. *Science* 301, 1365-1367.

Butzin, M., Prange, M., and Lohmann, G. (2005). Radiocarbon simulations for the glacial ocean: The effects of wind stress, Southern Ocean sea ice and Heinrich events. *Earth and Planetary Science Letters* 235, 45-61.

Cane, M. A. (1998). Climate change: A Role for the Tropical Pacific. *Science* 282, 59-61.

Cane, M., and Clement, A. C. (1999). A role for the tropical Pacific coupled ocean-atmosphere system on Milankovitch and millennial timescales. Part II: Global impacts. *In* "Mechanisms of Global Climate Change at Millennial Time Scales." pp. 373-383. Geophysical Monograph Series. Amer Geophysical Union, Washington.

Carter, R. M., and Gammon, P. (2004). New Zealand Maritime Glaciation: Millennial-Scale Southern Climate Change Since 3.9 Ma. *Science* 304, 1659-1662.

Chang, P., Yamagata, T., Schopf, P., Behera, S. K., Carton, J., Keesler, W. S., Meyers, G., Qu, T., Schott, F., Shetye, S., and Xie, S. P. (2006). Climate fluctuations of tropical coupled systems - The role of ocean dynamics, pp. 5122-5174. Amer Meteorological Soc.

Chappell, J. (2002). Sea level changes forced ice breakouts in the Last Glacial cycle: new results from coral terraces. *Quaternary Science Reviews* 21, 1229-1240.

Charles, C. D., LynchStieglitz, J., Ninnemann, U. S., and Fairbanks, R. G. (1996). Climate connections between the hemisphere revealed by deep sea sediment core ice core correlations. *Earth and Planetary Science Letters* 142, 19-27.

Chiang, J. C. H., Biasutti, M., and Battisti, D. S. (2003). Sensitivity of the Atlantic Intertropical Convergence Zone to Last Glacial Maximum boundary conditions. *Paleoceanography* 18, 18.

Clark, I. D., and Fritz, P. (1997). "Environmental isotopes in hydrogeology." Lewis Publishers, New York.

Clement, A. C., Cane, M. A., and Seager, R. (2001). An orbitally driven tropical source for abrupt climate change. *Journal of Climate* 14, 2369-2375.

Clement, A. C., Seager, R., and Cane, M. A. (1999). Orbital Controls on the El Nino/Southern Oscillation and the Tropical Climate. *Paleoceanography* 14, 441-456.

Corliss, B. H., McCorkle, D. C., and Higdon, D. M. (2002). Seasonal changes of the carbon isotopic composition of deep-sea benthic foraminifera. *Paleoceanography* 17.

Crowley, T. J. (1992). North Atlantic Deep Water Cools the Southern Hemisphere. *Paleoceanography* 7, 489-497.

Cruz, F. W., Burns, S. J., Karmann, I., Sharp, W. D., Vuille, M., Cardoso, A. O., Ferrari, J. A., Dias, P. L. S., and Viana, O. (2005). Insolation-driven changes in atmospheric circulation over the past 116,000 years in subtropical Brazil. *Nature* 434, 63-66.

Dannenmann, S., Linsley, B. K., Oppo, D. W., Rosenthal, Y., and Beaufort, L. (2003). East Asian monsoon forcing of suborbital variability in the Sulu Sea during Marine Isotope Stage 3: Link to Northern Hemisphere climate. *Geochemistry Geophysics Geosystems* 4, 13.

Dansgaard, W., Clausen, H. B., Gundestrup, N., Hammer, C. U., Johnsen, S. F., Kristinsdottir, P. M., and Reeh, N. (1982). A New Greenland Deep Ice Core. *Science* 218, 1273-1277.

Dansgaard, W., Johnsen, S. J., Clausen, H. B., Dahljensen, D., Gundestrup, N. S., Hammer, C. U., Hvidberg, C. S., Steffensen, J. P., Sveinbjornsdottir, A. E., Jouzel, J., and Bond, G. (1993). Evidence for general instability of past climate from a 250-kyr ice-core record. *Nature* 364, 218-220.

Dansgaard, W., Johnsen, S. J., Moller, J., and Langway, C. C., Jr. (1969). One Thousand Centuries of Climatic Record from Camp Century on the Greenland Ice Sheet. *Science* 166, 377-380.

D'Arrigo, R., and Wilson, R. (2006). On the Asian expression of the PDO. *International Journal of Climatology* 26, 1607-1617.

de Boer, A. M., Sigman, D. M., Toggweiler, J. R., and Russell, J. L. (2007). Effect of global ocean temperature change on deep ocean ventilation. *Paleoceanography* 22.

Dekens, P. S., Lea, D. W., Pak, D. K., and Spero, H. J. (2002). Core top calibration of Mg/Ca in tropical foraminifera: Refining paleotemperature estimation. *Geochemistry Geophysics Geosystems* 3.

Denis, D., Crosta, X., Schmidt, S., Carson, D., Ganeshram, R., Renssen, H., Bout-Roumazeilles,V., Zaragosi, S., Martin, B., Cremer, M., and Giraudeau, J. Holocene glacier and deep water dynamics, Adélie Land region, East Antarctica. *Quaternary Science Reviews*, accepted.

Denton, G. H., and Broecker, W. S. (2008). Wobbly ocean conveyor circulation during the Holocene? *Quaternary Science Reviews* 27, 1939-1950.

Duplessy, J. C., Arnold, M., Shackleton, N. J., Kallel, N., Labeyrie, L., and Juilletleclerc, A. (1988). Changes in the rate of ventilation of intermediate and deep-water masses in the Pacific-Ocean during the Last Deglaciation. *Chemical Geology* 70, 108-108.

Eberwein, A., and Mackensen, A. (2006). Regional primary productivity differences off Morocco (NW-Africa) recorded by modern benthic foraminifera and their stable carbon isotopic composition. *Deep Sea Research I* 53, 1379-1405.

Elliot, M., Labeyrie, L., and Duplessy, J. C. (2002). Changes in North Atlantic deep-water formation associated with the Dansgaard-Oeschger temperature oscillations (60-10 ka). *Quaternary Science Reviews* 21, 1153-1165.

Fairbanks, R. G., Evans, M. N., Rubenstone, J. L., Mortlock, R. A., Broad, K., Moore, M. D., and Charles, C. D. (1997). Evaluating climate indices and their geochemical proxies measured in corals. *Coral Reefs* 16, S93-S100.

Fedorov, A. V., and Philander, S. G. (2000). Is El Nino changing? *Science* 288, 1997-2002.

Ferguson, J. E., Henderson, G. M., Kucera, M., and Rickaby, R. E. M. (2008). Systematic change of foraminiferal Mg/Ca ratios across a strong salinity gradient *Earth and Planetary Science Letters* 265, 153-166.

Fine, R. A., Lukas, R., Bingham, F. M., Warner, M. J., and Gammon, R. H. (1994). The western equatorial Pacific: A water mass crossroads. *Journal of Geophysical Research* 99, 25063-25080.

Fischer, H., Fundel, F., Ruth, U., Twarloh, B., Wegner, A., Udisti, R., Becagli, S., Castellano, E., Morganti, A., Severi, M., Wolff, E., Littot, G., Rothlisberger, R., Mulvaney, R., Hutterli, M. A., Kaufmann, P., Federer, U., Lambert, F., Bigler, M., Hansson, M., Jonsell, U., de Angelis, M., Boutron, C., Siggaard-Andersen, M. L., Steffensen, J. P., Barbante, C., Gaspari, V., Gabrielli, P., and Wagenbach, D. (2007). Reconstruction of millennial changes in dust emission, transport and regional sea ice coverage using the deep EPICA ice cores from the Atlantic and Indian Ocean sector of Antarctica. *Earth and Planetary Science Letters* 260, 340-354.

Fontanier, C., Jorissen, F. J., Michel, E., Cortijo, E., Vidal, L., and Anschutz, P. (2008). Stable oxygen and carbon isotopes of live (stained) benthic foraminifera from Cap-Ferret Canyon (Bay of Biscay). *Journal of Foraminiferal Research* 38, 39-51.

Fontanier, C., Mackensen, A., Jorissen, F. J., Anschutz, P., Licari, L., and Griveaud, C. (2006). Stable oxygen and carbon isotopes of live benthic foraminifera from the Bay of Biscay: Microhabitat impact and seasonal variability. *Marine Micropaleontology* 58, 159-183.

Ganopolski, A., and Rahmstorf, S. (2001). Rapid changes of glacial climate simulated in a coupled climate model. *Nature* 409, 153-158.

Genty, D., Blamart, D., Ouahdi, R., Gilmour, M., Baker, A., Jouzel, J., and Van-Exter, S. (2003). Precise dating of Dansgaard-Oeschger climate oscillations in western Europe from stalagmite data. *Nature* 421, 833-837.

Gordon, A. L. (2005). Oceanography of the Indonesian Seas and their throughflow. *Oceanography* 18, 14-27.

Gordon, A. L., and Fine, R. A. (1996). Pathways of water between the Pacific and Indian oceans in the Indonesian seas. *Nature* 379, 146-149.

Gordon, A. L., Giulivi, C.F., Ilahude, A.G. (2003). Deep topographic barriers within the Indonesian seas. *Deep Sea Research II* 50, 2205-2228.

Haug, G. H., Hughen, K. A., Sigman, D. M., Peterson, L. C., and Rohl, U. (2001). Southward Migration of the Intertropical Convergence Zone Through the Holocene. *Science* 293, 1304-1308.

Hemming, S. R. (2004). Heinrich events: Massive late pleistocene detritus layers of the North Atlantic and their global climate imprint. *Reviews of Geophysics* 42, 43.

Hoerling, M. P., Hurrell, J. W., and Xu, T. (2001). Tropical Origins for Recent North Atlantic Climate Change. *Science* 292, 90-92.

Hoffmann, G., Jouzel, J., and Johnsen, S. (2001). Deuterium excess record from central Greenland over the last millennium: Hints of a North Atlantic signal during the Little Ice Age. *Journal of Geophysical Research* 106, 14265-14274.

Hu, C., Henderson, G. M., Huang, J., Xie, S., Sun, Y., and Johnson, K. R. (2008). Quantification of Holocene Asian monsoon rainfall from spatially separated cave records. *Earth and Planetary Science Letters* 266, 221-232.

Huang, K.-F., You, C.-F., Lin, H.-L., and Shieh, Y.-T. (2008). In situ calibration of Mg/Ca ratio in planktonic foraminiferal shell using time series sediment trap: A case study of intense dissolution artifact in the South China Sea. *Geochem. Geophys. Geosyst.* 9.

Hughes, M. K., and Diaz, H. F. (1994). Was there a "Medieval Warm Period" and if so, where and when? *Climatic Change* 26, 109-142.

Johnsen, S. J., Clausen, H. B., Dansgaar.W, and Langway, C. C. (1972). Oxygen isotope profiles through Antarctic and Greenland ice sheets. *Nature* 235, 429-434.

Jouzel, J., Vaikmae, R., Petit, J. R., Martin, M., Duclos, Y., Stievenard, M., Lorius, C., Toots, M., Melieres, M. A., Burckle, L. H., Barkov, N. I., and Kotlyakov, V. M. (1995). The 2-step shape and timing of the Last Deglaciation in Antarctica. *Climate Dynamics* 11, 151-161.

Kanfoush, S. L., Hodell, D. A., Charles, C. D., Guilderson, T. P., Mortyn, P. G., and Ninnemann, U. S. (2000). Millennial-scale instability of the antarctic ice sheet during the last glaciation. *Science* 288, 1815-1818.

Kawahata, H. (2005). Stable isotopic composition of two morphotypes of Globigerinoides ruber (white) in the subtropical gyre in the North Pacific. *Paleontological Research* 9, 27-35.

Kawahata, H., Nishimura, A., and Gagan, M. K. (2002). Seasonal change in foraminiferal production in the western equatorial Pacific warm pool: evidence from sediment trap experiments. *Deep Sea Research II* 49, 2783-2800.

Kawamura, K., Parrenin, F., Lisiecki, L., Uemura, R., Vimeux, F., Severinghaus, J. P., Hutterli, M. A., Nakazawa, T., Aoki, S., Jouzel, J., Raymo, M. E., Matsumoto, K., Nakata, H., Motoyama, H., Fujita, S., Goto-Azuma, K., Fujii, Y., and Watanabe, O. (2007). Northern Hemisphere forcing of climatic cycles in Antarctica over the past 360,000 years. *Nature* 448, 912-916.

Keigwin, L. D. (1998). Glacial-age hydrography of the far northwest Pacific Ocean. *Paleoceanography* 13, 323-339.

Keigwin, L. D., Cook, M.S. (2007). A role for North Pacific salinity in stabilizing North Atlantic climate. *Paleoceanography* 22, PA3102.

Keigwin, L. D., Jones, G. A., and Froelich, P. N. (1992). A 15,000 year paleoenvironmental record from Meiji Seamount, far northwestern Pacific. *Earth and Planetary Science Letters* 111, 425-440.

Kerr, R. A. (2000). A North Atlantic Climate Pacemaker for the Centuries. *Science* 288, 1984-1985.

Key, R. M., Kozyr, A., Sabine, C. L., Lee, K., Wanninkhof, R., Bullister, J. L., Feely, R. A., Millero, F. J., Mordy, C., and Peng, T. H. (2004). A global ocean carbon climatology: Results from Global Data Analysis Project (GLODAP). *Global Biogeochemical Cycles* 18.

Kienast, M., Kienast, S. S., Calvert, S. E., Eglinton, T. I., Mollenhauer, G., Francois, R., and Mix, A. C. (2006). Eastern Pacific cooling and Atlantic overturning circulation during the last deglaciation. *Nature* 443, 846-849.

Knorr, G., and Lohmann, G. (2003). Southern Ocean origin for the resumption of Atlantic thermohaline circulation during deglaciation. *Nature* 424, 532-536.

Knutti, R., Fluckiger, J., Stocker, T. F., and Timmermann, A. (2004). Strong hemispheric coupling of glacial climate through freshwater discharge and ocean circulation. *Nature* 430, 851-856.

Kreutz, K. J., Mayewski, P. A., Meeker, L. D., Twickler, M. S., Whitlow, S. I., and Pittalwala, I. I. (1997). Bipolar Changes in Atmospheric Circulation During the Little Ice Age. *Science* 277, 1294-1296.

Labracherie, M., Labeyrie, L. D., Dupral, J., Bard, E., Arnold, M., Pichon, J. J., and Duplessy, J. C. (1989). The last deglaciation in the Southern Ocean. *Paleoceanography* 4, 629-638.

Lamb, H. H. (1995). Climate, History and the Modern World. 171-186.

Lea, D. W., Mashiotta, T. A., and Spero, H. J. (1999). Controls on magnesium and strontium uptake in planktonic foraminifera determined by live culturing. *Geochimica et Cosmochimica Acta* 63, 2369-2379.

Lea, D. W., Pak, D. K., and Spero, H. J. (2000). Climate impact of late quaternary equatorial Pacific sea surface temperature variations. *Science* 289, 1719-1724.

Lean, J., Beer, J., and Bradley, R. (1995). Reconstruction of solar irradiance since 1610: Implications for climate change. *Geophysical Research Letters* 22, 3195-3198.

Lear, C. H., Elderfield, H., and Wilson, P. A. (2000). Cenozoic deep-sea temperatures and global ice volumes from Mg/Ca in benthic foraminiferal calcite. *Science* 287, 269-272.

Leduc, G., Vidal, L., Tachikawa, K., Rostek, F., Sonzogni, C., Beaufort, L., and Bard, E. (2007). Moisture transport across Central America as a positive feedback on abrupt climatic changes. *Nature* 445, 908-911.

Lorius, C., Jouzel, J., Ritz, C., Merlivat, L., Barkov, N. I., Korotkevich, Y. S., and Kotlyakov, V. M. (1985). A 150,000-year climatic record from Antarctic ice. *Nature* 316, 591-596.

Lutze, G. F., and Thiel, H. (1989). Epibenthic foraminifera from elevated microhabitats; Cibicidoides wuellerstorfi and Planulina ariminensis. *Journal of Foraminiferal Research* 19, 153-158.

Mackensen, A., Hubberten, H. W., Bickert, T., Fischer, G., and Futterer, D. K. (1993). The d13C in Benthic Foraminiferal Tests of Fontbotia Wuellerstorfi (Schwager) Relative to the d13C of Dissolved Inorganic Carbon in Southern Ocean Deep Water: Implications for Glacial Ocean Circulation Models. *Paleoceanography* 8, 587-610.

Mann, M. E., and Bradley, R. S. (1999). Northern Hemisphere temperatures during the past millennium: Inferences, uncertainties, and limitations. *Geophysical Research Letters* 26, 759-762.

Martin, P. A., Lea, D. W., Rosenthal, Y., Shackleton, N. J., Sarnthein, M., and Papenfuss, T. (2002). Quaternary deep sea temperature histories derived from benthic foraminiferal Mg/Ca. *Earth and Planetary Science Letters* 198, 193-209.

Martrat, B., Grimalt, J. O., Lopez-Martinez, C., Cacho, I., Sierro, F. J., Flores, J. A., Zahn, R., Canals, M., Curtis, J. H., and Hodell, D. A. (2004). Abrupt temperature changes in the Western Mediterranean over the past 250,000 years. *Science* 306, 1762-1765.

Martrat, B., Grimalt, J. O., Shackleton, N. J., de Abreu, L., Hutterli, M. A., and Stocker, T. F. (2007). Four climate cycles of recurring deep and surface water destabilizations on the Iberian margin. *Science* 317, 502-507.

Matsumoto, K. (2007). Radiocarbon-based circulation of the world oceans. *Journal of Geophysical Research* 112.

Matsumoto, K., Oba, T., Lynch-Stieglitz, J., and Yamamoto, H. (2002). Interior hydrography and circulation of the glacial Pacific Ocean. *Quaternary Science Reviews* 21, 1693-1704.

McCave, I. N., Carter, L., and Hall, I. R. (2008). Glacial-interglacial changes in water mass structure and flow in the SW Pacific Ocean. *Quaternary Science Reviews* 27, 1886-1908. Microclimate Press, Stony Point, NY.

McCorkle, D. C., and Keigwin, L. D. (1994). Depth Profiles of d13C in Bottom Water and Core Top C. wuellerstorfi on the Ontong Java Plateau and Emperor Seamounts. *Paleoceanography* 9, 197-208.

McCorkle, D. C., Corliss, B. H., and Farnham, C. A. (1997). Vertical distributions and stable isotopic compositions of live (stained) benthic foraminifera from the North Carolina and California continental margin. *Deep-Sea Research I* 44, 983-1024.

Meese, D. A., Gow, A. J., Alley, R. B., Zielinski, G. A., Grootes, P. M., Ram, M., Taylor, K. C., Mayewski, P. A., and Bolzan, J. F. (1997). The Greenland Ice Sheet Project 2 depth-age scale: Methods and results. *J. Geophys. Res.* 102, 26,411-26,423.

Mix, A. C., Lund, D. C., Pisias, N. G., Boden, P., Bornmalm, L., Lyle, M., and Pike, J. (1999). "Rapid climate oscillations in the northeast Pacific during the last deglaciation reflect northern and southern hemisphere sources." Geophysical Monograph.

Moberg, A., Sonechkin, D. M., Holmgren, K., Datsenko, N. M., and Karlen, W. (2005). Highly variable Northern Hemisphere temperatures reconstructed from low- and high-resolution proxy data. *Nature* 433, 613-617.

Morimoto, M., Abe, O., Kayanne, H., Kurita, N., Matsumoto, E., and Yoshida, N. (2002). Salinity records for the 1997-98 El Nino from Western Pacific corals. *Geophysical Research Letters* 29, 4.

Moy, C. M., Dunbar, R. B., Moreno, P. I., Francois, J.-P., Villa-Martínez, R., Mucciarone, D. M., Guilderson, T. P., and Garreaud, R. D. (2008). Isotopic evidence for hydrologic change related to the westerlies in SW Patagonia, Chile, during the last millennium. *Quaternary Science Reviews* 27, 1335-1349.

Muller, J., Kylander, M., Wust, R. A. J., Weiss, D., Martinez-Cortizas, A., LeGrande, A. N., Jennerjahn, T., Behling, H., Anderson, W. T., and Jacobson, G. (2008). Possible evidence for wet Heinrich phases in tropical NE Australia: the Lynch's Crater deposit. *Quaternary Science Reviews* 27, 468-475.

Newton, A., Thunell, R., and Stott, L. (2006). Climate and hydrographic variability in the Indo-Pacific Warm Pool during the last millennium. *Geophysical Research Letters* 33, L19710.

Ninnemann, U. S., and Charles, C. D. (2002). Changes in the mode of Southern Ocean circulation over the last glacial cycle revealed by foraminiferal stable isotopic variability. *Earth and Planetary Science Letters* 201, 383-396.

Nittrouer, C. A., Brunskill, G. J., and Figueiredo, A. G. (1995). Importance of tropical coastal environments. *Geo-Marine Letters* 15, 121-126.

Okumura, Y. M., Deser, C., Hu, A., Timmermann, A., and Xie, S.-P. (2008). North Pacific Climate Response to Freshwater Forcing in the Subarctic North Atlantic: Oceanic and Atmospheric Pathways. *Journal of Climate* preprint, 0000-0000.

Oppo, D.W., Linsley, B.K., Rosenthal, Y., Dannenmann, S. and Beaufort, L. (2003). Orbital and suborbital climate variability in the Sulu Sea, western tropical Pacific. *Geochemistry Geophysics Geosystems* 4, 1.

Oppo, D. W., Schmidt, G. A., and LeGrande, A. N. (2007). Seawater isotope constraints on tropical hydrology during the Holocene. *Geophysical Research Letters* 34, 5.

Ortiz, J. D., Mix, A. C., Rugh, W., Watkins, J. M., and Collier, R. W. (1996). Deep-dwelling planktonic foraminifera of the northeastern Pacific Ocean reveal environmental control of oxygen and carbon isotopic disequilibria. *Geochimica et Cosmochimica Acta* 60, 4509-4523.

Ostlund, W. G., and Stuiver, M. (1980). GEOSECS Pacific radiocarbon. *Radiocarbon* 22, 25-53.

Pahnke, K., and Zahn, R. (2005). Southern hemisphere water mass conversion linked with North Atlantic climate variability. *Science* 307, 1741-1746.

Pelejero, C., Grimalt, J. O., Heilig, S., Kienast, M., and Wang, L. J. (1999). High-resolution U-37(K) temperature reconstructions in the South China Sea over the past 220 kyr. *Paleoceanography* 14, 224-231.

Pichat, S., Sims, K. W. W., Francois, R., McManus, J. F., Leger, S. B., and Albarede, F. (2004). Lower export production during glacial periods in the equatorial Pacific derived from (Pa-231/Th-230) measurements in deep-sea sediments. *Paleoceanography* 19.

Porter, S. C. (2001). Chinese loess record of monsoon climate during the last glacial–interglacial cycle *Earth-Science Reviews* 54, 115-128.

Porter, S. C., and Zhisheng, A. (1995). Correlation between climate events in the North Atlantic and China during the last glaciation. *Nature* 375, 305-308.

Raisbeck, G. M., Yiou, F., Jouzel, J., and Stocker, T. F. (2007). Direct north-south synchronization of abrupt climate change record in ice cores using Beryllium 10. *Climate of the Past* 3, 541-547.

Rathburn, A. E., Perez, M. E., Martin, J. B., Day, S. A., Gieskes, J., Mahn, C., Ziebis, W., Williams, D., and Bahls, A. (2003). Relationships between the distribution and stable isotopic composition of living foraminifera and cold methane seep biogeochemistry in Monterey Bay, California. *Geochemistry, Geophysics and Geosystems* 4.

Rintoul, S. R., Sokolov, S., and Church, J. A. (2001). "Ocean Circulation and Climate. Observing and Modelling the Global Ocean." Academic Press, London.

Rohling, E. J., Marsh, R., Wells, N. C., Siddall, M., and Edwards, N. R. (2004). Similar meltwater contributions to glacial sea level changes from Antarctic and northern ice sheets. *Nature* 430, 1016-1021.

Rosenthal, Y., and Lohmann, G. P. (2002). Accurate estimation of sea surface temperatures using dissolution-corrected calibrations for Mg/Ca paleothermometry - art. no. 1044. *Paleoceanography* 17, 1044-1044.

Rosenthal, Y., Boyle, E. A., and Slowey, N. (1997). Temperature control on the incorporation of magnesium, strontium, fluorine, and cadmium into benthic foraminiferal shells from Little Bahama Bank: Prospects for thermocline paleoceanography. *Geochimica et Cosmochimica Acta* 61, 3633-3643.

Rosenthal, Y., Lohmann, G. P., Lohmann, K. C., and Sherrell, R. M. (2000). Incorporation and preservation of Mg in Globigerinoides sacculifer: Implications for reconstructing the temperature and O-18/O-16 of seawater. *Paleoceanography* 15, 135-145.

Russell, J. L., Dixon, K. W., Gnanadesikan, A., Stouffer, R. J., and Toggweiler, J. R. (2006). The Southern Hemisphere Westerlies in a Warming World: Propping Open the Door to the Deep Ocean. *Journal of Climate* 19, 6382-6390.

Schmiedl, G., Pfeilsticker, M., Hemleben, C., and Mackensen, A. (2004). Environmental and biological effects on the stable isotope composition of Recent deep-sea benthic foraminifera from the Mediterranean Sea. *Marine Micropaleontology* 51, 129-152.

Schulz, H., von Rad, U., and Erlenkeuser, H. (1998). Correlation between Arabian Sea and Greenland climate oscillations of the past 110,000 years. *Nature* 393, 54-57.

Seidov, D., and Maslin, M. (2001). Atlantic Ocean heat piracy and the bipolar climate see-saw during Heinrich and Dansgaard-Oeschger events. *Journal of Quaternary Science* 16, 321-328.

Seidov, D., Stouffer, R. J., and Haupt, B. J. (2005). Is there a simple bi-polar ocean seesaw? *Global and Planetary Change* 49, 19-27.

Shackleton, N. J. (1974). "Attainment of isotopic equilibrium between ocean water and the benthonic foraminifera genus Uvigerina: Isotopic changes in the ocean during the last glacial." Cent. Natl. de la Rech. Sci, Paris.

Shackleton, N. J., and Opdyke, N. D. (1973). Oxygen isotope and palaeomagnetic stratigraphy of Equatorial Pacific core V28-238: Oxygen isotope temperatures and ice volumes on a 105 year and 106 year scale. *Quaternary Research* 3, 39-55.

Shackleton, N. J., and Pisias, N. G. (1985). "Atmospheric CO2: Natural Variations, Archaean to Present." AGU.

Shackleton, N. J., Hall, M. A., and Vincent, E. (2000). Phase relationships between millennial-scale events 64,000-24,000 years ago. *Paleoceanography* 15, 565-569.

Shackleton, N. J., Imbrie, J., and Hall, M. A. (1983). Oxygen and carbon isotope record of East Pacific core V19-30 - implications for the formation of deep-water in the Late Pleistocene North-Atlantic. *Earth and Planetary Science Letters* 65, 233-244.

Shevenell, A. E., and Kennett, J. P. (2002). Antarctic Holocene climate change: A benthic foraminiferal stable isotope record from Palmer Deep. *Paleoceanography* 17, 1019.

Siddall, M., Rohling, E. J., Almogi, L. A., Hemleben, C., Meischner, D., Schmelzer, I., and Smeed, D. A. (2003). Sea-level fluctuations during the last glacial cycle. *Nature* 423, 853-858.

Sikes, E. L., Samson, C. R., Guilderson, T. P., and Howard, W. R. (2000). Old radiocarbon ages in the southwest Pacific Ocean during the last glacial period and deglaciation. *Nature* 405, 555-559.

Sirocko, F., Leuschner, D., Staubwasser, M., Maley, J., and Heusser, L. (1999). High-frequency oscillations of the last 70,000 years in the tropical/subtropical and polar climates. *In* "Mechanisms of Global Climate Change at Millennial Time Scales." pp. 113-126. Geophysical Monograph Series. Amer Geophysical Union, Washington.

Skinner, L. C., and Elderfield, H. (2007). Rapid fluctuations in the deep North Atlantic heat budget during the last glacial period. *Paleoceanography* 22, 9.

Skinner, L. C., and Shackleton, N. J. (2004). Rapid transient changes in northeast Atlantic deep water ventilation age across Termination I. *Paleoceanography* 19, 12.

Skinner, L. C., and Shackleton, N. J. (2005). An Atlantic lead over Pacific deep-water change across Termination I: implications for the application of the marine isotope stage stratigraphy. *Quaternary Science Reviews* 24, 571-580.

Skinner, L. C., Shackleton, N. J., and Elderfield, H. (2003). Millennial-scale variability of deep-water temperature and delta O-18(dw) indicating deep-water source variations in the Northeast Atlantic, 0-34 cal. ka BP. *Geochemistry Geophysics Geosystems* 4, 17.

Sowers, T., and Bender, M. (1995). Climate records covering the Last Deglaciation. *Science* 269, 210-214.

Spero, H. J., and Lea, D. W. (1993). Intraspecific stable isotope variability in the planktonic foraminifera Globigerinoides sacculifer: Results from laboratory experiments. *Mar. Micropaleontol.* 22, 221-234.

Stenni, B., Proposito, M., Gragnani, R., Flora, O., Jouzel, J., Falourd, S., and Frezzotti, M. (2002). Eight centuries of volcanic signal and climate change at Talos Dome (East Antarctica). *Journal of Geophysical Research* 107, 4076.

Stocker, T. F. (1998). Climate change - The seesaw effect. *Science* 282, 61-62.

Stocker, T. F., and Johnsen, S. J. (2003). A minimum thermodynamic model for the bipolar seesaw. *Paleoceanography* 18, 9.

Stocker, T. F., and Wright, D. G. (1996). Rapid Changes in Ocean Circulation and Atmospheric Radiocarbon. *Paleoceanography* 11, 773-795.

Stocker, T. F., Wright, D. G., and Mysak, L. A. (1992). A zonally averaged, coupled ocean atmosphere model for paleoclimate studies. *Journal of Climate* 5, 773-797.

Stott, L., Poulsen, C., Lund, S., and Thunell, R. (2002). Super ENSO and global climate oscillations at millennial time scales. *Science* 297, 222-226.

Stott, L., Timmermann, A., and Thunell, R. (2007). Southern Hemisphere and Deep-Sea Warming Led Deglacial Atmospheric CO2 Rise and Tropical Warming. *Science*.

Sun, D.-Z., Fasullo, J., Zhang, T., and Roubicek, A. (2003). On the Radiative and Dynamical Feedbacks over the Equatorial Pacific Cold Tongue. *Journal of Climate* 16, 2425-2432.

Timmermann, A., Lorenz, S. J., An, S. I., Clement, A., and Xie, S. P. (2007). The Effect of Orbital Forcing on the Mean Climate and Variability of the Tropical Pacific. *Journal of Climate* 20, 4147-4159.

Timmermann, A., Timm, O., Stott, L., and Menviel-Hessler, L. (in press). Local orbital forcing as a jump-starter for the last deglaciation. *Journal of Climate*.

Toggweiler, J. R., and Samuels, B. (1995). Effect of sea-ice on the salinity of Antarctic bottom waters. *Journal of Physical Oceanography* 25, 1980-1997.

Troelstra, S. R., and Kroon, D. (1989). Note on extant planktonic foraminifera from the Banda Sea, Indonesia (Snellius-II Expedition, cruise G5). *Netherlands Journal of Sea Research* 24, 459-463.

van Aken, H.M. (2000). The hydrography of the mid-latitude northeast Atlantic Ocean I: The deep water masses. *Deep Sea Research II* 47, 757-788.

van de Flierdt, T., Frank, M., Halliday, A. N., Hein, J. R., Hattendorf, B., Gunther, D., and Kubik, P. W. (2004). Deep and bottom water export from the Southern Ocean to the Pacific over the past 38 million years. *Paleoceanography* 19.

Verschuren, D., Laird, K. R., and Cumming, B. F. (2000). Rainfall and drought in equatorial east Africa during the past 1,100 years. *Nature* 403, 410-414.

Wang, L. (2000). Isotopic signals in two morphotypes of Globigerinoides ruber (white) from the South China Sea: implications for monsoon climate change during the last glacial cycle. *Palaeogeography, Palaeoclimatology, Palaeoecology* 161, 381-394.

Wang, L., Sarnthein, M., Erlenkeuser, H., Grootes, P. M., Grimalt, J. O., Pelejero, C., and Linck, G. (1999). Holocene variations in Asian Monsoon moisture: a bidecadal sediment record from the South China Sea. *Geophysical Research Letters* 26, 2889-2892.

Wang, X. F., Auler, A. S., Edwards, R. L., Cheng, H., Cristalli, P. S., Smart, P. L., Richards, D. A., and Shen, C. C. (2004). Wet periods in northeastern Brazil over the past 210 kyr linked to distant climate anomalies. *Nature* 432, 740-743.

Wang, Y. J., Cheng, H., Edwards, R. L., An, Z. S., Wu, J. Y., Shen, C. C., and Dorale, J. A. (2001). A high-resolution absolute-dated Late Pleistocene monsoon record from Hulu Cave, China. *Science* 294, 2345-2348.

Watanabe, T., Winter, A., and Oba, T. (2001). Seasonal changes in sea surface temperature and salinity during the Little Ice Age in the Caribbean Sea deduced from Mg/Ca and 18O/16O ratios in corals. *Marine Geology* 173, 21-35.

Weaver, A. J., Saenko, O. A., Clark, P. U., and Mitrovica, J. X. (2003). Meltwater pulse 1A from Antarctica as a trigger of the bolling-allerod warm interval. *Science* 299, 1709-1713.

Wolf-Gladrow, D. A., Riebesell, U., Burkhardt, S., and Bijma, J. (1999). Direct effects of CO2 concentration on growth and isotopic composition of marine plankton. *Tellus B* 51, 461-476.

Wunsch, C. (2006). Abrupt climate change: An alternative view. *Quaternary Research* 65, 191-203.

Wunsch, C., and Heimbach, P. (2008). How long to oceanic tracer and proxy equilibrium? *Quaternary Science Reviews* 27, 637-651.

Xie, S.-P., Okumura, Y., Miyama, T., and Timmermann, A. (2008). Influences of Atlantic Climate Change on the Tropical Pacific via the Central American Isthmus. *Journal of Climate* 21, 3914-3928.

Zeebe, R. E. (1999). An explanation of the effect of seawater carbonate concentration on foraminiferal oxygen isotopes *Geochimica et Cosmochimica Acta* 63, 2001-2007.

Zhang, P., Cheng, H., Edwards, R. L., Chen, F., Wang, Y., Yang, X., Liu, J., Tan, M., Wang, X., Liu, J., An, C., Dai, Z., Zhou, J., Zhang, D., Jia, J., Jin, L., and Johnson, K. R. (2008). A Test of Climate, Sun, and Culture Relationships from an 1810-Year Chinese Cave Record. *Science* 322, 940-942.

Zhang, Y., Sperber, K. R., Boyle, J. S., Dix, M., Ferranti, L., Kitoh, A., Lau, K. M., Miyakoda, K., D., R., Takacs, L., and Wetherald, R. (1997). East Asian winter monsoon: results from eight AMIP models. *Climate Dynamics* 13,

Appendix A

The following data were presented in Project I in graphical form. 13C data for *G. ruber* and infaunal benthic species *U. hispida* is also included.

Depth (cm)	*G. ruber* $\delta^{13}C$ (per mil)	*G. ruber* $\delta^{18}O$ (per mil)	*G. ruber* Mg/Ca (mmol/mol)	*U. hispida* $\delta^{13}C$ (per mil)	*U. hispida* $\delta^{18}O$ (per mil)
1804	0.95	-1.26	4.18		
1806	1.21	-1.21	4.02	-0.56	4.12
1808	1.10	-1.38			
1810	1.00	-1.38	4.29	-0.74	4.36
1812	1.20	-1.17	4.05	-0.76	4.41
1813				-0.76	4.52
1814	1.17	-1.18	4.11		
1816	1.25	-1.12	3.94		
1818	1.15	-1.05	3.82		
1820	1.17	-1.08			
1822	1.11	-1.08		-0.73	4.46
1824	1.22	-1.19			
1826			3.90		
1828	0.83	-1.02	4.08	-0.70	4.57
1831				-0.62	4.42
1832			3.89		
1834				-0.61	4.54
1836	1.32	-1.16	4.00		
1842	1.21	-1.16	4.17		
1846				-0.65	4.53
1847	1.20	-1.18	4.28		
1848				-0.73	4.46
1850				-0.68	4.52
1852	1.37	-1.07	4.00	-0.72	4.57
1854				-0.62	4.46
1856	1.18	-1.33	3.95	-0.62	4.48
1858	1.27	-1.31			
1858				-0.81	4.54
1860	1.20	-1.12	4.13		
1862	1.24	-1.19		-0.68	4.43
1864	1.20	-1.36		-0.57	4.47
1866	1.09				
1868	1.23				
1870	1.19				
1872	1.18				
1873	1.10	-1.23			
1874	1.34	-1.24			
1876	1.28				

1878	1.16	-1.32			
1882	0.98	-1.34	3.93		
1884			3.90		
1886	1.27	-1.23			
1888				-0.37	4.42
1888	1.24	-1.31	3.83	-0.64	4.46
1893				-0.35	4.39
1894			3.86		
1896	1.18	-1.31	4.12	-0.40	4.28
1898	1.10	-1.16		-0.09	4.05
1904			4.29	-0.39	4.16
1906	1.09	-1.41			
1908	1.09	-1.30			
1910	1.17	-1.30	4.12		
1911				-0.37	4.25
1912			4.13		
1914	0.98	-1.44		-0.54	3.99
1916			4.12		
1918	1.04	-1.30	4.03		
1919				-0.57	4.25
1920	1.22	-1.18	3.97		
1922	1.29	-1.20			
1924			3.81	-0.65	4.03
1928	1.08	-1.19			
1929				-0.64	4.29
1930	1.19	-1.24	4.08		
1934			4.18		
1936				-0.70	4.18
1937	1.30	-1.23	4.09		
1939				-0.64	4.33
1942	1.17	-1.40	4.03	-0.78	4.10
1944	1.32	-1.51	3.86		
1946	1.37	-1.42	3.99		
1947				-0.40	4.30
1948			3.84		
1950	1.05	-1.54	4.03	-0.28	4.04
1952	1.22	-1.38	3.99		
1954	1.06	-1.38	4.00	-0.41	4.04
1956			3.81		
1958	1.20	-1.51	4.03		
1959				-0.53	4.40
1960	1.12	-1.37	3.97		
1962				-0.64	4.35
1962	1.23	-1.08	3.89		
1964	1.30	-1.15		-0.45	4.37
1966	1.36	-1.16	3.85	-0.52	4.34
1968				-0.85	4.20

1969	1.30	-1.14			
1970				-0.93	4.25
1974				-0.87	3.98
1976				-0.77	3.98
1977	1.24	-1.22			
1980				-0.52	4.20
1981	1.26	-1.19	3.79		
1982				-0.80	4.29
1984				-0.82	4.34
1985			3.79		
1986				-0.77	4.18
1988	1.20	-1.36	4.20	-0.80	4.35
1990	1.03	-1.33	4.09		
1991				-0.75	4.22
1992	1.17	-1.50	4.14		
1994				-0.88	4.24
1995	1.12	-1.41	3.92		
1996				-0.67	4.25
1998	1.24	-1.32	3.93	-0.70	4.23
2001				-0.84	4.28
2004	1.21	-1.42	4.05		
2006	1.05	-1.50	4.14	-0.74	4.28
2008	0.93	-1.40	4.09		
2010			3.99		
2012	1.03	-1.32	4.08		
2014	0.91	-1.52	4.00		
2016	1.24	-1.46	3.92		
2018	1.03	-1.23		-0.89	4.06
2020	1.19	-1.30	3.93	-0.59	4.19
2022	1.26	-1.19	4.17	-0.73	4.15
2024			4.04	-0.66	4.04
2028			3.91		
2032	1.30	-1.25	3.95	-0.68	4.09
2034	1.29	-1.16	3.88	-0.66	4.11
2036	1.59	-1.06	4.06	-0.60	4.15
2038	1.27	-1.19		-0.63	4.20
2040	1.27	-1.30	4.15		
2041				-0.80	4.13
2044			3.95	-0.75	4.22
2046			4.02	-0.83	4.21
2048	1.16	-1.42	4.02	-0.89	4.17
2050	1.12	-1.50	3.94	-0.72	4.26
2052	1.26	-1.14	4.14	-0.51	4.20
2054	1.13	-1.15	4.17	-0.50	4.28
2056	1.33	-1.09	4.05		
2058	1.19	-1.20	3.97	-0.66	4.28
2060	0.95	-1.38	4.04		

2061				-0.80	4.33
2062	1.27	-1.25	3.90		
2064	1.21	-1.30	4.01		
2066	1.32	-1.37	3.92		
2068			3.96	-0.93	4.18
2070	1.08	-1.32	3.94	-0.55	4.38
2074			3.87		
2075				-1.03	4.22
2076	1.31	-1.37			
2078	1.06	-1.46	4.06		
2080	1.03	-1.40	4.12		
2082	1.07	-1.34	4.13	-0.74	4.24
2084	0.93	-1.36		-0.94	4.31
2085				-0.76	4.38
2086	1.12	-1.38			
2088	1.16	-1.37	4.00		
2090	1.02	-1.49			
2091				-0.75	4.23
2092	1.10	-1.42	4.00		
2094	1.11	-1.37	4.03		
2096	1.10	-1.28	4.17	-1.00	4.24
2098	1.03	-1.39	4.08		
2099				-0.65	4.38
2100	1.09	-1.27	4.10		
2102	0.96	-1.33			
2104	1.10	-1.45	4.10		
2106	1.04	-1.31	4.11	-0.66	4.38
2110	0.88	-1.41	4.32		
2112	0.98	-1.46	4.04		
2114	1.00	-1.44	4.18		
2116	1.04	-1.36	4.29		
2118	1.15	-1.37	4.10		
2120	1.26	-1.46	4.35	-0.66	4.34
2124	1.15	-1.51	4.19		
2124	1.15	-1.51	4.18		
2126	0.96	-1.50	4.25		
2128	1.03	-1.51	4.26		
2130	0.96	-1.61			
2132	0.97	-1.66	4.25		
2138	1.07	-1.66	4.27		
2140	1.03	-1.55			
2142				-0.38	4.35
2144	0.96	-1.54	4.24		
2146			4.08		
2146			3.98		
2148	1.43	-1.42			
2150			4.00	-0.52	4.17

2152			4.06		
2153				-0.61	4.03
2154	1.38	-1.29	4.05		
2158	1.11	-1.39	3.97		
2160	0.96	-1.45	3.83		
2162	0.95	-1.46	3.85		
2164	1.21	-1.24	3.90		
2166	1.38	-1.34	3.94	-0.77	4.16
2168	1.06	-1.53			
2170	1.23	-1.37	3.82		
2172	0.96	-1.47	3.96	-0.69	4.05
2174			3.91		
2174	0.79	-1.56	3.88		
2176	0.97	-1.51	4.03		
2178	0.99	-1.39	3.99	-0.75	4.08
2180	1.24	-1.39	3.92		
2182	1.29	-1.37	4.05	-0.67	4.04
2184	1.31	-1.39	3.80		
2186	1.22	-1.57	3.83		
2187				-0.72	4.08
2189			3.90		
2194			4.01	-0.31	4.14
2197	0.67	-1.54			
2198			4.20		
2201	0.83	-1.29	3.97		
2202				-0.80	4.02
2204	0.89	-1.22	3.99		
2204			4.06		
2206	0.74	-1.43	3.99		
2206			3.96		
2207				-0.60	4.03
2208	0.85	-1.48	4.16		
2210	0.80	-1.44	4.14	-0.63	4.07
2210			4.06		
2211				-0.74	4.10
2212	1.22	-1.21	3.90		
2212			3.88		
2214	1.26	-1.04	3.78		
2214			3.80		
2215				-0.70	4.01
2216	1.13	-1.10	3.99	-0.65	4.06
2218	0.96	-1.25			
2219				-0.76	4.09
2220	1.31	-1.20	3.92	-0.47	4.44
2220			3.87		
2222			3.89		
2224			3.81	-0.75	4.34

2226			3.84	-0.81	4.49
2228	1.08	-1.24	3.92		
2230	1.16	-1.20		-0.52	4.26
2232	1.19	-1.26		-0.56	4.39
2240				-0.63	4.47
2242			3.80		
2244	1.36	-0.95	4.01	-0.30	4.42
2245				-0.77	4.36
2246			3.85	-0.57	4.33
2248	1.24	-1.01	4.07		
2249				-0.58	4.32
2250	1.31	-1.10	3.88		
2252	1.23	-1.15	4.00		
2254				-0.64	4.43
2256	1.20	-1.20	4.06		
2258	1.10	-1.11	4.03		
2260				-0.63	4.53
2260	1.26	-1.02	3.92		
2260			3.84		
2262	1.22	-1.27	3.91		
2262			3.75		
2264				-0.24	4.38
2265			3.86		
2266			3.78	-0.02	4.35
2268			3.82	0.14	4.28
2268	1.29	-1.11	3.81		
2270	1.27	-1.26	3.88	0.09	4.25
2272	1.27	-1.16	3.77	-0.07	4.47
2274	1.24	-1.31	3.94	-0.66	4.48
2276	1.18	-1.16		-0.17	4.40
2278	1.33	-1.03	3.94	-0.21	4.52
2280				-0.65	4.46
2280	1.01	-1.18	3.95		
2282	1.20	-1.17	3.92		
2284	1.22	-1.24	3.88		
2286	1.15	-1.20	3.83	-0.77	4.46
2288			3.78		
2290	1.12	-1.13		-0.62	4.45
2292	1.24	-1.21	4.09		
2294	1.21	-1.32	4.04	-0.74	4.43
2296	1.20	-1.30	4.04		
2298	1.22	-1.38	4.02		
2300	1.08	-1.38	4.01	-0.64	4.46
2302	1.19	-1.44	4.10		
2304	1.20	-1.52		-0.65	4.39
2306	1.34	-1.22	3.96		
2308	1.19	-1.32	4.01		

2310	0.98	-1.59	3.95		
2312	1.13	-1.31			
2314	1.11	-1.54	3.93	-0.36	4.40
2316	1.22	-1.35	4.03	-0.49	4.32
2318	1.18	-1.37	4.19	-0.61	4.22
2320	1.15	-1.61	3.87		
2321				-0.85	4.24
2322	1.08	-1.43	3.98		
2324	1.11	-1.32	3.88	-0.81	4.34
2326	0.97	-1.35	4.16	-0.65	4.36
2328	1.08	-1.39	4.18		
2330	1.27				
2332	1.27				
2334	1.03				
2336	1.03				
2338	1.26	-1.38	3.92		
2340	1.04	-1.33			
2342	1.19	-1.36			
2344	1.15	-1.48	3.87		
2345				-0.73	4.47
2346	1.31	-1.26			
2348	1.15	-1.43	3.74		
2350	1.09	-1.29	3.87		
2352	1.20	-1.39		-0.66	4.43
2354	0.92	-1.35			
2356	0.98	-1.32	3.84	-0.57	4.48
2358	1.17	-1.37	3.97	-0.72	4.38
2359				-0.70	3.92
2360	1.30	-1.21	3.89		
2362	1.34	-1.34		-0.96	3.88
2363				-0.55	3.91
2376			3.86		
2378	1.15	-1.46	3.71		
2380	1.06	-1.53	3.77		
2382	0.75	-1.55	3.88	-0.27	4.24
2384			3.94	-0.57	4.12
2386				-0.66	4.08
2388	0.98	-1.56	3.99	-0.56	3.99
2390	0.95	-1.41	3.97		
2392	1.43	-1.48	4.13		
2394			4.22	-0.59	4.27
2396			3.97	-0.52	4.35
2398	1.32	-1.36	3.88	-0.67	4.04
2400			3.92		
2401				-0.28	4.30
2402	0.98	-1.30	4.07		
2404				-0.54	4.11

2404	1.44	-1.27			
2406	1.13	-1.24	3.85	-0.16	4.39
2408				-0.63	4.13
2410	1.34	-1.15	3.62	-0.35	4.33
2411				-0.61	4.38
2414	1.23	-1.37	3.91		
2416	1.12	-1.27	3.84		
2418	1.21	-1.18	3.70	-0.69	4.31
2420			3.93	-0.45	4.40
2422	1.41	-1.26	4.04		
2424	1.31	-1.17	3.84		
2425				-0.56	4.38
2426	1.51	-1.28	4.12		
2428			4.05		
2430	1.30	-1.32	4.22		
2432	1.30	-1.25	3.95	-0.68	4.24
2434			4.00		
2435				-0.31	4.26
2436	1.20	-1.23	4.11		
2438	1.43	-1.25			
2439				-0.69	4.24
2440	1.00	-1.39	3.92		
2442	1.13	-1.26	3.99		
2444	1.34	-1.32	4.21		
2448	1.22	-1.26	3.87		
2450	1.38	-1.32	4.07		
2452			3.95	-0.70	4.17
2452	1.18	-1.52	3.84		
2454	1.21	-1.50	3.96	-0.54	4.35
2456	1.05	-1.63	4.28	-0.66	4.33
2456			4.13		
2457				-0.89	4.17
2458	1.09	-1.60	4.24		
2458			4.26		
2458			3.96		
2460	1.25	-1.70	4.04		
2460	1.21	-1.67	3.87		
2460			4.01		
2462			4.06	-0.92	4.15
2462	1.26	-1.72	3.84		
2464	1.14	-1.61			
2464	1.07	-1.63	4.01		
2466	1.16	-1.62	4.00		
2466	1.11	-1.71	3.96		
2468	0.93	-1.70	4.12		
2468			4.00		
2470			4.26		

2470	1.11	-1.76	4.24		
2472	1.05	-1.69	4.07		
2473	1.11	-1.65			
2474	1.09	-1.62	4.15		
2474	1.30	-1.62			
2476	1.13	-1.76			
2476	1.12	-1.68	3.72		
2478	1.10	-1.53	3.88		
2480	1.05	-1.58	3.77		
2480			3.91		
2482	0.70	-1.55	3.94	-0.67	4.29
2483			3.84		
2484	0.81	-1.62	3.88	-0.71	4.28
2484	0.86	-1.55			
2486	0.85	-1.58	3.83	-0.67	4.25
2486	1.05	-1.53	4.06		
2487				-0.83	4.14
2488	1.05	-1.56			
2489			4.03	-0.64	4.19
2490	0.66	-1.57			
2492	0.98	-1.52	4.05	-0.76	4.20
2493			3.99		
2494	0.81	-1.60	4.13		
2495				-0.76	4.20
2496	1.04	-1.44			
2497	1.09	-1.61			
2498	1.00	-1.41		-0.78	4.11
2498				-0.77	4.18
2500	1.06	-1.50	4.20	-0.65	4.19
2501	0.97	-1.54	4.03		
2502	1.00	-1.56	4.06		
2504	1.15	-1.44		-0.81	3.98
2505			4.01		
2506	0.84	-1.38			
2508	1.33	-1.52		-0.90	4.04
2509			4.03		
2510	1.09	-1.47	3.91	-0.84	4.06
2513			3.98		
2515				-0.74	4.03
2524			3.89	-0.78	3.91
2524	1.02	-1.51	4.19		
2526	1.04	-1.51		-0.65	4.01
2527			3.87		
2528	1.25	-1.43	4.12	-0.81	3.95
2530	1.02	-1.52	3.99		
2531	0.86	-1.60	3.90		
2532	0.96	-1.51	3.99		

2534	0.88	-1.72	4.02		
2536	1.05	-1.65	4.23		
2537			4.00		
2538	1.28	-1.64		-0.69	4.03
2540			4.16		
2542	0.84	-1.48	4.01	-0.39	3.99
2544	1.08	-1.44	4.09		
2544			4.08		
2545				-0.51	4.03
2546	0.88	-1.57	4.12		
2546			4.28		
2548	1.02	-1.46			
2549	1.03	-1.59	4.32		
2550	1.00	-1.58			
2552	1.17	-1.47		-0.57	3.89
2552	1.21	-1.59	4.07		
2554	0.93	-1.62	4.15	-0.72	3.80
2554	1.09	-1.42			
2556	1.09	-1.66	4.16		
2557				-0.58	3.97
2558	1.05	-1.52	4.17		
2558	1.23	-1.49			
2562				-0.45	3.94
2562			4.14		
2564			3.90	-0.34	4.02
2564	1.11	-1.39			
2565	1.25	-1.36	3.94		
2566	1.39	-1.39	3.91		
2568	1.08	-1.40	3.89	-0.60	3.92
2569	1.08	-1.41	3.95		
2570	1.03	-1.54	4.01		
2572			3.92		
2572	1.01	-1.42	4.06		
2574	0.76	-1.61	3.98		
2574	0.93	-1.56	3.85		
2576	1.14	-1.63	3.92		
2578	1.08	-1.56	3.97		
2580			4.08	-0.52	3.85
2580	0.88	-1.39	3.84		
2582	1.03	-1.41	4.04	-0.60	3.89
2582			4.08		
2584			3.90	-0.56	3.86
2585	1.19	-1.33	3.92		
2586	0.92	-1.39			
2588	0.98	-1.32			
2588	0.96	-1.27			
2590	0.96	-1.21	4.00	-0.87	3.77

2590	0.82	-1.44	4.10		
2592	1.21	-1.30		-0.78	3.81
2592	1.36	-1.24	3.81		
2594	1.01	-1.40		-0.62	4.01
2594	1.38	-1.23	3.92		
2596	1.03	-1.33	3.85		
2597			4.06		
2598	1.27	-1.39	3.86		
2598	1.67	-1.37	3.86		
2600	1.01	-1.33		-0.54	3.98
2602	0.95	-1.31	3.86	-0.81	4.00
2602	1.07	-1.41			
2604	1.14	-1.49	3.85		
2606	0.74	-1.44	3.83	-0.73	4.09
2608				-0.68	4.14
2608	0.84	-1.42			
2610	1.00	-1.39	3.84	-1.11	4.05
2610				-0.69	4.13
2612	0.58	-1.47		-0.70	4.09
2613			3.80		
2614	1.12	-1.42		-0.63	4.06
2615				-0.69	4.26
2616	1.11	-1.31	3.99	-0.74	4.10
2618	0.91	-1.47		-0.74	4.13
2620	1.23	-1.38		-0.80	4.27
2622			3.94	-0.54	4.15
2624	0.99	-1.33	3.80	-0.78	4.29
2624			3.80		
2626	1.08	-1.42	4.05	-0.72	4.34
2626	0.94	-1.35	4.05		
2628	1.04	-1.39	3.98	-0.65	4.24
2630	1.04	-1.42	4.03	-0.94	4.20
2632			4.01	-0.84	4.25
2634	0.64	-1.42	4.03	-0.72	4.14
2637			3.81		
2638	1.01	-1.41		-0.49	4.27
2640				-0.80	4.14
2641	0.57	-1.51			
2642	1.05	-1.49		-0.81	4.21
2648	1.04	-1.54	3.88	-0.78	4.14
2650	0.67	-1.49		-0.85	3.99
2652	0.87	-1.52	3.85	-0.92	3.89
2654	0.83	-1.58		-0.82	3.94
2655			3.93		
2656	0.92	-1.46		-0.86	4.16
2658	0.81	-1.51		-0.73	4.07
2659	1.14	-1.54	4.19		

2660	0.91	-1.52		-0.62	4.08
2662	0.72	-1.60		-0.66	4.00
2664	0.93	-1.71		-0.78	3.93
2666	0.89	-1.54		-0.56	3.98
2676	0.89	-1.61			
2678	0.83	-1.63			
2679				-1.03	4.16
2680	0.94	-1.77		-1.01	4.25
2681			4.23		
2682	0.81	-1.84		-0.88	4.20
2684	0.83	-1.48		-0.94	4.22
2686				-0.96	4.16
2688	0.87	-1.64	4.36	-0.88	4.13
2690	0.92	-1.51		-0.79	4.21
2692	0.95	-1.52		-0.80	4.12
2694	0.75	-1.78		-0.85	4.21
2695			4.04		
2696	1.26	-1.78		-0.95	4.15
2698	0.97	-1.76			
2699			3.98		
2700	1.28	-1.55			
2701				-0.69	4.23
2702	0.80	-1.49			
2702			3.91		
2708	0.95	-1.56	4.02		
2709				-0.85	4.29
2710	0.92	-1.47	4.38		
2712	0.83	-1.40	4.19		
2713				-0.73	4.28
2714	1.06	-1.30	3.95		
2716	0.87	-1.31	3.96	-0.94	4.18
2718	0.94	-1.47	4.32	-0.66	4.33
2720	0.78	-1.65		-0.83	4.27
2722	0.87	-1.66	4.19	-0.91	4.14
2724			4.17	-0.63	4.31
2726			4.12	-0.75	4.28
2728	0.99	-1.50	4.02	-0.75	4.09
2730	1.02	-1.56			
2732				-0.80	4.28
2732	1.06	-1.45	4.11		
2734	1.03	-1.43	4.03	-0.76	4.05
2736			4.07	-0.97	4.30
2738	1.14	-1.44	4.02	-0.79	4.27
2740	1.08	-1.54	4.32	-0.86	4.11
2742	0.97	-1.64	4.40	-0.78	4.33
2744	1.07	-1.64	4.42	-0.81	4.29
2745				-0.87	4.14

2746	1.05	-1.53	4.56	-0.77	4.36
2748	1.05	-1.52		-0.83	4.14
2750	1.04	-1.57	4.33	-0.70	4.12
2752				-0.82	4.29
2754			4.25	-0.78	4.25
2756	1.06	-1.52	4.54	-0.60	4.23
2758	0.93	-1.57	4.19	-0.84	4.10
2760	0.87	-1.79		-1.00	4.15
2761				-0.94	4.11
2762			4.29	-0.84	4.24
2764			4.41	-1.04	4.11
2765				-0.61	4.07
2766			4.38	-0.71	4.10
2768	0.99	-1.84	4.45	-1.02	4.16
2769				-0.83	4.06
2770	0.88	-1.78	4.21	-0.90	4.15
2772			4.39	-0.79	4.04
2780	1.04	-1.73		-0.90	4.19
2781				-0.81	4.05
2782	0.99	-1.58	4.25	-0.92	4.11
2784	0.96	-1.75	4.13	-1.05	4.05
2786	1.03	-1.67	4.04		
2788	0.99	-1.55	4.34		
2789				-0.97	4.06
2790	0.96	-1.80	4.36		
2791				-0.81	4.06
2792	0.82	-1.77	4.36	-1.02	3.99
2794				-0.92	4.19
2795				-0.59	4.13
2802	0.96	-1.74	4.32	-1.00	4.04
2808	1.24	-1.70	4.47		
2810	0.97	-1.71	4.31	-0.91	4.03
2812	0.96	-1.73	4.18	-1.03	4.15
2814	1.04	-1.69	4.29	-1.06	4.19
2816				-0.80	3.97
2816	1.03	-1.74	4.27		
2822	1.12	-1.83	4.45	-1.06	4.17
2823				-0.87	3.96
2824	0.93	-1.88	4.15	-1.04	4.14
2826	0.96	-1.73	4.24		
2827				-0.89	3.97
2828	1.04	-1.90	4.39	-1.04	4.10
2830	0.83	-1.87	4.36	-1.01	4.14
2832	1.00	-1.74	4.47	-1.06	4.00
2834	0.93	-1.72	4.54	-1.08	4.12
2836	0.79	-1.86	4.39		
2837				-0.88	3.96

2838	1.21	-1.72	4.17	-1.11	4.02
2840	0.94	-1.80	4.16	-1.02	4.10
2842	1.16	-1.68	4.20	-0.99	3.98
2844	1.00	-1.98	4.32	-1.16	3.91
2846	1.11	-1.77	4.19	-0.86	4.01
2848	0.98	-1.90	4.47	-0.86	4.02
2850			4.27		
2852	0.99	-1.94	4.32	-0.83	4.08
2853				-0.79	3.94
2854	0.87	-1.84	4.44	-0.90	3.87
2856	0.87	-1.77	4.65	-1.10	3.99
2858	0.88	-1.98	4.65	-0.94	3.91
2860	1.20	-1.83	4.21		
2862	0.96	-1.71	4.25	-0.77	4.00
2864	0.97	-1.82	4.34	-0.99	4.03
2866	0.77	-1.76	4.28	-0.75	4.07
2868	1.05	-1.74	4.24		
2870	0.78	-1.77	4.19	-0.84	4.10
2872	0.56	-1.82	4.36	-0.92	3.94
2874	0.75	-1.74	4.57		
2876	0.95	-1.80	4.29	-1.04	3.91
2878	1.04	-1.66	4.19	-0.93	3.91
2880			4.44		
2882	1.04	-1.68	4.13		
2883				-0.81	3.90
2884	0.82	-1.77	4.09	-0.90	3.93
2886	1.07	-1.76	4.27		
2888	0.77	-1.58	4.19		
2890	0.90	-1.64	4.38		
2891				-0.75	3.89
2892	1.23	-1.82	4.51		
2894	0.80	-1.74	4.45		
2896	1.03	-1.61	4.45	-0.79	3.92
2898	0.99	-1.69	4.19	-0.89	3.87
2900	0.88	-1.56	4.27	-0.72	3.97
2902	1.10	-1.59	4.47		
2904	1.08	-1.64	4.36	-0.84	3.83
2906	1.16	-1.62			
2908			4.15		
2910	1.06	-1.54	4.10		
2912			4.14	-0.79	3.75
2914	1.27	-1.57	4.31		
2916	1.20	-1.61	4.20		
2918	1.04	-1.52	4.41	-0.77	3.84
2920	0.96	-1.51		-0.75	3.97
2922	1.12	-1.55	4.16		
2924	0.87	-1.52	4.32	-0.80	3.92

2926	1.04	-1.55	4.15	-0.50	4.02
2928			4.20	-0.61	3.97
2930	0.86	-1.53	4.09	-0.97	3.93
2932	0.95	-1.51	4.18	-0.66	4.05
2934	0.83	-1.53	4.00		
2936				-0.84	3.90
2936	1.19	-1.55	4.13		
2938	0.69	-1.69	4.18	-0.72	4.13
2940	1.03	-1.71	4.30	-0.89	4.04
2942	0.94	-1.71	4.31	-1.05	3.99
2944			4.12	-0.73	4.15
2946	0.86	-1.35	3.97	-0.84	4.05
2947				-1.00	3.92
2948	0.79	-1.38	4.26	-0.88	4.02
2950	0.87	-1.56	4.24	-0.87	3.92
2952			4.03	-0.81	3.95
2953				-0.86	3.97
2954	0.93	-1.58	4.15		
2956	0.82	-1.47	4.07	-0.80	4.01
2958	0.91	-1.46	4.22		
2959				-0.68	4.03
2960	1.09	-1.59			
2962	1.07	-1.65	4.01	-0.88	4.12
2964	0.90	-1.68	4.29		
2966	1.13	-1.62	4.21	-0.61	4.19
2968	1.00	-1.77		-1.06	4.05
2970	0.94	-1.67	4.25		
2972	1.00	-1.77	4.25		
2974	0.95	-1.66	4.30	-0.99	4.08
2976	0.58	-1.66	4.22	-0.78	4.17
2982	0.99	-1.38			
2983				-0.94	3.97
2984	1.03	-1.55	4.46		
2986	0.68	-1.49	4.24		
2987				-0.88	3.95
2988	1.02	-1.48	4.39		
2994	1.04	-1.54	4.04		
2995				-1.04	3.97
2996	0.90	-1.56	4.16	-1.09	4.08
2998	0.96	-1.41			
3000				-0.94	4.14
3002	0.99	-1.38	3.99	-0.99	4.20
3004				-1.19	4.14
3006	0.98	-1.46		-0.92	4.20
3008	0.70	-1.63	4.06	-0.77	4.29
3010	0.79	-1.60	3.96	-0.82	4.23
3012	0.87	-1.61	3.97	-0.62	4.29

3014	0.76	-1.67	4.24	-0.96	4.08
3016	0.62	-1.64	4.07	-0.98	4.17
3017				-0.96	4.07
3018	0.77	-1.67	4.30	-0.99	4.13
3020			4.08	-1.13	4.24
3021				-1.07	4.13
3022			4.19	-1.06	4.19
3024	0.60	-1.64	4.31	-1.13	4.22
3026			4.27	-1.22	4.19
3028	0.60	-1.65		-1.07	4.23
3030	0.87	-1.66		-1.15	4.08
3032			4.06	-0.90	4.22
3034	0.69	-1.79	4.30	-0.92	4.15
3036	0.75	-1.74	4.20		
3037				-1.16	4.10
3038	0.94	-1.78		-1.09	4.05
3040			4.06	-1.13	4.20
3042	1.00	-1.55		-0.95	4.10
3044	0.94	-1.53	4.07		
3046			4.26		
3047				-0.79	4.10
3048	0.86	-1.57	4.26		
3050	0.86	-1.61		-1.07	4.26
3052	0.66	-1.66	4.34		
3054	0.91	-1.66	4.18		
3056				-1.01	4.14
3058	0.91	-1.79		-1.17	4.12
3059				-1.10	3.96
3060	0.58	-1.74			
3062	0.54	-1.78	4.23	-1.20	4.07
3064			4.28	-1.14	3.95
3066	0.62	-1.73	4.12	-0.93	4.10
3068	0.58	-1.68	4.22	-1.13	4.09
3070	0.92	-1.74		-1.07	3.95
3072	0.73	-1.74	4.24	-1.12	4.06
3074	0.69	-1.87	4.33		
3075				-1.21	4.07
3076	0.68	-1.77	4.10		
3078	0.75	-1.96		-0.78	4.15
3080	0.77	-1.81	4.15	-1.03	3.94
3082	0.80	-1.88	4.31	-1.12	4.20
3084	0.77	-1.82	4.16	-0.96	4.15
3086	0.72	-1.93	4.04	-0.98	3.84
3088			3.97	-1.03	4.12
3090	0.78	-1.87	4.34	-0.96	4.07
3092			4.31	-1.02	4.00
3094	0.68	-1.82	4.04	-1.13	3.82

3096			4.19	-0.98	4.08
3098	0.68	-1.74	4.13	-0.96	4.17
3100	0.83	-1.73	4.20	-1.02	3.92
3102	0.73	-1.70	4.31		
3106	0.67	-1.62	4.44		
3112	0.67	-1.58		-1.03	3.76
3114	0.66	-1.69	4.41	-0.86	4.09
3116	0.58	-1.64	4.14		
3117				-1.07	3.93
3118	0.72	-1.76	4.39		
3120	0.58	-1.68		-0.85	3.99
3122	0.82	-1.72	4.17	-1.11	3.81
3124	0.47	-1.72			
3126			4.15		
3128			4.39	-1.02	3.79
3130	0.81	-1.69			
3132			4.51		
3134			4.51	-1.17	3.82
3136			4.22		
3138	0.66	-1.85	4.30		
3140				-1.05	3.92
3142			4.29		
3144	0.63	-1.88			
3146			4.36	-0.96	3.88
3148	0.85	-1.80	4.38		
3150	0.83	-1.71	4.28	-1.14	3.87
3151				-0.98	3.87
3152	0.58	-1.89			
3154				-1.03	3.97

Appendix B

The following data were presented in Project II in graphical form. 13C data for *G. ruber* and benthic foraminifera *U. hispida* (infaunal) and *U. costata* (infaunal) is also included.

MD81 Depth (cm)	***G. ruber* $\delta^{18}O$ (per mil)**	***G. ruber* $\delta^{13}C$ (per mil)**	***G. ruber* Mg/Ca (mmol/mol)**	***C. wuellerstorfi* $\delta^{18}O$ (per mil)**	***C. wuellerstorfi* $\delta^{13}C$ (per mil)**	***U. costata* $\delta^{18}O$ (per mil)**	***U. costata* $\delta^{13}C$ (per mil)**
2.50	-2.83	0.82	4.98	2.58	0.26	3.17	-0.58
5.00	-2.74	1.01	5.09	2.56	0.35	3.12	-0.84
6.00						3.16	-0.60
6.50	-2.85	0.80	4.93				
8.00	-3.02	0.76	5.09				
9.00	-2.80	1.06		2.57	0.36	3.21	-0.61
11.00				2.69	0.14		
11.50	-2.54	0.94	5.15			3.16	-0.65
13.00	-2.69	1.07	5.14	2.59	0.32	3.15	-0.57
16.00	-2.61	1.14	5.25	2.44	0.26	3.20	-0.57
19.00			5.24	2.63	0.47	3.20	-0.57
22.50				2.54	0.43	3.25	-0.42
25.00	-3.01	0.85	5.27	2.45	0.42	3.24	-0.72
28.00	-2.49	1.13	5.32	2.44	0.37	3.25	-0.53
31.00			5.27	2.63	0.34	3.14	-0.81
34.00	-2.55	1.07	5.09	2.51	0.32		
36.00				2.42	0.38	3.13	-0.22
37.00	-2.72	0.90	4.98				
39.00	-2.74	1.27	4.97	2.61	0.45	3.42	-0.63
41.00	-2.77	1.00					
42.50	-2.87	1.27					
44.00	-2.78	1.26	4.98	2.65	0.52	3.11	-0.84
46.00						3.17	-0.47
47.00	-2.63	0.95	4.96				
48.00	-2.95	1.34		2.51	0.42	3.13	-0.73
51.00	-2.68	1.06		2.36	0.33	3.33	-0.76
54.00	-2.76	1.16	4.91	2.56	0.40	3.03	-0.70
56.50	-3.05	1.00				3.03	-0.87
59.00	-2.82	0.91	4.91			3.23	-0.71
61.00	-3.05	0.99	4.89	2.39	0.43	3.22	-0.62
63.00	-2.90	1.68					
64.00	-2.58	1.06		2.35	0.29	3.17	-0.80
66.50	-2.78	1.16		2.56	0.42	3.14	-0.75
69.00	-2.93	0.98	5.16	2.60	0.44	3.26	-0.66
72.00	-2.89	1.06	4.65	2.60	0.38	3.12	-0.74

75.00			4.74	2.59	0.41	2.98	-0.84
79.00	-3.05	0.20	5.03	2.58	0.36	3.01	-0.97
82.00	-2.96	1.20	5.16	2.65	0.46	3.28	-0.75
85.00	-3.11	1.10	5.07	2.69	0.42	3.28	-0.69
87.50	-3.10	0.99	5.19	2.59	0.44	3.24	-0.80
89.00	-3.03	1.11	4.99				
92.00	-3.14	1.15	5.12	2.64	0.36	3.32	-0.73
93.00			5.11				
94.50	-2.96	0.89	4.83			3.26	-0.73
97.00	-3.01	1.35	4.88	2.69	0.41	3.34	-0.72
98.50			4.87				
100.00			4.76	2.72	0.50	3.24	-0.75
103.00	-2.98	1.46					
103.50	-3.16	1.10	5.08			3.32	-0.59
105.50	-2.96	1.41	5.16	2.77	0.40		
107.00	-3.13	1.04					
108.00	-3.05	1.17		2.79	0.31		
109.00						3.30	-0.68
110.50			4.93	2.73	0.42		
111.00			4.86				
113.00			4.81	2.67	0.48	3.27	-0.60
115.50			4.66	2.81	0.57	3.36	-0.64
118.00	-2.93	1.27	4.91	2.75	0.39		
120.50			4.76	2.86	0.52		
123.00			4.75				
123.50				2.78	0.43		
126.00	-2.90	1.14	4.83	2.66	0.35		
129.00	-2.81	1.09					
131.50				2.74	0.54		
133.00			4.99				
134.00				2.70	0.34		
136.50				2.87	0.46		
138.00	-2.76	1.11					
139.00	-2.81	1.56		2.78	0.34		
141.50				2.84	0.43		
143.00	-2.87	1.13					
144.50				2.84	0.45		
146.50				2.74	0.45		
147.00	-2.97	1.27	4.85				
149.00	-3.09	0.84	4.80	2.89	0.44		
151.00				2.73	0.37		
152.00	-3.18	0.92	4.69				
156.00	-3.33	0.66	4.83				
161.00			4.79	2.71	0.40		
163.00	-3.21	0.81					
165.00				2.69	0.46		
166.00	-3.28	0.85	5.00				

169.00	-3.20	0.76	5.02	2.70	0.48		
171.00	-3.09	1.44		2.68	0.34		
172.00	-2.93	1.17	4.67				
174.00				2.80	0.56		
175.00			4.89				
177.00	-3.03	0.98	4.77				
179.00	-3.20	0.83	5.10	2.77	0.63		
181.00			5.02	2.51	0.63		
183.00	-2.98	0.91		2.53	0.26		
185.00			5.21				
187.00			5.36	2.71	0.44		
189.00	-2.82	0.90	5.40	2.55	0.30		
191.00	-2.94	0.73	4.95	2.59	0.10		
193.00			5.26				
196.00	-2.96	0.85					
198.00				2.43	0.31		
201.00				2.39	0.26		
203.00				2.51	0.40		
205.00			4.98	2.73	0.38		
207.00			5.02	2.54	0.25		
209.00	-3.28	0.92	5.22				
211.00	-3.19	1.06	5.14	2.53	0.33		
213.00	-3.04	0.98	5.28	2.65	0.15		
215.00	-2.95	0.97	5.14	2.46	0.25		
217.00	-3.20	0.89	5.37	2.49	0.36		
219.00	-3.00	1.01	5.16	2.60	0.25		
221.00	-3.28	0.79	5.26	2.73	0.29		
223.00			5.18	2.53	0.24		
227.00	-3.03	1.26					
229.00	-2.94	0.88	5.26				
231.00	-2.96	0.65	5.18	2.34	0.17		
233.00			4.91				
235.00	-3.06	1.08					
237.00	-2.98	0.52	4.99	2.62	0.48		
239.00			4.84				
241.00	-3.07	0.86	5.02				
243.00	-2.85	1.10	5.19	2.33	0.26		
245.00	-2.89	1.14					
247.00				2.35	0.31		
248.00	-2.90	1.03					
251.00	-3.02	0.88	5.03				
254.00	-3.05	0.65	5.06				
262.00	-3.03	0.73	5.22				
265.00	-2.99	1.19					
267.00	-2.88	0.95	4.69	2.34	0.45		
269.00	-2.99	0.73	4.71				
271.00	-2.78	1.06					

272.00				2.24	0.38		
274.00	-2.90	0.69	4.60				
277.00	-2.85	1.24					
279.00	-3.03	0.91	5.08				
281.00	-2.92	0.97	4.86				
283.00	-2.91	0.97	4.49				
285.00	-3.06	0.62	4.67				
286.00				2.38	0.37		
287.00	-2.76	1.08	4.85				
289.00				2.44	0.34		
290.00	-2.88	0.76	5.06				
291.00				2.46	0.46		
293.00	-2.99	0.87	4.85	2.32	0.32		
295.00	-2.90	0.95		2.26	0.39		
297.00	-3.08	1.07	4.91				
299.00	-2.78	0.95		2.54	0.33		

MD77 Depth (cm)	***G. ruber* $\delta^{18}O$ (per mil)**	***G. ruber* $\delta^{13}C$ (per mil)**	***G. ruber* Mg/Ca (mmol/mol)**	***U. hispida* $\delta^{18}O$ (per mil)**	***U. hispida* $\delta^{13}C$ (per mil)**	***U. costata* $\delta^{18}O$ (per mil)**	***U. costata* $\delta^{13}C$ (per mil)**
2.50	-3.21	1.17	5.20				
3.00				2.58	-0.05		
3.50	-3.17	1.21	5.04				
4.50	-3.13	1.25	5.25				
5.00				2.49	-0.16	2.81	-0.06
5.50	-3.17	1.16	5.00				
6.50	-3.05	1.02	4.71				
7.00				2.38	-0.14		
7.50	-3.08	1.09	4.93				
8.50	-3.17	1.06	5.09				
9.50	-3.04	1.16	4.95			2.51	-0.48
10.00				2.44	-0.04		
10.50	-3.09	1.30	4.95			2.62	-0.43
13.50	-3.13	1.21	4.85				
14.00						2.72	-0.08
14.50	-3.17	1.12	4.67				
15.50	-3.17	1.27	4.68				
16.50	-3.08	1.14	4.77	2.63	0.07	2.70	-0.19
17.50	-2.99	1.30	4.83	2.55	-0.13		
18.50	-3.15	1.09	5.00	2.54	-0.07		
19.50	-3.21	1.08	4.98			2.61	0.18
23.50	-3.35	1.12	4.89				
24.50			4.76	2.52	0.28		
25.50	-3.16	1.21	5.08				
26.50	-3.09	1.28	4.94				
27.50	-3.12	1.35	4.76				
28.50	-3.42	1.12	5.12	2.47	0.19		

29.50	-3.23	1.11	5.00				
30.50	-2.99	1.40	5.14				
31.50	-2.99	1.45	5.03				
32.50	-3.21	0.95	4.99	2.51	0.06		
33.50	-3.02	1.09	5.07				
34.00						2.54	-0.49
34.50	-2.96	1.03	5.03	2.51	-0.19		
37.50	-3.21	1.00	5.14	2.49	-0.05		
38.50	-3.31	0.92	5.06				
39.00						2.56	-0.25
39.50	-3.06	1.10	5.13				
40.50	-3.29	-3.36	4.85	2.56	0.09		
41.00						2.76	-0.20
41.50	-3.37	0.87	5.02				
42.50	-3.04	0.94	4.91	2.37	0.04		
43.50	-3.26	1.07	5.02	2.69	0.00	2.48	-0.52
44.50	-3.16	0.90	5.11	2.60	0.21		
45.50	-3.02	1.13	4.78	2.48	0.16		
46.50	-3.16	1.12	4.95			2.49	-0.31
47.50	-3.22	1.08	5.02				
48.00				2.50	-0.01		
48.50	-3.01	1.29	4.95				
49.50	-3.08	1.17	5.11	2.43	-0.04		
50.50	-3.11	1.13	5.11			2.47	-0.25
51.00				2.46	-0.10		
51.50	-3.13	1.25	5.78				
52.50	-3.14	1.13	5.20				
53.50	-3.04	1.08	5.42				
54.00				2.51	0.03		
54.50	-3.19	1.20	5.58				
55.50	-3.20	1.12	5.34				
56.50	-3.16	1.15	5.22				
57.50	-3.12	1.07	5.13	2.56	0.28	2.64	-0.27
58.50	-3.07	1.23	5.10	2.60	0.08	2.57	0.01
59.50	-3.02	1.22	5.51				
60.50	-3.23	0.89	5.71	2.49	0.12		
61.50	-3.15	1.16	5.39	2.53	-0.16	2.38	-0.45
62.50	-3.05	1.36	4.97	2.52	0.11	2.47	-0.34
63.50	-3.12	1.09	5.57			2.50	-0.26
64.00				2.46	-0.08		
64.50	-3.11	1.08	5.26				
65.50	-3.02	1.23	5.58	2.53	0.06		
66.50	-2.97	1.16	5.18	2.49	0.02	2.54	-0.20
67.50	-3.12	1.22	5.26				
68.00				2.64	0.05		
68.50	-3.08	1.08	5.31				
69.00						2.47	-0.18

69.50	-3.21	1.18	5.26				
70.50	-2.99	1.26	5.62				
71.50	-3.02	0.98	5.10	2.45	0.05		
72.50	-3.19	1.16	4.73				
73.00				2.51	-0.01		
73.50	-3.12	1.14	5.15				
74.50			5.25				
75.50	-3.02	1.07	5.50				
76.50	-3.12	1.39	5.04				
77.00						2.49	-0.30
77.50	-3.14	1.32	5.12				
78.50	-3.27	1.09	5.44				
79.50	-3.27	0.87	5.11				
80.00				2.49	-0.09		
80.50	-3.10	1.03	5.07			2.52	-0.28
81.50	-3.16	1.20	5.25	2.52	0.09		
82.50	-3.07	1.21	5.24				
83.00				2.53	0.15		
83.50	-3.22	1.26	5.14			2.51	0.01
84.50	-3.25	1.31	5.07				
85.50	-3.24	1.32	4.94				
86.00				2.42	-0.02		
86.50	-3.22	1.36	5.21				
87.00						2.44	-0.37
87.50			5.06				
88.00				2.54	0.05		
88.50	-3.08	1.26	5.04			2.33	-0.26
89.50	-3.12	1.30	5.12			2.53	-0.43
90.00				2.52	-0.04		
90.50	-2.91	0.90	4.93				
91.00						2.49	-0.04
91.50	-3.28	1.38	5.24				
92.50	-2.95	1.25	4.95				
93.00				2.54	-0.04		
93.50	-3.05	1.16					
94.50	-3.07	1.29	5.37				
95.50	-3.28	1.38	5.23			2.58	-0.34
96.00				2.46	-0.02		
96.50	-3.04	1.08	5.45				
97.50	-3.01	1.24	5.32				
98.50	-3.35	1.09	5.14				
99.50	-3.16	0.85	4.98				
100.00				2.48	0.00		
100.50	-2.98	0.98	5.24				
101.50	-3.22	0.95	4.97				
102.50	-3.23	0.92	5.08	2.51	-0.01	2.52	-0.22
103.50	-3.01	1.34	4.92				

104.50	-3.24	1.11	5.12				
105.00				2.71	-0.07		
105.50	-3.34	1.05	4.92				
106.50	-3.12	1.02	5.30	2.61	0.12		
107.00						2.42	-0.35
107.50	-3.06	1.15	5.32				
108.00				2.54	0.06		
108.50	-3.08	1.28	5.02				
109.50	-2.96	1.29	5.10				
110.00				2.66	0.09		
110.50	-3.27	1.00	5.06				
111.50	-3.17	1.14	5.07	2.44	-0.03		
112.00						2.38	-0.41
112.50	-3.19	1.11	4.99				
113.00				2.60	-0.11		
113.50	-3.23	0.97	4.93				
114.50	-3.21	0.93	5.13	2.64	-0.15	2.59	0.09
115.50	-3.20	1.11	5.15				
116.00				2.67	0.02		
116.50	-3.16	1.06	4.96				
117.50	-3.06	0.87	5.07				
118.50	-3.09	0.91	5.12	2.56	0.05		
119.50	-3.15	1.27	5.04			2.53	-0.07
120.50	-3.09	1.19	5.45	2.54	-0.15		
121.50	-3.16	1.13	5.49	2.59	-0.03		
122.00						2.68	-0.14
122.50	-3.11	1.33	5.25	2.61	-0.14		
123.50	-3.10	1.29	4.99				
124.00						2.36	-0.49
124.50	-3.22	1.14	5.35				
125.50	-3.51	0.98	4.90	2.59	0.01		
126.00						2.51	-0.26
126.50	-3.38	1.13	4.93				
127.50	-3.42	0.93	5.05				
128.00				2.59	-0.02	2.49	-0.28
128.50	-3.24	1.02	4.92				
129.50	-3.23	1.08	4.94			2.33	-0.11
130.50	-3.22	1.24	5.38			2.41	-0.08
131.50	-2.80	1.69	5.00	2.54	0.10		
132.50	-3.00	1.02	5.28				
133.00						2.50	-0.35
133.50	-3.10	1.11	4.90				
134.00				2.56	-0.16		
134.50	-3.11	1.29	5.23				
135.00						2.53	-0.31
135.50	-3.08	0.89	5.24				
136.50	-3.16	1.16	5.20	2.51	-0.16		

137.50	-3.19	1.13	5.28				
138.50	-3.23	1.26	5.18			2.64	0.21
139.00				2.70	0.02		
139.50	-3.36	0.91	5.35				
141.00	-3.10	1.06	5.20	2.32	0.08	2.48	-0.21
142.50	-3.02	1.13	4.84				
143.00				2.37	0.26	2.32	-0.41
143.50	-3.20	1.20	5.31				
144.50	-3.08	1.06	5.29				
145.50	-3.19	1.30	5.39				